

AMERICAN UNIVERSITY OF BEIRUT

INTENSIFYING THE RECARBONATION PROCESS OF WATER

by
GABI ANTOINE ALTABASH

A thesis
submitted in partial fulfillment of the requirements
for the degree of Master of Science
to the Department of Chemical and Petroleum Engineering
of the Maroun Semaan Faculty of Engineering and Architecture
at the American University of Beirut

Beirut, Lebanon
September 2018

AMERICAN UNIVERSITY OF BEIRUT

INTENSIFYING THE RE-CARBONATION PROCESS OF WATER

by
GABI ANTOINE ALTABASH

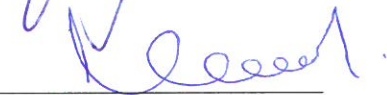
Approved by:

Dr. Fouad Azizi, Associate Professor
Department of Chemical and Petroleum Engineering



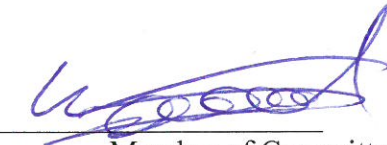
Advisor

Dr. Mahmoud Al - Hindi, Associate Professor
Department of Chemical and Petroleum Engineering



Member of Committee

Dr. Walid Saad, Associate Professor,
Department of Chemical and Petroleum Engineering



Member of Committee

Date of thesis defense: Sep 6, 2018

AMERICAN UNIVERSITY OF BEIRUT

THESIS, DISSERTATION, PROJECT RELEASE FORM

Student Name:

Altabash Gabi Antoine
Last First Middle

Master's Thesis Master's Project Doctoral Dissertation

I authorize the American University of Beirut to: (a) reproduce hard or electronic copies of my thesis, dissertation, or project; (b) include such copies in the archives and digital repositories of the University; and (c) make freely available such copies to third parties for research or educational purposes.

I authorize the American University of Beirut, to: (a) reproduce hard or electronic copies of it; (b) include such copies in the archives and digital repositories of the University; and (c) make freely available such copies to third parties for research or educational purposes after:

One ---- years from the date of submission of my thesis, dissertation, or project.

Two ---- years from the date of submission of my thesis, dissertation, or project.

Three ---- years from the date of submission of my thesis, dissertation, or project.



September 12, 2018

Signature

Date

ACKNOWLEDGMENTS

I would like to express my deepest gratitude and appreciation to my thesis advisor Dr. Fouad Azizi for his great guidance and assistance throughout my research. Without his countless support and involvement in every step, this work would have never been accomplished.

I would like to thank my thesis committee, Dr. Mahmoud Al-Hindi and Dr. Walid Saad for their valuable advice, constructive comments and suggestions on the manuscript of my thesis paper.

Finally, I would like to thank my dearest family and friends for their great encouragement, support, and unconditional love. Their faith in my capabilities has motivated me to accomplish this work with all confidence and persistence.

AN ABSTRACT OF THE THESIS OF

Gabi Antoine Altabash for Master of Science
Major: Chemical Engineering

Title: Intensifying the re-carbonation process of water

Gas–liquid contacting operations emphasize the enhancement of inter-phase mass transfer which is usually achieved by dispersing the gases into fine bubbles. Several reactor/contactors types are used for this purpose; however, many of which remain improperly designed because of their complex hydrodynamics. Lately, the interest is growing in the use of tubular reactors equipped with static mixers as they present an attractive alternative whereby the hydrodynamics are better controlled in order to enhance the mixing efficiency and mass transfer performance of the operations. A new type of static mixing element was recently introduced in which screens or grids are used and were found to be very effective at processing multiphase operations. Therefore, this study aimed at employing these static mixers in an attempt to intensify the absorption of CO₂ in RO water without chemical reactions. Its success would allow achieving smaller reactor volumes and introducing various economical and safety enhancements to the process. Faster and more efficient re-carbonation processes can thus be conducted at lower energy consumption and space requirements. In addition, the success of the work would also impact the design of photo-bioreactors and influence various applications of biogas upgrading.

To assess the efficiency of the reactor, the amount of absorbed CO₂ was tracked along the reactor using two methods, namely, pH measurements and direct CO₂ measurements using a CO₂ analyzer. The effect of varying the liquid and gas flow rates, screen geometry, and inter-screen spacing on the mass transfer performance were investigated and analyzed. It was found that the measured volumetric mass transfer coefficients, k_{LA} , were several orders of magnitude larger than those reported using conventional reactors. k_{LA} values increased with increasing both the liquid and gas flow rates and reached a maximum value of 1.01 s⁻¹ at low specific energy consumption rates (0.013 kWh/tonne). In addition, as the screen open area decreased, the k_{LA} value increased. However, decreasing the inter-screen spacing did not affect the value of k_{LA} , but only caused an increase in the energy consumption rates. This indicated that CO₂ absorption in RO water might be limited by the kinetics of the absorption and not by mass transfer.

CONTENTS

ACKNOWLEDGEMENTS	v
ABSTRACT.....	vi
LIST OF ILLUSTRATIONS	ix
LIST OF TABLES.....	xi
NOMENCLATURE.....	xiii
Chapter	
1. INTRODUCTION	1
2. LITERATURE REVIEW	9
2.1. CO ₂ absorption in aqueous solutions with chemical reaction	9
2.2. Physical absorption of CO ₂ using nanofluids in methanol, Deionized water, and NaCl solution	12
2.3. CO ₂ physical absorption in water systems with no chemical reactions..	16
3. METHODOLOGY.....	21
3.1. Experimental setup	21
3.1. Screen-type static mixers	23
3.2. System investigated	25
3.3. Method of analysis	28
3.3.1. Volumetric Mass Transfer Coefficient, k_{La}	28
3.4.1.1. pH measurements	30

3.4.1.2. CO ₂ Direct Measurements	31
3.5. Energy Dissipation and Power Consumption	33
4. RESULTS AND DISCUSSION	36
4.1. Pressure drop	36
4.2. pH and CO ₂ analyzer measurements	39
4.3. Volumetric mass transfer coefficient	42
4.3.1. Effect of liquid flow rate	43
4.3.2. Effect of gas holdup	45
4.4. Effect of Reynolds number	47
4.5. Energy requirements	52
4.6. Effect of inter-screen spacing	54
5. CONCLUSION	56
Appendix	
I. FIGURES	58
II. RAW DATA FROM EXPERIMENTS	71
III. SAMPLE CALCULATION (k_{La})	80
IV. ERROR ANALYSIS	85
BIBLIOGRAPHY	92

ILLUSTRATIONS

Figure	Page
1. Schematic Representation of the Experimental Setup	23
2. Screen Type Mixers	24
3. Pressure drop for four different screen geometries versus: (a) Empty pipe Reynolds number, Re_{pipe} and (b) Wire Reynolds number, Re_b	37
4. Effect of gas holdup on the pressure per screen: (a) pressure drop versus liquid velocity and (b) pressure drop versus superficial velocity of gas – liquid mixture	38
5. Raw data measurements versus residence time: (a) pH and (b) CO_2 concentrations	40
6. Comparing the measured and calculated data versus residence time: (a) measured and calculated pH (b) measured and calculated CO_2 concentrations	42
7. k_{LA} from pH, CO_2 analyzer, and average k_{LA} versus total superficial velocity ($L = 70$ mm): (a) Mesh 30, $\phi = 10\%$, (b) Mesh 50, $\phi = 20\%$, (c) Mesh 80, $\phi = 30\%$ and (d) Mesh 100, $\phi = 30\%$	43
8. Effect of Superficial velocity and gas holdup on k_{LA} ($L = 70$ mm): (a) Mesh 30, (b) Mesh 50, (c) Mesh 80 and (d) Mesh 100	45
9. Effect of superficial velocity and gas holdup on k_{LA} ($L = 33.5$ mm): (a) Mesh 30, (b) Mesh 50, (c) Mesh 80, (d) Mesh 100	47
10. The variation of k_{LA} with Reynolds number for all four screen geometries ($L = 70$ mm): (a) Re , (b) Re_b , (c) Re_M , (d) Re_j and (e) Re_{jet}	50
11. The variation of k_{LA} with Reynolds number for all four screen geometries ($L = 33.5$ mm): (a) Re , (b) Re_b , (c) Re_M , (d) Re_j and (e) Re_{jet}	52
12. k_{LA} versus the energy needed to process a unit of the flowing mixture, E_{spm} , ($L = 70$ mm): (a) Mesh 30, (b) Mesh 50, (c) Mesh 80 and (d) Mesh 100	53
13. k_{LA} versus the energy needed to process a unit of the flowing mixture, E_{spm} , ($L = 33.5$ mm): (a) Mesh 30, (b) Mesh 50, (c) Mesh 80 and (d) Mesh 100	54

14.	Parity plot of determined k_{LA} at $L = 33.5$ mm against k_{LA} at $L = 70$ mm	55
15.	Effect of gas holdup and superficial liquid velocity on the pressure drop per screen: (a) Mesh 30, (b) Mesh 50 and (c) Mesh 100	58
16.	Effect of gas holdup and total superficial velocity on pressure drop per screen: (a) Mesh 30, (b) Mesh 50 and (c) Mesh 100	59
17.	k_{LA} from pH, CO ₂ analyzer and average k_{LA} versus U_T at $\phi = 10\%$ ($L = 70$ mm): (a) Mesh 50, (b) Mesh 80 and (c) Mesh 100	60
18.	k_{LA} from pH, CO ₂ analyzer and average k_{LA} versus U_T at $\phi = 20\%$ ($L = 70$ mm): (a) Mesh 30 and (b) Mesh 80	61
19.	k_{LA} from pH, CO ₂ analyzer and average k_{LA} versus U_T at $\phi = 30\%$ ($L = 70$ mm): (a) Mesh 30, (b) Mesh 50 and (c) Mesh 100	62
20.	k_{LA} from pH, CO ₂ analyzer and average k_{LA} versus U_T at $\phi = 10\%$ ($L = 33.5$ mm): (a) Mesh 30, (b) Mesh 50, (c) Mesh 80 and (d) Mesh 100 ...	63
21.	k_{LA} from pH, CO ₂ analyzer and average k_{LA} versus U_T at $\phi = 20\%$ ($L = 33.5$ mm): (a) Mesh 30, (b) Mesh 50, (c) Mesh 80 and (d) Mesh 100 ...	64
22.	k_{LA} from pH, CO ₂ analyzer and average k_{LA} versus U_T at $\phi = 30\%$ ($L = 33.5$ mm): (a) Mesh 30, (b) Mesh 50, (c) Mesh 80 and (d) Mesh 100 ...	65
23.	The variation of k_{LA} with Reynolds number for all four screen geometries ($L = 70$ mm and $\phi = 10\%$): (a) Re , (b) Re_b , (c) Re_M , (d) Re_j and (e) Re_{jet}	66
24.	The variation of k_{LA} with Reynolds number for all four screen geometries ($L = 70$ mm and $\phi = 20\%$): (a) Re , (b) Re_b , (c) Re_M , (d) Re_j and (e) Re_{jet}	67
25.	The variation of k_{LA} with Reynolds number for all four screen geometries ($L = 33.5$ mm and $\phi = 10\%$): (a) Re , (b) Re_b , (c) Re_M , (d) Re_j and (e) Re_{jet}	69
26.	The variation of k_{LA} with Reynolds number for all four screen geometries ($L = 33.5$ mm and $\phi = 20\%$): (a) Re , (b) Re_b , (c) Re_M , (d) Re_j and (e) Re_{jet}	70

TABLES

Table		Page
1.	Characteristics of the investigated stainless steel plain weave wire cloth	25
2.	Data Representing the Experimental Conditions	28
3.	Raw data for Mn = 30 at L = 70 mm and $\phi = 10\%$	71
4.	Raw data for Mn = 30 at L = 70 mm and $\phi = 20\%$	71
5.	Raw data for Mn = 30 at L = 70 mm and $\phi = 30\%$	72
6.	Raw data for Mn = 50 at L = 70 mm and $\phi = 10\%$	72
7.	Raw data for Mn = 50 at L = 70 mm and $\phi = 20\%$	72
8.	Raw data for Mn = 50 at L = 70 mm and $\phi = 30\%$	73
9.	Raw data for Mn = 80 at L = 70 mm and $\phi = 10\%$	73
10.	Raw data for Mn = 80 at L = 70 mm and $\phi = 20\%$	73
11.	Raw data for Mn = 80 at L = 70 mm and $\phi = 30\%$	74
12.	Raw data for Mn = 100 at L = 70 mm and $\phi = 10\%$	74
13.	Raw data for Mn = 100 at L = 70 mm and $\phi = 20\%$	74
14.	Raw data for Mn = 100 at L = 70 mm and $\phi = 30\%$	75
15.	Raw data for Mn = 30 at L = 33.5 mm and $\phi = 10\%$	75
16.	Raw data for Mn = 30 at L = 33.5 mm and $\phi = 20\%$	76
17.	Raw data for Mn = 30 at L = 33.5 mm and $\phi = 30\%$	76
18.	Raw data for Mn = 50 at L = 33.5 mm and $\phi = 10\%$	76
19.	Raw data for Mn = 50 at L = 33.5 mm and $\phi = 20\%$	77
20.	Raw data for Mn = 50 at L = 33.5 mm and $\phi = 30\%$	77

21.	Raw data for Mn = 80 at $L = 33.5$ mm and $\phi = 10\%$	77
22.	Raw data for Mn = 80 at $L = 33.5$ mm and $\phi = 20\%$	78
23.	Raw data for Mn = 80 at $L = 33.5$ mm and $\phi = 30\%$	78
24.	Raw data for Mn = 100 at $L = 33.5$ mm and $\phi = 10\%$	78
25.	Raw data for Mn = 100 at $L = 33.5$ mm and $\phi = 20\%$	79
26.	Raw data for Mn = 100 at $L = 33.5$ mm and $\phi = 30\%$	79
27.	Sample calculation operating and design conditions	80
28.	Calculated variables	81
29.	Data Used to Calculate k_{LA}	83
30.	Calculated variables for determining k_{LA} using pH	83
31.	Calculated variables for determining k_{LA} using CO ₂ analyzer	84
32.	Errors associated with measured physical quantities	85
33.	Error analysis for superficial velocity of gas and liquid mixture	86
34.	Error on residence time	87
35.	Error propagation on the calculated CO ₂ from pH	88
36.	Error propagation on back calculated pH from CO ₂ analyzer	89
37.	Error propagation on k_{LA}	89
38.	Error on Reynolds number	90

NOMENCLATURE

a	Interfacial are of contact	[m ² /m ³]
b	Screen wire diameter	[μm]
$(C_{H_2CO_3})^*$	Concentration of CO ₂ at equilibrium with the gas phase	[mol·L ⁻¹]
D	Pipe diameter	[m]
E	Energy dissipation rate	[kW]
E_{spm}	Specific energy consumption rate per unit mass of liquid processed	[kWh/kg]
H_{CO_2}	Henry's law constant	[mol·atm ⁻¹ ·L ⁻¹]
K_0, K_1 and K_2	Equilibrium constants	[M]
k, k_1 and k_2	Factor for volume increase	[-]
k_L	Mass-transfer coefficient	[m·s ⁻¹]
k_{LA}	Volumetric mass transfer coefficient	[s ⁻¹]
K_s	Solubility of the gas in the liquid sample	[bar ⁻¹]
L	Inter-screen spacing in the mixing section	[m]
M	Wire mesh size	[m]
Mn	Mesh number	[-]
p'	Partial pressure of a gas	[atm]
p_o	Original saturation pressure of the gas in the liquid	[atm]
p	Equilibrium pressure measured	[atm]
p_s	Standard pressure of 1 bar	[atm]
P_{CO_2}	Partial pressure of CO ₂	[atm]
Q	Volumetric flow rate	[m ³ /s]
R	Gas constant	[atm·L·mol ⁻¹ ·K ⁻¹]
Re	Reynolds number, $\frac{\rho UD}{\mu}$	[-]
Re_{pipe}	Empty pipe Reynolds number, $\frac{\rho U_T D}{\mu}$	[-]
Re_b	Wire Reynolds number, $\frac{\rho U_T b}{\mu}$	[-]
Re_M	Mesh Reynolds number, $\frac{\rho U_T M}{\mu}$	[-]
Re_j	Individual-jet Reynolds number, $\frac{\rho U_T 2(M-b)}{\mu \alpha \sqrt{\pi}}$	[-]
Re_{jet}	Macroscopic jet Reynolds number, $\frac{\rho U_T D}{\alpha \mu}$	[-]
S	Salinity	[g/kg]
t	Residence time	[h]
T	Temperature	[K]
U	Superficial velocity	[m/s]
V	Volume	[L]
X	First gas species present in the sample	[-]
Y	Second gas species present in the sample	[-]
Greek Symbols		
α	Percentage open area of screen	[%]

ΔP	Pressure drop in the pipe	[Pa]
ε	Turbulent kinetic energy dissipation rate	[W/kg]
ρ	Density	[kg/m ³]
φ	Gas holdup	[%]
<i>Subscripts</i>		
g	Gas	
L	Liquid	
T	Total	
mix	Mixture properties	

CHAPTER 1

INTRODUCTION

It is well known that CO₂ represents an important component of the greenhouse gas effect and its capture and storage are of extreme importance. CO₂ emissions from fossil fuels and industry comprise approximately 90% of all CO₂ emissions from human activities (Jackson et al., 2017). The largest emitting countries like China, U.S.A, India, Russia, Japan, and the European Union account for 68% of the total global CO₂ emissions and 63% of the total global greenhouse gas emissions (Olivier et al., 2017). According to various studies, CO₂ emissions were steady between 2014 and 2016, with a reported ~35.7 Gt CO₂ released, however, a 2% increase was recorded in 2017 and a further increase is projected for 2018 (Jackson et al., 2017; Olivier et al., 2017). The impact of these large amounts of released CO₂ is being felt by warmer temperatures around the globe, a situation that is expected to further escalate with its subsequent environmental hazards. Reducing CO₂ emissions therefore becomes of utmost necessity. (Bloder et al., 2005)

Numerous works focused on reducing the CO₂ emissions into the atmosphere, while a larger number investigated CO₂ capture methods which consist of the three major methods: post-combustion, pre-combustion and oxy-fuel combustion (Wang et al., 2017). For the post-combustion capture, after completely burning the fuels, the CO₂ is sequestered from the flue gas. In pre-combustion, the syngas produced from the coal gasification is composed mainly of CO₂ and H₂. Generally, CO₂ is removed before H₂

combustion takes place. For the oxy-fuel combustion, it takes place under pure oxygen condition to produce high CO₂ concentration that is readily transported and stored. Several investigations targeted the post-combustion capture with several technologies including chemical absorption methods or scrubbing processes which are considered the most suitable and possible for implementation. In addition, Membrane-based CO₂ separation processes recently appear to be a competitive substitution for conventional chemical absorption technology. No chemical reaction in membrane-based separation process takes place unlike chemical absorption process, and thus it has less environmental impact with much less energy consumption expected (Wang et al., 2017).

Basically, chemical absorption is commonly achieved by chemisorption using ionic liquids (Hasib-ur-Rahman et al., 2010; Wappel et al., 2010) or amine-based solvents (Rubia et al., 2010; ZHANG et al., 2007). Some of the major ionic solvents reported by MacDowell et al. (2010) are the alkanolamines such as monoethanolamine (MEA), diethanolamine (DEA), and methyldiethanolamine (MDEA). Mechanically agitated tanks, bubble columns, packed bed reactors and absorption columns are major reactors/contactors used for the purpose of capturing CO₂ from flue gas, then compressing and transporting the absorbed gas for storage in geological formations, oceans, oil fields, or water aquifers (Ali et al., 2011; Momeni et al., 2012). In addition, the captured CO₂ can be used as a feedstock for some industrial processes (Wang et al., 2017). Some investigators used these solvents with other solutions. For instance, Chavez and Guadarrama (2010) used sodium hydroxide solution in absorption columns,

while Bishnoi and Rochelle (2000) used a mixture of DEA and MDEA solutions in wetted wall contactor for his investigations.

However, fewer investigators considered the direct solubility of CO₂ in pure water systems without chemical reactions. These studies are of great importance as they can contribute to great advancements in the remineralization of soft waters, the design of photobioreactors and biogas upgrading to biomethane. For example, desalinated (soft) water from Reverse Osmosis (RO) and thermal desalination is highly reactive and characterized by a very low salinity, and high aggressiveness and corrosivity (Al-Deffeeri, 2008; Glade et al., 2005). Consequently, re-mineralizing this water to render it non-corrosive, non-aggressive and palatable is a crucial step before its distribution for civil consumption (Al-Anezi and Hilal, 2006). This is frequently achieved by increasing its mineral content of the desalinated water (Withers, 2005). Several re-mineralization processes are currently employed such as chemical addition, carbon dioxide addition followed by limestone dissolution, carbon dioxide addition followed by lime dosing, or blending with water containing a high mineral content (Hasson and Bendrihem, 2006; Withers, 2005). However, the dissolution of limestone or lime by using CO₂ is most widely used. In these processes, the CO₂ released in multi-stage flash (MSF) plants can be used for re-carbonating the distillate, while injection of CO₂, produced from gas generators, into the permeate line is the method commonly used in RO plants. The injected CO₂ is critical to increase the mineral content of the water because it dissolves the calcium ions from lime or limestone (Hasson and Bendrihem, 2006). Other works tackled the carbon dioxide stripping in cell-culture reactors. In these operations, the

CO₂-enriched waters are used as a source of carbon in bioreactors, where it is converted to organic carbon by living cells such as photosynthetic algae (Hill, 2006; Kordac and Linek, 2008).

To perform these absorption operations, a wide array of gas-liquid contactors is typically employed. These contactors vary between mechanically agitated vessels (Gómez-Díaz and Navaza, 2005; Hill, 2006; Kordac and Linek, 2008), bubble columns (Álvarez et al., 2008; Thaker and Rao, 2007), packed bed (Evren et al., 1999), absorption column and hollow fiber membranes (Boributh et al., 2011; Mansourizadeh, 2012). For instance, Hill (2006) and Kordač and Linek (2008) studied the absorption of CO₂ in RO water and water containing NaCl using a mechanically agitated vessel. Their study was conducted for the purpose of studying the mass transfer performance of the reactor to increase the concentration of absorbed CO₂ in water, which is considered as a source of carbon for photosynthetic cell cultures. In addition, Gomez et al. (2005) studied the mass transfer of CO₂ using carbon dioxide/alkane systems in a stirred vessel. Thaker and Rao (2007) investigated the CO₂ absorption in water and using a bubble column, while Álvarez et al. (2008) studied the gas/liquid mass transfer process of carbon dioxide in polluted aqueous solutions with surface active substances by employing a thermostated cylindrical bubble column. Moreover, Evren et al. (1999) investigated the absorption of carbon dioxide-air mixtures in water using a packed-bed absorption column and developed a numerical model for the same system. Mansourizadeh et al. (2012) investigated the absorption and desorption of CO₂ in distilled water using structurally developed hydrophobic polyvinylidene fluoride

(PVDF) hollow fiber membranes in a membrane contactor. Whereas, boributh et al. (2011) developed a mathematical model to investigate the physical absorption of CO₂ using hollow fiber membrane contactors. The pore size distribution was studied, and the simulation was performed under various operating conditions.

In addition, some investigators tackled the removal of CO₂ from biogas using water for the purpose of upgrading biogas to biomethane. Biogas is normally produced by bacterial conversion of organic matter under anaerobic (oxygen free) environment. Biogas is mainly composed of methane and carbon dioxide with smaller proportions of other gases such as hydrogen sulfide, water vapor and other minor compounds like nitrogen, oxygen and ammonia (Belaissaoui and Favre, 2018). Typically, the percentage of the carbon dioxide gas present in biogas can reach 35 to 45%, while methane gas can reach 55 to 65% (Nock et al., 2014). To produce biomethane, biogas undergoes purification processes such as sulfur removal, CO₂ removal and dehydration. This biomethane can be used as a green source of energy for vehicle fuel, substituent for natural gas and for combined heat and power plants. Pressurized water absorption using packed column or water scrubbing is the most established and most widely used technology for removing CO₂ from biogas (Nock et al., 2014). This technology comes with great amount of energy expenditure ranging between 0.2 – 0.6 kWh/Nm corresponding to 2 – 11% of the energy content of the upgraded biomethane (Bauer et al., 2013; Berglund and Börjesson, 2006; Nock et al., 2014; Persson, 2003; Smyth et al., 2009). The amount of CO₂ removed depends on several factors including the design of the column, interfacial area, and the solubility of CO₂ in the solvent. Water is

considered as substantial solvent due to its low cost and high availability. In addition, the solubility of CO₂ in water is 26 times more than methane (Dawoud et al., 2007). A recent study by Belaïssaoui and Favre (2018) investigated the use of hollow fiber membrane contactor in a novel absorption/desorption loop with water as an absorbent. Based on their study 96.6% of CO₂ removal and 98% purity of biogas was achieved with 68% reduction in volume of the absorption unit used in water scrubbing (Belaïssaoui and Favre, 2018).

In all these reactors/contactors gas-liquid mass transfer remains the rate limiting step (Laakkonen et al., 2006). Gas-liquid mass transfer relies on the efficient dispersion of gases into liquids to increase the area of contact between the phases and consequently the rate of transfer. The varying hydrodynamic conditions prevailing in the aforementioned reactor types, leads to the observed wide variations in their mass transfer effectiveness. In addition, the design of these units is very difficult without employing empirical knowledge and experience because of the spatial inhomogeneity of their hydrodynamics (Azizi and Al Taweel, 2012). The ability to enhance interphase mass transfer by better dispersing the gases into fine bubbles thus becomes an area of great interest (Azizi and Al Taweel, 2012). This can be achieved by providing valuable concentration profiles in the different phases and by dispersing the gases into fine bubbles that have large interfacial area of contact, a , (Azizi and Al Taweel, 2012). Moreover, achieving high k_{LA} allows for the use of smaller and safer reactors as well as increasing the selectivity and yield of mass-transfer controlled reactions (Boodhoo and Harvey, 2013a; Zhang et al., 2012). For this purpose, tubular reactors equipped with

static mixers became of great interest because of their great potential (Azizi and Al Taweel, 2015). Al Taweel and Chen. (1996) highlighted that high multiphase mass transfer rates that can be achieved with tubular reactors equipped with static mixing elements while using very large flow rates (Ghanem et al., 2014; Peschel et al., 2012).

These static mixers presented are motionless inserts to a pipeline. They are used to promote mixing. There are various types of static mixer designs for the wide range of applications including laminar and turbulent mixing in single phase and multiphase systems and blending of viscous materials. For the case of turbulent flows, static mixers seek to enhance the formation of turbulent eddies in the flow streams (Boodhoo and Harvey, 2013b). Normally, the fluids to be mixed are liquid, but static mixers can be used to mix gas streams, disperse gas into liquid in multiphase flow or blend immiscible liquids (Boodhoo and Harvey, 2013b). One variant of these mixers, the screen-type static mixer, is used to repetitively superimpose an adjustable, radially uniform, highly turbulent field on the nearly plug flow conditions encountered in high-velocity pipe flows. Those type of static mixers were able to achieve an interfacial area of $2200 \text{ m}^2/\text{m}^3$ in the case of gas-liquid contacting (Al Taweel and Chen, 1996). According to Azizi and Al Taweel (2012), the very high turbulence intensities generated in the regions adjacent to the screens resulted in the formation of fine dispersed phase entities and enhanced the value of the interphase mass transfer coefficient. These mixers were found very efficient in processing oxygenation/deoxygenation operations as well as liquid-liquid extractive separations. In a recent study conducted by Luo et al. (2017), they found that the use of stainless steel wire mesh packings similar to the screen type

static mixer in a rotating packed bed enhanced the interfacial area and thus more CO₂ absorbed in NaOH solution-based solvent. Moreover, in a previous study by Al Taweel et al. (2005), they found that interphase mass transfer can be significantly enhanced by inserting a screen-type static mixing element into the two-phase pipeline flow. Therefore, tubular reactors equipped with static mixers has become an attractive alternative to conventional agitation because of their better performance at lower capital and operating costs (Azizi and Al Taweel, 2015).

Therefore, the main objective of this study is to investigate the possibility of using screen-type static mixing elements to intensify the mass transfer of CO₂ from the gaseous phase into aqueous phase with no chemical reactions. To achieve this, A plug flow reactor/contactator equipped with screen-type static mixers will be employed. The amount of the carbon dioxide dissolved is measured across the reactor and used to determine the mass transfer performance of this reactor.

CHAPTER 2

LITERATURE REVIEW

CO₂ absorption can be classified as physical or chemical absorption. This section will primarily discuss the previous investigations on the absorption of CO₂ in aqueous solutions where no chemical reaction is taking place. In addition, it will briefly discuss the CO₂ absorption in solvents where chemical reactions take place.

2.1. CO₂ absorption in aqueous solutions with chemical reaction

Most of the research investigating CO₂ absorption in the literature were undertaken with the purpose of sequestering this gas for environmental reasons. Numerous works focused on removing CO₂ from the gas phase into liquid solvent using chemical reactions. In these methods, CO₂ reacts reversibly with the solvent to form water-soluble salts and the solvents are then regenerated and introduced again to the absorption unit. The most commonly used absorption solvents are the alkanolamines, such as MEA, DEA, and MDEA (Aroonwilas et al., 1999; MacDowell et al., 2010). For instance, Chavez and Guadarrama (2010) and Aroonwilas et al. (1999) investigated CO₂ absorption into aqueous solution in absorption columns with structured packings using sodium hydroxide and MEA as solvents. Whereas, Bishnoi and Rochelle (2000) investigated the absorption of CO₂ into aqueous solutions using a mixture of DEA and MDEA in a wetted wall contactor. In addition, Gomez-Diaz and Navaza (2005) worked with the carbon dioxide absorption in binary mixtures of normal alkanes as liquid phase in stirred tanks. Maceiras et al. (2007) studied the process of carbon dioxide absorption

using a bubble column reactor and DEA solutions as solvent, while La Rubia et al. (2010) considered CO₂ absorption in aqueous solutions using bubble column reactor and triethanolamine (TEA) as solvent. So, all the mentioned studies are related to the absorption of CO₂ in aqueous solutions using alkaolamines. Nevertheless, In a review made by Afkhamipour and Mofarahi (2017), they investigated the mass transfer performance for CO₂ absorption in amine based solvents in packed columns for environmental purposes. Volumetric mass transfer models were discussed for several type of amine solvents like conventional amines like alkanolamines and newly developed amines such as N,N-diethylethanolamine (DEEA), 4- diethylamino-2-butanol (DEAB), and diethylenetriamine (DETA) (Afkhamipour and Mofarahi, 2017).

Other investigators focused on the enhancement of CO₂ absorption in ionic solvents. For this purpose, they investigated the hydrodynamics and mass transfer performance of some reactors. For instance, Ganapathy et al. (2016) studied the process intensification characteristics of a microreactor absorber for enhancing the post combustion capture of CO₂ in DEA solvent. Basically, microreactor performance can be enhanced significantly by increasing the surface area needed for the reaction. The new model of the reactor proposed by Ganapathy et al. (2016) was characterized by increased number of straight parallel channels with relatively low hydrodynamic diameter, and the absorption efficiency, mass transfer coefficient, acid loading ratio and the pressure drop were investigated to determine the mass transfer performance of the microreactor. They found that the absorption efficiency enhanced when the liquid

velocity increase while gas flowrate decreases. The mass transfer coefficient was determined to be 17 s^{-1} . This is considered as one to three orders of magnitude higher than the values reported for conventional absorption units indicating the increased level of process intensification of their reactor (Ganapathy et al., 2016). Lin and Chu (2015) and Lin and Kuo (2016) investigated the mass transfer performance of rotating packed beds with blade packings in carbon dioxide absorption into sodium hydroxide solution and MEA solution in two studies. In both investigations, increasing the rotational speed of the rotational packed bed, the inner diameter of the bed, liquid flowrate and the gas flow rate increased the volumetric mass transfer of the system (Lin and Chu, 2015; Lin and Kuo, 2016). However, the mass transfer efficiency was found to be higher when using MEA solution than in the case of NaOH solution. In addition, rotational packed bed equipped with blade packings were found to be more effective than structured packings in capturing CO_2 . Moreover, Luo et al. (2017) studied the mass transfer performance and the effect of the interfacial area on CO_2 absorption in rotating packed bed equipped with stainless steel wire mesh packings. NaOH solution was used in this investigation, and it was found that the increase in rotational speed, gas and liquid flow rate increased the value of the interfacial area (Luo et al., 2017). Unlike the aforementioned studies, Xu et al. (2016) investigated the mass transfer performance of CO_2 absorption into aqueous DEEA using packed columns. Several factors including CO_2 partial pressure, lean CO_2 loading, liquid flow rate and inert gas flow rate were considered. It was found that as the temperature and the flow rate of the liquid increase, the overall mass transfer coefficient, k_{GA} , increased. Moreover, increasing the DEEA

concentrations increased the mass transfer performance. However, when the CO₂ partial pressure and the CO₂ loading increase, k_{GA} value decreased. It was found that the volumetric mass transfer coefficient was higher when using DEEA than using MDEA. Structured packings also enhanced the mass transfer coefficient more effectively than random packings (Xu et al., 2016).

2.2. Physical absorption of CO₂ using nanofluids in methanol, Deionized water, and NaCl solution

This section considers several studies concerning the absorption of CO₂ in methanol, deionized water and NaCl in water solutions. In these studies, the use of metal oxide nanoparticles such as Al₂O₃, SiO₂, TiO₂ and carbon nanotubes (CNTs) were investigated. These nanoparticles along with the solution used form nanofluids. Different reactors were employed to study the absorption rate of CO₂ including tray column absorber (Torres Pineda et al., 2012), Taylor-Couette absorber (Torres Pineda and Kang, 2016), vertical annular contactor (Pineda et al., 2014), bubble column (Lee et al., 2016, 2011), hollow fiber membrane contactors (Golkhar et al., 2013) and a lab scale absorption/regeneration system (Lee et al., 2015).

For instance, Torres Pineda et al. (2012) investigated the enhancement of CO₂ absorption in methanol using Al₂O₃ and SiO₂ nanofluids in tray column absorber for the purpose of capturing CO₂ for environmental reasons. Twelve sieve trays were used in the absorber. The use of Al₂O₃ and SiO₂ in methanol based nanofluids promoted the detachment of the bubbles from the orifice which resulted in enhancement in the absorption rate compared with the use of pure methanol. The mass flow rate of CO₂ is

measured at the outlet of the tray column through a mass flow meter, and it is used to determine the amount of CO₂ absorbed. An enhancement of 9.4% and 9.7% was achieved with a 0.05 vol% of Al₂O₃ and SiO₂ respectively (Torres Pineda et al., 2012). In addition, Torres Pineda and Kang (2016) investigated the CO₂ absorption in Taylor-Couette absorber, where flow takes place between two concentric cylinders. They used methanol and aluminum oxide methanol-based nanoabsorbents at low concentrations. The addition of nanoparticles to methanol reduced the energy consumption required in the case of absorption and regeneration processes. According to the same authors, the turbulent regime in the reactor enhanced the CO₂ absorption in methanol up to 20% and the volumetric mass transfer coefficient for the counter current operation enhanced by 27% when using nanoabsorbents in turbulent regimes compared with methanol and 53% in the case of stagnant fluid (Torres Pineda and Kang, 2016).

In another work, Pineda et al. (2014) compared the use of new nanoparticles such as SiO₂ and TiO₂ to Al₂O₃ with methanol as solvent. These nanofluids were used for CO₂ absorption in a vertical annular contactor and the performance was compared to similar contactor equipped with trays (Pineda et al., 2014). These studies target the post combustion capture of CO₂ emitted from fossil fuels-based industry. Two flow configurations the co-current and counter-current flows were applied and compared, and it was found that there is no enhancement in the case of co-current flow with pure methanol. For the counter-current flow, a 7% increase in performance was obtained. In addition, the presence of trays in the annular contactor enhanced the absorption rate for counter-current flows up to 9%, 10% 6% and 5% for pure methanol, Al₂O₃, SiO₂ and

TiO₂ respectively (Pineda et al., 2014). It was found that the SiO₂ nanofluids did not enhance the mass transfer under hydrodynamic conditions of the liquid phase unlike the case of Al₂O₃ and TiO₂. However, the SiO₂ nanoparticles are found to be more suitable for the combined CO₂ absorption/regeneration process in a study performed by Lee et al (2016). Moreover, it was found that the bicarbonate and carbonate species formed by binding of CO₂ with the nanoparticles of Al₂O₃ decreased the absorption/regeneration performance. Consequently, SiO₂ nanoparticles with methanol is more suitable for the combined CO₂ absorption/regeneration(Lee et al., 2016). Lee et al. (2011) also studied the absorption of CO₂ in a bubble column. The optimum concentration for Al₂O₃ and SiO₂ in methanol for the best CO₂ absorption was found to be between 0.01 and 0.05 vol% (Lee et al., 2011). At a temperature of 20 °C, the absorption enhancement was 4.5% at 0.01 vol% of Al₂O₃ in methanol. However, at -20 °C, the absorption enhancement was found to be 5.6% at 0.01 vol% of SiO₂ in methanol (Lee et al., 2011). Furthermore, Lee and Kang (2013) investigated the enhancement of CO₂ absorption using Al₂O₃ nanoparticles in a 3.5 wt% NaCl aqueous solution. Experiments were performed in a bubble column absorber. It was found that the CO₂ solubility increases as the particle concentration increases to 0.01 vol%. The CO₂ solubility increased by 11%, 12.5% and 8.7% for 0.01 vol% of Al₂O₃ in NaCl solution at 30, 20 and 10 °C (Lee and Kang, 2013).

Moreover, Lee et al. (2015) in another study investigated enhancement of the absorption and regeneration cycle of CO₂ in an integrated gasification combined cycle (IGCC), which is a physical method. Generally, chemical methods are characterized by

higher absorption rates than that of physical methods. However, the regeneration process requires less energy in physical methods than that of chemical methods. In this study, dispersed nanoparticles such as SiO_2 and Al_2O_3 in deionized water solution were used. The amount of CO_2 absorbed was determined by measuring the time needed to reach the saturation pressure of 500 kPa and was compared to the time needed in the case of a base fluid (348 s). It was found that the optimum concentration for the best CO_2 absorption and regeneration is 0.01 vol% of SiO_2 and the enhancement in absorption and regeneration was 23.5% and 11.8% respectively. However, for the case of Al_2O_3 , the CO_2 absorption rate increased by 23.5% similar to the case of SiO_2 , but the regeneration decreased by 11.2% for a 0.01 vol% of Al_2O_3 . This is attributed to the reaction of CO_2 with Al_2O_3 surface which resulted in the formation of absorbed bicarbonate and carbonate species (Lee et al., 2015).

Golkar et al. (2013) studied CO_2 capture from air and CO_2 mixture by silica and carbon nanotubes (CNTs) nanofluids in distilled water using hollow fiber membrane contactors. Factors such as type of nanofluids, nanoparticle concentration, gas and liquid flow rates, temperature and CO_2 inlet concentration were investigated to determine their effect on the efficiency of CO_2 absorption. The gas flow through the shell side and the liquid flowed through the lumen side of the hollow fibers co-currently. The CO_2 removal efficiency was calculated by measuring the inlet and outlet gas flow rate and tracking the composition of the inlet and outlet streams using gas chromatography. At 0.05 wt% of SiO_2 , a 20% enhancement in absorption rate was achieved compared to pure distilled water. However, at similar concentrations, with

CNT nanofluid about 40% enhancement was achieved. Therefore, the absorption rate of CNT nanofluids is higher than SiO₂ nanofluids, and this result recommend the use of CNT nanofluids as an alternative to metal oxide nanofluids in hollow fiber membrane contactors (Golkhar et al., 2013).

2.3. CO₂ physical absorption in water systems with no chemical reactions

On the other hand, only few investigators considered the physical absorption of CO₂ in pure water without chemical reactions. For instance, Hill (2006) studied the mass transfer of carbon dioxide into water using a direct pH measurement technique to track the dissolution of CO₂ in water. He employed a baffled stirred tank reactor equipped with a six-blade Rushton-type impeller. In addition, Hill (2006) presented a model based on temperature, aeration rate and stirring speed to evaluate the mass transfer performance. He also studied the effect of dissolved salts on k_{LA} by using 2.85% NaCl solution. Hill (2006) developed a model based on the chemistry of the dissolution of CO₂ in water and assuming that the carbonate and the hydroxide ions can be neglected to determine k_{LA} . The obtained k_{LA} values fit those reported in the literature. He deduced that using the diffusion coefficient correction can be used to obtain the carbon dioxide transfer rates form the oxygen transfer rates. However, no improvement was achieved by the addition of salt to water. In fact, the addition of salt to water decreased the value of k_{LA} which contradicts the literature. This study, however, led Kordač and Linek (2008) to replicate Hill's (2006) work to prove that his analysis of the experimental data were erroneous. They also employed a baffled stirred

tank reactor equipped with a vaned-disc impeller. The newly developed model was independent on the reaction equilibrium constant, the experiment start time and or initial and final pH readings. The model assumes ideal mixing in the gas phase, negligible gas-phase mass-transfer resistance and a reversible reaction in the liquid phase, which is fast enough to keep the concentrations of carbonate, bicarbonate and hydronium ions in equilibrium. Higher k_{LA} values were obtained compared to Hill especially in saline solutions (Kordac and Linek, 2008).

Other investigations tackled the desorption of CO₂ in pure water. For instance, Lisitsin et al. (2008) conducted studies on CO₂ desorption from pure water. Their overall volumetric mass transfer coefficient was calculated based on the difference between the bulk CO₂ concentration and that at equilibrium following the work of Vázquez et al. (1997). Furthermore, Nieves-Remacha et al. (2013) explored the hydrodynamics and mass transfer of gas-liquid flow in an advanced flow reactor using carbon dioxide and water. The gas liquid mass transfer was obtained by determining the amount of CO₂ absorbed using a titration method with sodium hydroxide and hydrochloric acid. the experiments were made under ambient conditions and with low flowrates of the gas and liquid, 5.6-103 mL/min and 10-80 mL/min respectively, which does not reflect the industrial scale conditions. They deduced that the bubble size distribution is greatly affected by the gas and liquid flowrates and that at a constant gas flow rate, the average bubble size decreases continuously while increasing the liquid

flowrate. In addition, the gas holdup decrease along the length of the reactor with the increase in the interfacial mass transfer rates (Nieves-Remacha et al., 2013).

Moreover, Panja and Rao (1993) investigated the CO₂ absorption in water using a mechanically agitated contactor. They proposed a dynamic response method for the evaluation of k_{LA} by sparging pure CO₂ to the reactor and measuring the change in the electrical conductivity as a function of time. The conductivity changes are attributed to the formation of carbonic acid. Extensive amount of mathematical processing is required to evaluate k_{LA} for every run using an approximate guess for the k_{LA} value to solve the various sets of differential equations. The solution of the first set of differential equations provides an estimate to the various ion concentrations in the solution. These concentrations are then used in algebraic equations to obtain a theoretical value of the temporal change in conductivity that is also used in another differential equation to obtain the actual increase in the conductivity of the solution. Finally, the sum of squares of differences between the computed and measured values of the conductivity for the initial guesses of k_{LA} is calculated. The actual value for k_{LA} is the minimum value of the computed sum of squares. They observed an increase in the k_{LA} value as the gas flow rate increase which is in accordance to most investigations (Panja and Rao, 1993). In a similar study, Thaker and Rao (2007) investigated the hydrodynamics of CO₂ absorption in distilled water using a bubble column. They relied on conductivity measurements and the technique developed by Panja and Rao (1993) which consists of measuring the conductivity as a function of time to obtain k_{LA} , with

the aid of a mathematical model. The feed gas was saturated with water vapor was fed to a packed bed disperser and analysis of water samples were made with titration. Similar to the findings of Panja and Rao (1993), the k_{La} value increase as the gas flow rate increase. However, they found higher water level in the column caused an increase in the gas holdup with decrease in the value of k_{La} . Furthermore, Thaker and Rao (2007) investigated the effect of staging the column by adding a redistributor plate at a height four times its diameter. The plate increased the gas holdup and thus the interfacial area of contact between the phases. A 20 to 40% increase in k_{La} value was achieved. In addition, higher k_{La} values were obtained when conducting desorption experiments into air rather than absorption experiments into water (Thaker and Rao, 2007).

In another study, Evren et al. (1999) investigated the absorption of CO₂ and air mixture in water using a packed-bed recirculating absorption column. They derived a model based on mass balance to obtain the k_{La} value numerically similar to the method of Panja and Rao. They observed that as the water flow rate and gas holdup increase, the k_{La} value increase. Also, the temperature and gas flow rate did not affect the value of k_{La} (Evren et al., 1999). Other studies considered the absorption of CO₂ in sea water with no solvents. For instance, Tokumura et al. (2007) investigated CO₂ absorption in seawater using a cylindrical bubble column. they investigated the salinity, temperature and gas flow rate on the absorption capacity. They found that increasing salinity concentration and temperature caused inhibition to the CO₂ absorption, while CO₂ injection rate enhanced the CO₂ absorption rate (Tokumura et al., 2007). Furthermore,

Chen and Vallabh (1970) studied the effect of cylindrical screen packings on rate of mass transfer in counter-current gas-liquid bubble column over a range of different gas and liquid flow rates. Mixtures of CO₂ and air of known proportions were used, and the rate of CO₂ absorption in water was determined by a titration method. The volumetric mass transfer coefficient was obtained from liquid phase composition changes and from the amount of CO₂ absorbed in water. An increase in the gas flow rate caused an increase in k_La values until it remains constant at a certain gas flow rate. Also, the screen packings affected k_La , where increase in k_La values were observed with smaller screen opening areas due to decrease in bubbles size (Chen and Vallabh, 1970).

It can be deduced that the value of the volumetric mass transfer coefficient is affected by both the interfacial area of contact between the phases, a , and the mass transfer coefficient, k_L . The presented studies showed that as the gas flow rate increase independent of the reactor/contactator type an increase in the k_La value is observed.

CHAPTER 3

METHODOLOGY

In order to meet the research objectives, a plug flow reactor/contactor design equipped with screen type static mixers will be employed to test and quantify the transfer rates of CO₂ into RO water. The method of analysis will be similar to that proposed by Kordač and Linek (2008) in addition to a new patented method that relies on measuring directly the dissolved CO₂ concentrations.

3.1. Experimental Setup

The experimental setup that was used in this investigation is shown in Figure 1. The aqueous phase was stored in a large tank, fed to the static mixer loop using a centrifugal pump (Pedrollo[®], model AL-RED 135m), and its flow rate measured using a paddle flow meter (King Instrument Company, model 7520, precision: ± 1.5 L/min). The desired flow of gas will be adjusted using two mass flow meters, one for low range gas flow rates ($Q_g \leq 8$ L/min) (Omega Engineering, model FMA 3811, precision: $\pm 4\%$) and the second one for larger range gas flow rates ($Q_g > 8$ L/min) (Omega Engineering, model FMA-A2417, precision: $\pm 4\%$). Pure CO₂ gas will be used to study the mass transfer characteristics of this setup.

Gas-liquid contacting will be conducted using a 25 mm inner diameter vertical pipeline whose mixing section will be 560 mm long. The vertical placement is chosen to eliminate the introduction of flow non-uniformities due to gravity. Stainless steel woven

wire mesh placed 33.5 and 70 mm apart will be used to enhance the mixing in the reactor/contacter. Samples will be collected from various points along the length of the reactor (e.g. before the entrance to the mixing section, inside the mixing section, and downstream from the mixing section).

The pressure at the inlet to the mixing section, as well as the pressure and temperature at the exit of the mixing section were measured using pressure transducers (Siemens Building Technologies, model QBE2002-P1 and QBE2002-P5, precision: ± 0.4 kPa), and all the information was collected using a data acquisition board (National Instruments, model NI USB-6218), and a specially developed LabVIEW[®] program.

Two physical techniques for measuring the volumetric mass transfer coefficient (namely, pH and direct CO₂ measurements) were selected in order to eliminate the influence of the reagents needed for the various chemical techniques on bubble breakage and coalescence rates. To determine the value of k_{LA} , the pH of the liquid entering the mixing section, and that in the flowing dispersion was measured using a pH probe (Adwa, model AD 131, precision ± 0.01 , and Omega Engineering, model PHTX-271-2P, precision: ± 0.03). In addition, a CO₂ analyzer (Anton Paar[®], model CarboQC At-line, precision: ± 40 mg/L) that uses direct methods to determine the concentration of absorbed CO₂ was also used. The obtained concentrations from the CO₂ analyzer will be used to further validate the concentrations of absorbed CO₂ calculated using the pH probe. Six sampling ports installed equidistantly along the length of the reactor were used to analyze the dissolution of carbon dioxide in the flowing mixture.

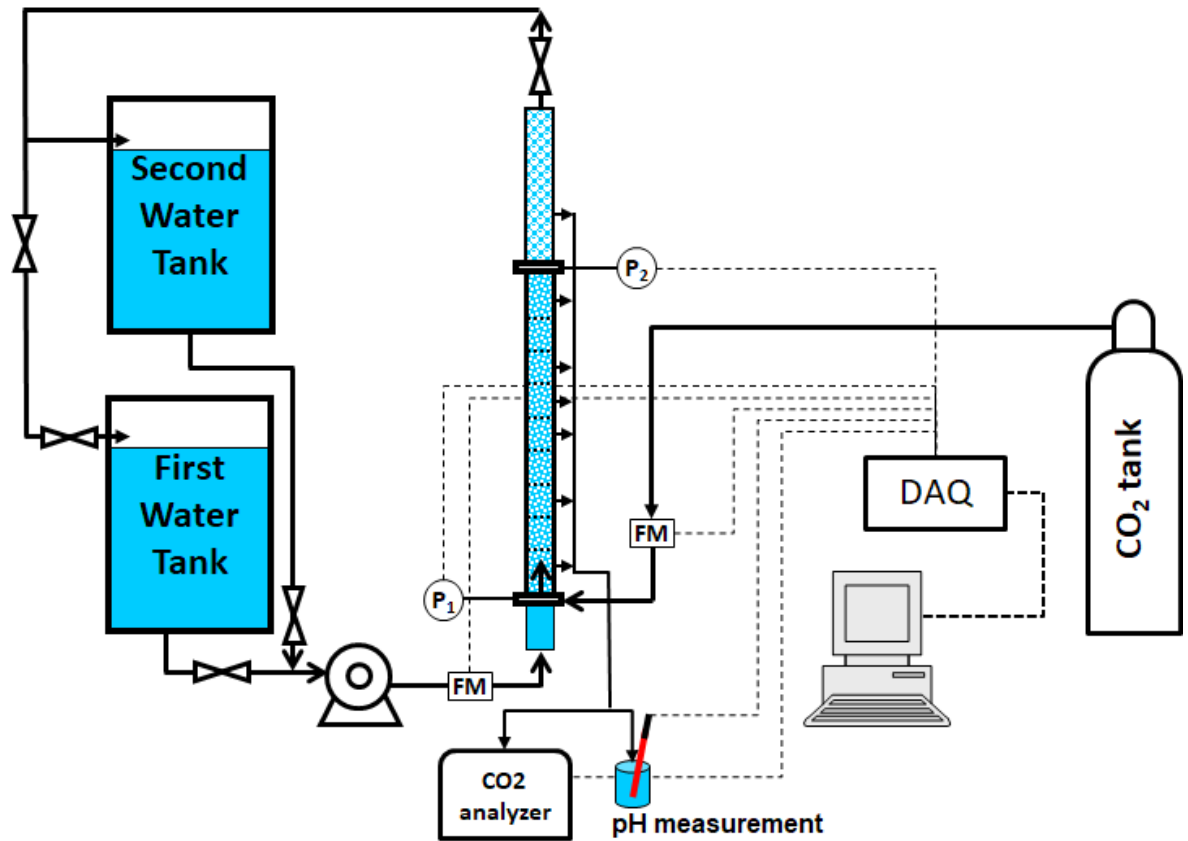


Figure 1: Schematic Representation of the Experimental Setup

Although the setup can operate in the recycle (continuous) mode, all the experiments in this investigation were conducted using a once through approach.

3.2. Screen-type static mixers

The screen-type static mixing elements that were used in this work are plain weave meshes that are generally characterized by their mesh size (M), wire diameter (b) and screen open area (α). These screens are also commonly referred to by their mesh number (Mn), which indicates the number of openings per inch. For example, a screen of mesh number, $Mn = 30$, indicates that the woven mesh has 30 openings per inch,

which indirectly implies the mesh size, M . Figure 2 shows a sketch of a screen element, and highlights its various geometric/design parameters.

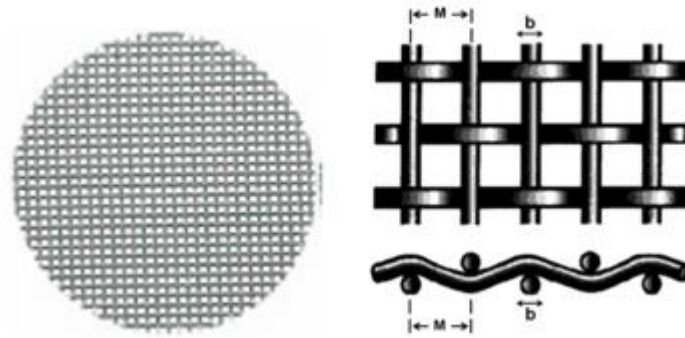


Figure 2: Screen Type Mixers

The percentage screen open area, α , of a screen is also inherently linked to the other design parameters according to Equation (1).

$$\alpha = \left(\frac{M - b}{M} \right)^2 \times 100 \quad (1)$$

Where M is the mesh size and b is the wire diameter.

In this investigation, screen-type static mixers (the characteristics of which are given in Table 1) were inserted in the column equidistantly from each other. The choice of using screens emanates from their ability to generate reasonably uniform hydrodynamic conditions over the entire cross-sectional area of the pipe with energy dissipation rates that change drastically within very short distances (Azizi and Al Taweel, 2011). In addition, they have been efficiently used to disperse liquid-liquid and gas-liquid flows

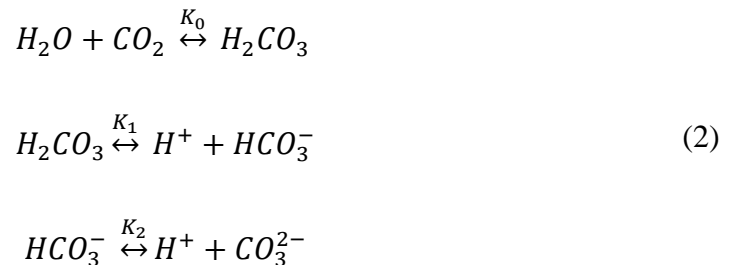
(Turunen and Haario 1994; Al Taweel et al., 2007; Munter, 2010; Azizi and Al Taweel, 2015) as well as intensify mass-transfer limited reactions (Al Taweel et al., 2013). In the current work, the effect of the screen geometry as well as the inter-screen spacing was investigated. For this reason, four different screen geometries were tested under two different reactor designs (i.e. inter-screen spacing). First, 8 screens were inserted at 70 mm inter-screen spacing, while in the second case, 16 screens were placed at a distance of 33.5 mm. This allows for a total mixing section length of 560 mm.

Table 1: Characteristics of the investigated stainless steel plain weave wire cloth

<i>Mesh Mn</i>	<i>Number,</i>	<i>Wire size, b (μm)</i>	<i>Mesh M (μm)</i>	<i>Size,</i>	<i>Open α (%)</i>	<i>Area,</i>
30		304.8	838.2		40.5	
50		228.6	508		30.25	
80		139.7	317.5		31.36	
100		114.3	254		30.25	

3.3. System investigated

The dissolution of CO₂ takes place via the following reactions (Hill, 2006; Kordac and Linek, 2008),



Where K_0 , K_1 and K_2 are the equilibrium constants and are known functions of temperature and salt concentrations.

The low value of the dissociation constant K_0 (7×10^{-7} M), implies that the concentration of dissolved CO_2 is by far greater than that of H_2CO_3 , and therefore the two components can be considered as one (Kordac and Linek, 2008). The equilibrium concentration of carbonic acid, H_2CO_3 , can then be inferred using Henry's constant, according to Equation (3).

$$[\text{H}_2\text{CO}_3]^* = P_{\text{CO}_2} \times H_{\text{CO}_2} \quad (3)$$

where P_{CO_2} is the partial pressure of CO_2 in atm, H_{CO_2} is Henry's law constant in $\text{mol} \cdot \text{atm}^{-1} \cdot \text{L}^{-1}$ and $[\text{H}_2\text{CO}_3]^*$ is the concentration of physically dissolved CO_2 in $\text{mol} \cdot \text{L}^{-1}$ in equilibrium with P_{CO_2} in the gas phase.

In the temperature range of $273 < T < 313$ K and the salinity range of $0 < S < 40$ g/kg, Henry's constant can be determined, according to Weiss (1974), using Equation (4).

$$\begin{aligned} \ln H_{\text{CO}_2} = & -60.24 + 93.45 \left(\frac{100}{T} \right) + 23.36 \ln \left(\frac{T}{100} \right) \\ & + S \left[0.0235 - 0.0236 \left(\frac{T}{100} \right) + 0.0047 \left(\frac{T}{100} \right)^2 \right] \end{aligned} \quad (4)$$

Furthermore, the dissociation constants K_1 and K_2 are in $\text{mol} \cdot \text{L}^{-1}$ and are defined as follows,

$$K_1 = \frac{[\text{H}^+][\text{HCO}_3^-]}{[\text{H}_2\text{CO}_3]} \quad (5)$$

$$K_2 = \frac{[H^+][CO_3^{2-}]}{[HCO_3^-]} \quad (6)$$

From these expressions, the values of the various species can be deduced especially that K_1 and K_2 can be easily calculated since they are known functions of temperature and salinity. For example, according to Millero (1995), and for RO water, K_1 can be expressed as,

$$\begin{aligned} \ln K_1 = & 290.9097 - \frac{14554.21}{T} - 45.0575 \ln T \\ & + \left(-228.39774 + \frac{9714.36839}{T} + 34.485796 \ln T \right) S^{0.5} \\ & + \left(54.20871 - \frac{2310.48919}{T} - 8.19515 \ln T \right) S \\ & + \left(-3.969101 + \frac{170.22169}{T} + 0.603627 \ln T \right) S^{1.5} \\ & - 0.00258768S^2 \end{aligned} \quad (7)$$

Where T is the temperature in K, and S is the salinity in $\text{g}\cdot\text{kg}^{-1}$. Other relationships that apply for various types of water with varying degrees of salinity and alkalinity can be found, summarized, in Al-Hindi and Azizi (2017).

In order to quantify the mass transfer performance of the current reactor, various operating and design conditions will be tested. These are summarized in Table 2.

Table 2: Data Representing the Experimental Conditions

Condition	Value
Pipe diameter (mm)	25
Number of screen elements	8 and 16
Inter screen spacing (mm)	33.5 and 70
Screen open area (%)	30.25 – 40.5
Liquid superficial velocity (m/s)	0.7 – 1.8
Dispersed phase holdup (%)	10, 20 and 30
Pipe Reynolds number	19,600 – 44,800
Residence time (s)	0.35 – 0.7

3.4. Method of Analysis

The performance of the reactor at hand will be evaluated based on the achievable rates of mass transfer as well as the required energy to achieve them. The following sections will therefore highlight the various methods and equations used to evaluate these two major parameters.

3.4.1. Volumetric Mass Transfer Coefficient, k_La

The calculation of the volumetric mass transfer coefficient is the primary parameter for evaluating the efficiency of the reactor. For this reason, tracking the amount of dissolved CO₂ in the water becomes of utmost importance. Several methods are available for this purpose. They rely on either pH, electrical conductivity or direct CO₂ measurements. In this work, two techniques were employed, namely, pH measurements and direct CO₂ measurements based on the patented multiple volume expansion method.

These two techniques will be highlighted in the subsections that follow to delineate how the concentration of dissolved CO₂ is calculated.

Knowledge of temporal change of [H₂CO₃] (also denoted as C_{H₂CO₃}) along the reactor will be used to calculate the volumetric mass transfer coefficient, *k_{LA}*, following the method proposed by Kordač and Linek (2008). According to these authors, carbon dioxide is physically absorbed and undergoes a fast reversible reaction, according to Equation (2), that maintains the bulk concentrations of carbonic acid, bicarbonate ion, and hydrogen ion in equilibrium. Assuming an ideal mixing of the gas phase and a negligible mass transfer resistance in the gas phase, the authors related the value of *k_{LA}* to the temporal change of [H₂CO₃] according to the following equation,

$$\frac{dc_{H_2CO_3}}{dt} = k_{LA} \frac{A}{1 + A} [(C_{H_2CO_3})^* - C_{H_2CO_3}] \times \left[\frac{2}{2 + (K_1/c_{H_2CO_3})^{0.5}} \right] \quad (8)$$

where,

$$A = \frac{Q_G}{k_{LA} V_L R T H_{CO_2}} \quad (9)$$

Measuring the concentration of H₂CO₃ along the length of the reactor and numerically solving for the value of *k_{LA}* that satisfies the equation for all measurements will help determine the value of the volumetric mass transfer coefficient, *k_{LA}*. To measure this change in concentration, two techniques were adopted in the current work, namely, pH, and direct dissolved CO₂ measurements. These methods are highlighted in the following sections.

3.4.1.1. pH Measurements

The equilibrium concentrations of carbon dioxide, carbonic acid, bicarbonate ion, and carbonate ion are functions of the local pH. The dissolution of CO₂ results in a change of pH in the reactor, the extent of which is linked to the rate of mass transfer in the reactor (Nieves-Remacha et al., 2013). The change in pH emanates from the fact that carbonic acid and bicarbonate ions dissolve reversibly to give hydrogen ions in the water.

According to Kordač and Linek (2008), who used a pH meter to track the dissolution of CO₂ in water in a stirred tank reactor, and from Equation (5), the concentration of carbonic acid can be calculated as,

$$[H_2CO_3] = [CO_2] = \frac{[H^+][HCO_3^-]}{K_1} \quad (10)$$

For solutions where pH is less than 6, the solution becomes acidic, rendering negligible the concentration of the hydroxide ion. In addition, the concentration of carbonate ions (CO₃²⁻) also becomes insignificant. Thus, according to the principle of electroneutrality, it can be deduced that the concentration of hydrogen and bicarbonate ions are equal (Kordac and Linek, 2008), where the former can be directly calculated from pH measurements according to Equation (12).

$$[H^+] = [HCO_3^-] \quad (11)$$

$$[H^+] = 10^{-pH} \quad (12)$$

As a result, Equation (10) can be re-written as,

$$[H_2CO_3] = [CO_2] = \frac{10^{-2pH}}{K_1} \quad (13)$$

Equation 13 can be re-written for pH as shown below:

$$pH = -\frac{1}{2} \log(K_1 \times [CO_2]) \quad (14)$$

3.4.1.2. CO₂ Direct Measurements

The multiple volume expansion method (MVE) is a patented technique by Anton Paar® (US Patent 6,874,351), to determine the dissolved CO₂ content without the influence of other gases, namely, O₂ and N₂. Originally developed to measure the CO₂ content in beverage samples, this method is deemed accurate and the analysis is based on absolute temperature and pressure measurements.

It relies on measuring the equilibrium temperature and pressure of a liquid sample after expanding its volume. The measurement is performed twice during which expansion to a pre-specified value (larger than 1) is performed and the CO₂ content of the sample is calculated by solving a system of equations.

When expanding the volume of the measuring chamber, the partial pressure of air decreases much more than that of CO₂ due to the difference in the solubility of air and CO₂. When equilibrium is attained at the first and second volume expansions, the resulted pressure and temperature are measured. The difference between the pressures

measured at the two volume expansions is used to calculate the amount of dissolved air and CO₂ in the liquid.

To calculate the gas content, solubility and saturation pressures, Henry's and Boyle's laws are applied to obtain the partial pressure in the gas phase using the following equation (Bloder et al., 2005):

$$p' = \frac{p_o}{\left(1 + \frac{k}{K_s \times p_s}\right)} \quad (15)$$

The measured pressure, which represents the equilibrium pressure, is the sum of the partial pressure of the gases in the sample.

$$p_i = p'X + p'Y \quad (16)$$

From the measured equilibrium pressures p_1 and p_2 corresponding to volume increases k_1 and k_2 , and by knowing the solubilities $K_s(X)$ and $K_s(Y)$ of the two dissolved gases, the original saturation pressures p_oX and p_oY (e.g. p_oCO_2 and p_oN_2) can be calculated by solving the system of equations represented below (Bloder et al., 2005).

$$p_1 = \frac{p_oX}{1 + \frac{k_1}{K_s(X) \times p_s}} + \frac{p_oY}{1 + \frac{k_1}{K_s(Y) \times p_s}} \quad (17)$$

$$p_2 = \frac{p_oX}{1 + \frac{k_2}{K_s(X) \times p_s}} + \frac{p_oY}{1 + \frac{k_2}{K_s(Y) \times p_s}} \quad (18)$$

To obtain the gas content in the liquid sample, the saturation pressures p_oX and p_oY are multiplied by the respective gas solubility $K_s(X)$ and $K_s(Y)$.

If only one gas is dissolved in the liquid, then the saturation pressure and the solubility can be determined from the measured pressures p_1 and p_2 according to the following equations (Bloder et al., 2005).

$$K_s(X) = \frac{(p_1 \times k_1 - p_2 \times k_2)}{\frac{(p_2 - p_1)}{p_s}} \quad (19)$$

$$p_oX = \frac{p_1 \times (1 + k_1)}{K_s(X) \times p_s} \quad (20)$$

Where X represents the dissolved species such as CO_2

One main advantage of this method is that it eliminates the influence of dissolved residual gas (i.e. air or nitrogen) on the final measurement. This is accomplished by the fact that the pressure for the larger volume expansion is lower than that for the smaller volume expansion, with the difference between the two being used to calculate the correction value to eliminate the influence of dissolved residual gas. The partial pressure of CO_2 in the sample is then converted to concentration using Henry's law.

3.5. Energy Dissipation and Power Consumption

Power consumption is one of the most important design criteria since it determines the economic desirability and viability of the reactor/contactator. Several methods to quantify the power consumption exist, for example, pressure drop, power per unit volume, energy dissipation rate. The latter parameter is of utmost importance as it directly affects the rates of breakage and coalescence and therefore the bubble size distribution

of the flowing dispersion. In the reactor at hand, three main factors contribute to the overall pressure drop in the system, namely,

- Pressure drop due to skin friction at the reactor wall
- Pressure drop due to the difference in the static head caused by the vertical orientation of the mixer
- Pressure drop caused due to the blockage of flow by the screen mixers

These factors are, in turn, affected by several operational and design parameters such as the length of the reactor, number of screens, liquid and gas flowrates, and screen geometry (Azizi and Al Taweel, 2015). Under the turbulent flow conditions encountered in the current study, the pressure drop due to the screens is expected to dominate the other energy sinks.

To characterize the average hydrodynamic conditions in multiphase systems, the volume average turbulent energy dissipation rate per unit mass was calculated using the measured pressure drop values as shown in the following expression (Azizi and Al Taweel, 2015):

$$\varepsilon = \frac{Q_L \Delta P}{1000 \times \rho_L V_L} = \frac{U_L \Delta P}{\rho_L L (1 - \phi/100)} \quad (21)$$

Other approaches and parameters can be considered to characterize the energy requirement to achieve good gas-liquid contacting. These parameters were discussed at length by Azizi and Al Taweel (2015), and the reader is referred to their work. These

parameters include the energy consumption in the reactor (in W), energy dissipation per unit volume (in W/m³), or the energy dissipation per unit mass (in W/kg).

However, the aforementioned parameters may present a distorted large value that undermines the benefits of using a static mixer because they do not factor the residence time requirements for various mixer types, a factor that significantly affect power consumption. To overcome this, several previous studies used the concept of energy needed to process a unit of the flowing mixture, E_{spm} , (Koglin et al; Azizi and Al Taweel, Al Taweel and Walker) because it allows the comparison between several types of reactors with varying mixing times.

$$E_{spm} = \frac{E}{V \cdot \rho_{mix}} \times t = \frac{\Delta P \cdot (Q_L + Q_G)}{V \cdot \rho_{mix}} \times t \quad (28)$$

CHAPTER 4

RESULTS AND DISCUSSION

In the current work, the effect of varying the operating conditions as well as the reactor configuration on the rate of CO₂ absorption into RO water were investigated. Pressure drop measurements as well as the energy required to operate the reactor will be presented in the following sections in addition to the effect of the operating conditions on the final results.

4.1. Pressure Drop Measurements

Pressure drop is an important criterion in determining the energy dissipation rate inside the reactor as well as its power requirements. In addition, knowledge of the local pressure is vital in determining the partial pressure of CO₂ and hence the concentration driving force needed for the quantification of the mass transfer coefficient. In the current work, pressure drop measurements were conducted for four different screen geometries used in two distinct reactor designs ($L = 33.5$ mm and $L = 70$ mm) under various operating conditions.

Pressure drop across the screens is caused by the contribution of both viscous and inertial resistances. However, at high superficial liquid velocities, inertial forces dominate whereas viscous forces are dominant in the laminar flow regime. The pressure losses are due to the turbulent vortices associated to the sudden expansion and contraction caused by the existing screens across the flow in the reactor (Azizi and Al

Taweel, 2011). The pressure drop is therefore expected to be a direct function of the screen geometry where smaller screen openings exhibit larger pressure drops. However, regardless of the screen geometry, the pressure drop per screen is expected to increase with an increase in the flow rate. In the current work, it was found that ΔP increased with the pipe Reynolds number as shown in Figure 3a, however, screens with $Mn = 80$ rendered the highest pressure drop values despite having an open area slightly larger than that of $Mn = 100$. But, the pipe Reynolds number might not always reflect the true hydrodynamics of screen-type static mixers, hence, using different characteristic lengths in calculating Re might be required to better reflect the situation (Azizi and Abou Hweij, 2017). This is clearly demonstrated in Figure 3b where the pressure drop per screen was plotted against the wire Reynolds number. Under these conditions and as expected, screens with $Mn = 100$ showed the largest pressure drop.

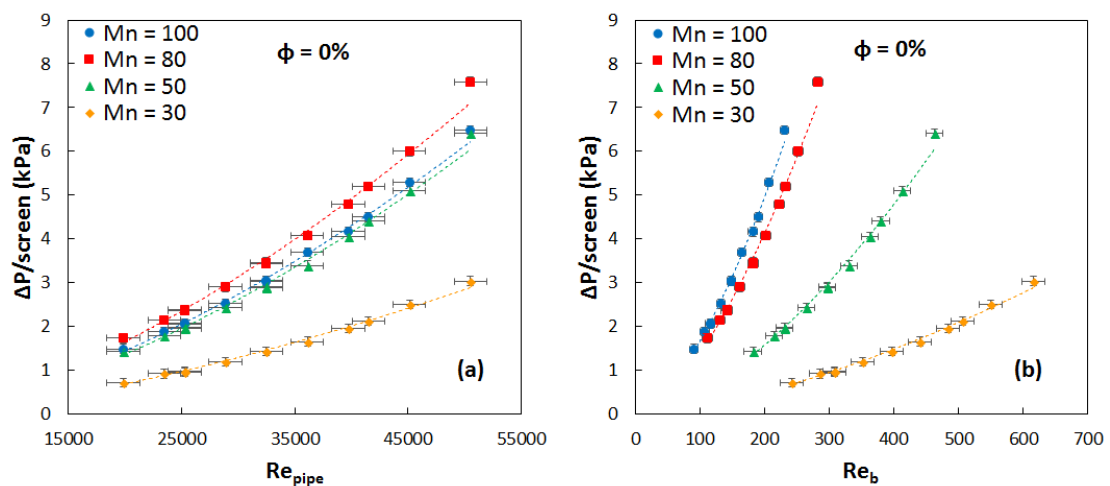


Figure 3: Pressure drop for four different screen geometries versus: (a) Empty pipe Reynolds number, Re_{pipe} and (b) Wire Reynolds number, Re_b

The pressure drop was also measured for two-phase gas-liquid flows. Under these conditions, and as can be seen from Figure 4a, the pressure drop was found to decrease with an increase in the gas holdup for the same total superficial gas velocity. This can be explained by a reduced dispersion density and the consequent reduction in the kinetic energy of the microjets formed by the screen (Azizi and Al Taweel, 2011). Another factor that might contribute to this reduction in pressure drop is the reduced drag coefficient of screens in the presence of fine bubbles in a two-phase pipe flow (Azizi and Al Taweel, 2015, 2011). However, when plotted against the liquid phase velocity it can be seen that the gas phase did not cause any changes in the value of the pressure drop (Figure 4b). This is in-line with the results obtained by Azizi and Al Taweel (2015) who found that the pressure drop is independent of the gas-phase flow rate and can be correlated against the liquid flow rate only. Plots for other meshes ($Mn = 30, 50$ and 100) are presented in Appendix I (Figure 15 and 16).

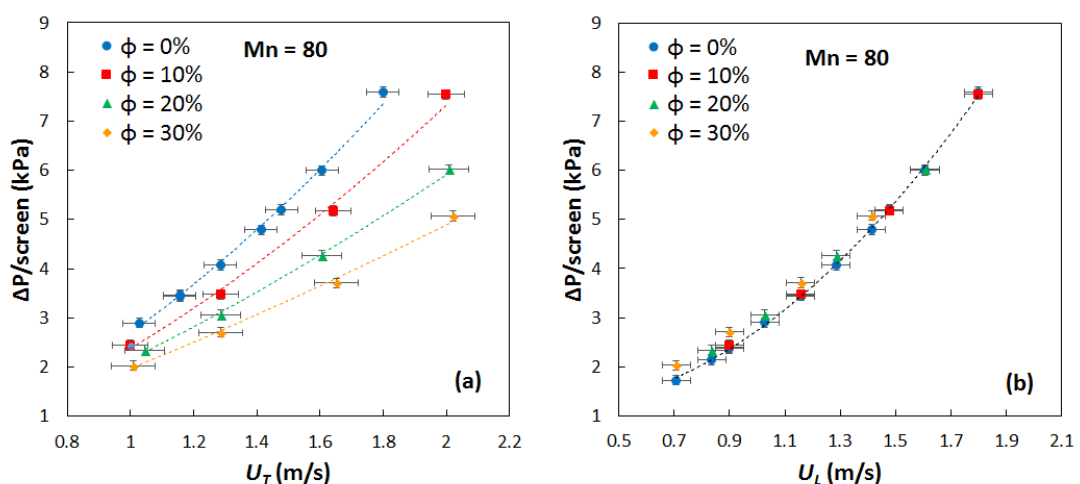


Figure 4: Effect of gas holdup on the pressure per screen: (a) pressure drop versus superficial velocity of gas – liquid mixture and (b) pressure drop versus liquid velocity

4.2. pH and CO₂ Analyzer Measurements

The dissolution of CO₂ in water leads to the formation of carbonic acid and bicarbonate ions which in turn dissolve reversibly to form hydrogen ions in water. The presence of hydrogen ions in water cause a decrease in pH value of water. Thus, monitoring the variation of pH is a good indicator of the amount of dissolved CO₂ in water. In the current work, six pH measurements were taken along the length of the reactor equidistantly and their variation along the reactor are represented in Figure 5a for a model case. It should be noted that pH at point zero represents the pH of water before the injection of CO₂ gas. It can be clearly discerned that a sudden decrease in pH takes place initially due to the introduction of CO₂ gas to the liquid phase stream which keeps on decreasing until a pseudo-steady state is reached. This condition is reached only under certain operating conditions. In this work, steady state was considered to be attained when the change between two consecutive pH measurements is less than 1%. For the conditions presented in Figure 5a, steady state was reached at the 4th pH measurement. Similar trends (decreasing pH) were obtained for all the operating conditions investigated in the current work and this is in line with all the data from the literature (Al-Hindi and Azizi, 2017; Hill, 2006; Kordac and Linek, 2008; Nieves-Remacha et al., 2013). The raw pH measurements are presented in Appendix II.

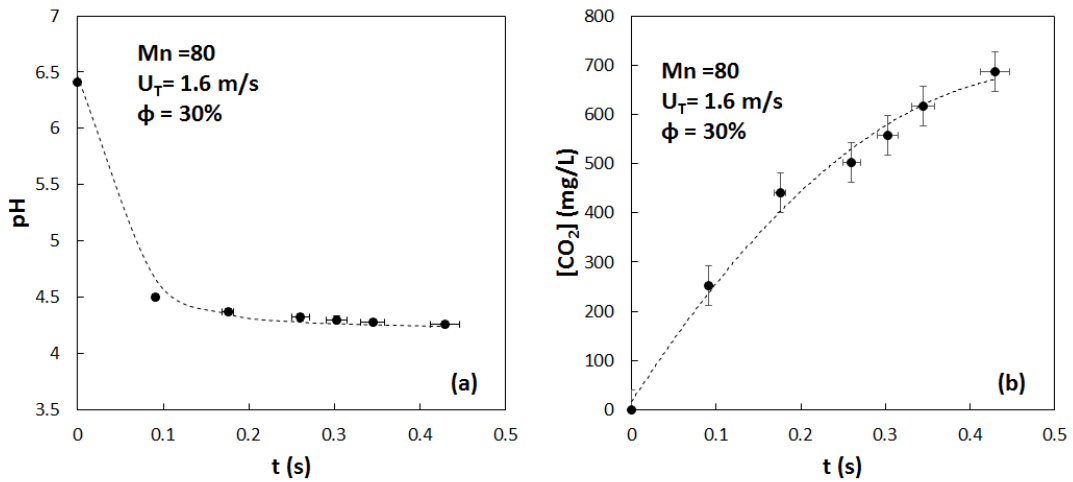


Figure 5: Raw data measurements versus residence time: (a) pH and (b) CO_2 concentrations

Alternatively, another method was employed in the current work to track the amount of dissolved CO_2 in water and validate the results obtained from pH measurements. This technique consisted of direct CO_2 concentration measurements using a CO_2 analyzer. These measurements took place simultaneously with pH measurements as highlighted in the previous Experimental Setup section. A sample measurement of CO_2 concentrations, obtained in mg/L, are plotted against the residence time in the reactor in Figure 5b. The trend shows that the CO_2 concentration increases rapidly across the reactor with the slope slowing down at large residence times. The CO_2 concentration at time zero represents that of pure water before the injection of CO_2 . The raw CO_2 concentration measurements are presented in Appendix II.

To validate the CO_2 measurements, it was decided to use the CO_2 analyzer data to calculate the equivalent pH and compare them to pH measurements and simultaneously calculate the CO_2 concentrations from pH data and compare them to the analyzer

measurements. This was performed for all the measurements obtained using a screen with $Mn = 50$ and $L = 70$ mm. The plot of pH values (pH meter and CO₂ analyzer) are shown in Figure 6a while that of CO₂ concentrations is shown in Figure 6b. First, it was observed that the CO₂ analyzer measured larger CO₂ concentrations which correspond to lower pH values. While Figure 6b shows a substantial difference between the CO₂ concentration values, the difference in pH measurements ranged between 2 and 10% for all screen geometries. This clearly shows that a small pH variation can induce a significant change in CO₂ concentrations. Therefore, the difference between measurement techniques was considered a systematic error in both the pH meter and CO₂ analyzer. These systematic errors typically result from calibration, hysteresis and nonlinearity in the instrument response. It should be noted that the precision error associated with the pH meter resulted in a 15% error propagation in the CO₂ concentrations whereas the precision error associated with the CO₂ analyzer resulted in an error of 0.5%. This indicates that direct CO₂ measurements could be a more accurate method than pH measurements.

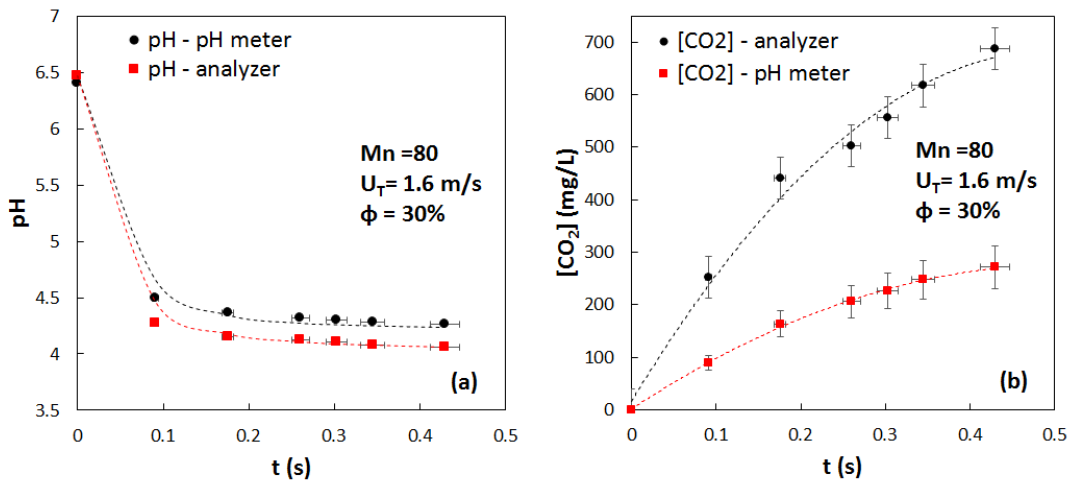


Figure 6: Comparing the measured and calculated data versus residence time: (a) measured and calculated pH (b) measured and calculated CO_2 concentrations

4.3. Volumetric Mass Transfer Coefficient

The volumetric mass transfer coefficient is considered the most important criterion in characterizing mass transfer operations in multiphase reactors/contactors. To obtain k_{LA} , the concentration of dissolved CO_2 should be first determined. As previously mentioned, two measurement techniques were employed (pH and CO_2 analyzer) where each method resulted in a different CO_2 concentration which would consequently render a different k_{LA} value. Figure 7a-d clearly show the k_{LA} values obtained from pH and CO_2 analyzer for four different screen geometries at different operating conditions. It is evident that k_{LA} from CO_2 analyzer is consistently greater than that obtained using pH measurements. This is attributed to the aforementioned difference in measurements (Figure 6). It is also clear from Figure 7 that the errors on k_{LA} associated to the precision error of CO_2 analyzer can reach much higher values than the ones associated to the

precision error of pH. However, to minimize the errors, it was decided to use an arithmetic average k_{LA} (from both measurement techniques) and be used throughout the study. The remaining figures for other operating and design conditions are shown in Appendix I (Figure 17, 18, 19, 20, 21 and 22).

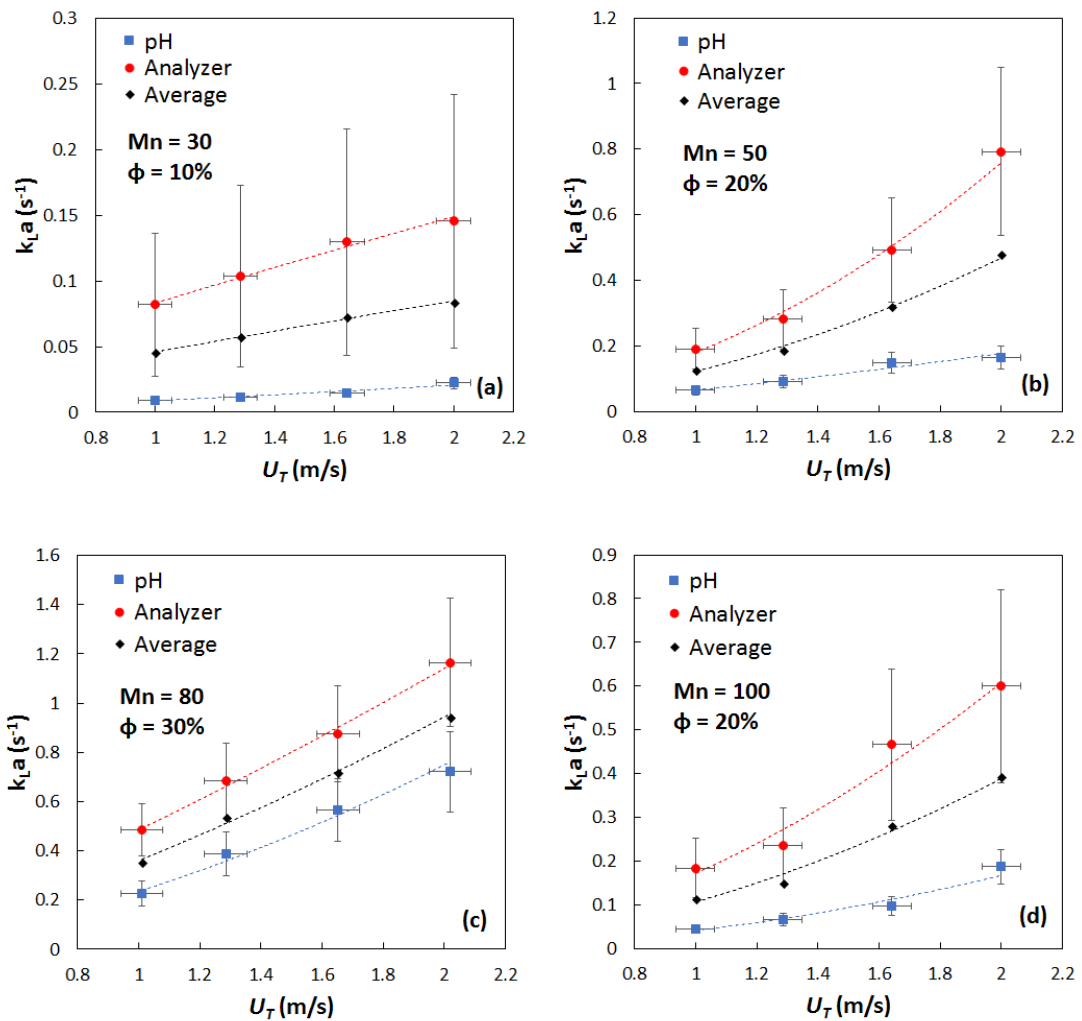


Figure 7: k_{LA} from pH, CO₂ analyzer and k_{LA} average versus total superficial velocity ($L = 70$ mm): (a) Mesh 30, $\phi = 10\%$, (b) Mesh 50, $\phi = 20\%$, (c) Mesh 80, $\phi = 30\%$ and (d) Mesh 100, $\phi = 30\%$

4.3.1. Effect of liquid flow rate

The liquid flow rate controls the residence time in the reactor as well as the extent of the turbulence generated within the mixer and its dissipation rate (Al Taweel et al., 2005).

An increase in the superficial liquid velocity therefore reduces the residence time however it increases the pressure drop and the average turbulent energy dissipation rate throughout the reactor/contactors (Azizi and Al Taweel, 2015). As a multiphase flow passes through screen-type static mixers, bubble breakage becomes dominant and hence a larger interfacial area of contact between the phases is generated. This typically leads to enhanced mass transfer and thus larger values of k_{La} (Azizi and Al Taweel, 2007; Turunen and Haario, 1994; Alves et al., 2004; Lezhnin et al., 2003; Moucha et al., 2012). The variation of k_{La} with total superficial velocity for all four screen geometries ($L = 70$ mm and $L = 33.5$ mm) are shown in Figure 8 and 9. It is evident that highest k_{La} values are obtained at the highest liquid flow rates for any gas holdup with values ranging between 0.006 and 1.01 s⁻¹.

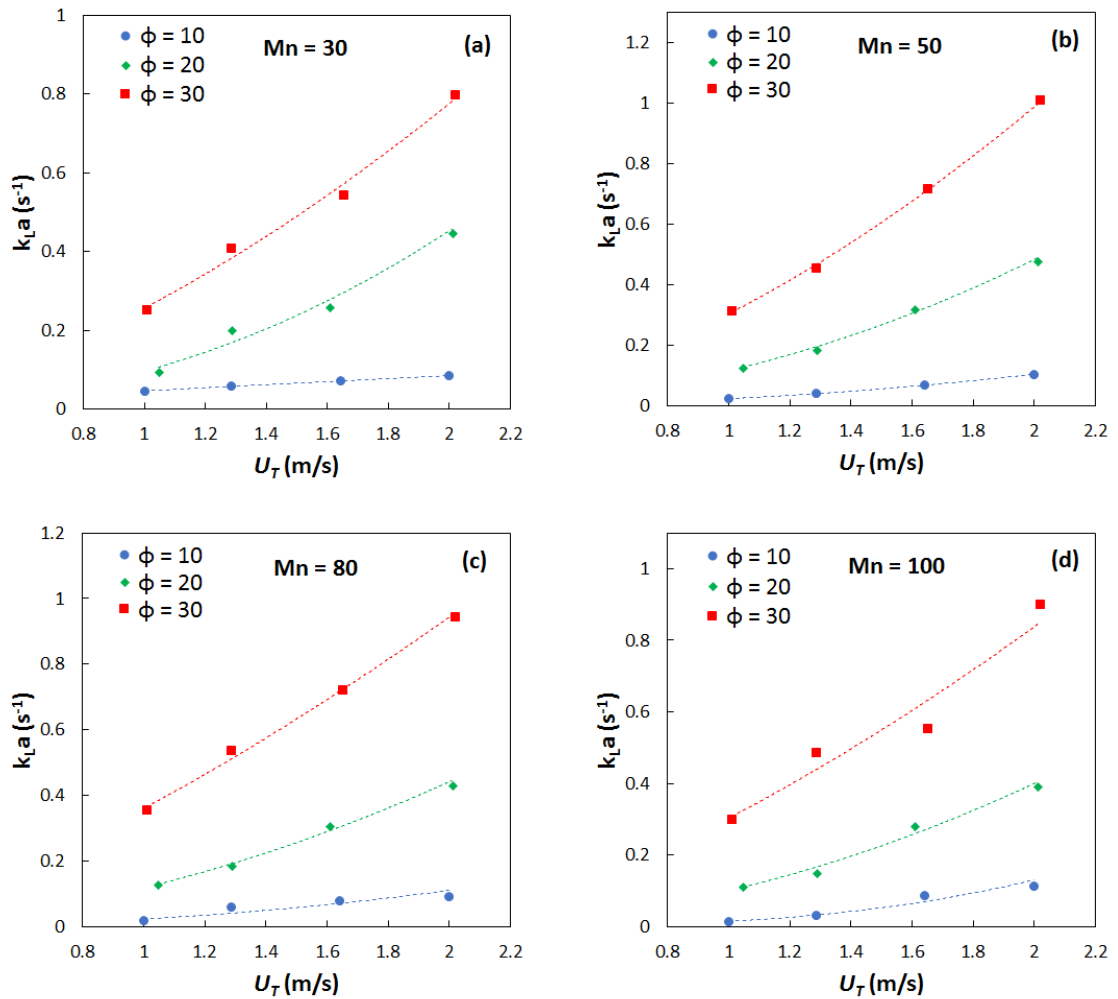


Figure 8: Effect of Superficial velocity and gas holdup on k_{La} ($L = 70$ mm): (a) Mesh 30, (b) Mesh 50, (c) Mesh 80 and (d) Mesh 100

4.3.2. Effect of gas holdup

An increase in the gas-liquid flow ratio typically increases the mean bubble diameter due to the increase in the bubble population density and the subsequent increase in the coalescence rate. However, the impact of increasing the gas holdup on the volumetric mass transfer coefficient k_{La} depends on the balance between the values of both k_L and

a , independently (Al Taweel et al., 2013; Azizi and Al Taweel, 2015). In the current work, the effect of the gas holdup on the volumetric mass transfer coefficient is clearly shown in Figure 8 and 9. It is evident that k_{LA} increases with an increase in gas holdup. It should be noted that the highest k_{LA} values were achieved at the highest gas holdups ($\phi = 30\%$) and the obtained results are in-line with several other investigators (Azizi and Al Taweel, 2015; Nieves-Remacha et al., 2013) who reported similar trends.

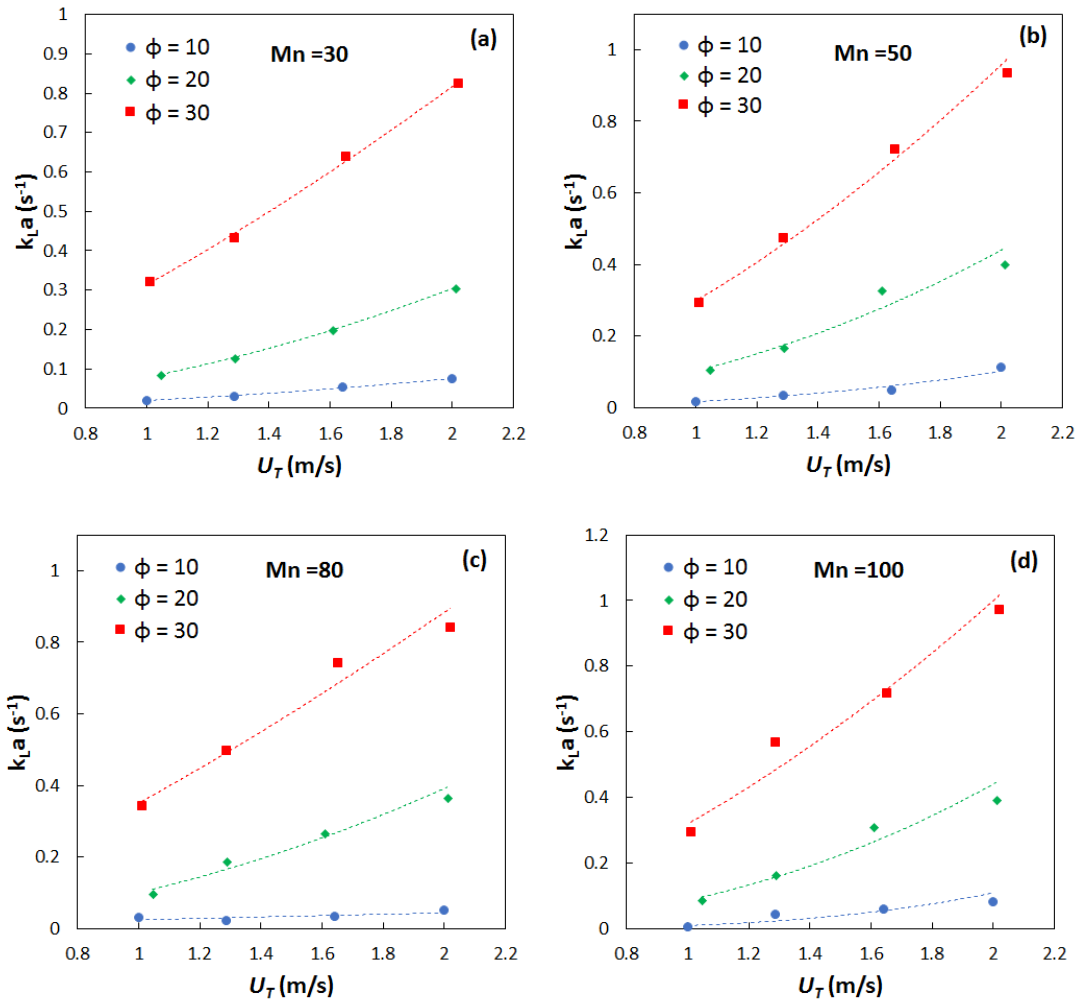


Figure 9: Effect of superficial velocity and gas holdup on k_{LA} ($L = 33.5$ mm): (a) Mesh 30, (b) Mesh 50, (c) Mesh 80, (d) Mesh 100

4.4. Effect of Reynolds number

When dealing with screen-type static mixers, the characteristic length of the Reynolds number is critical in highlighting the effect of the screen geometry on the measured results. This was clearly highlighted by Abou Hweij and Azizi (2015) and Azizi and Abou Hweij (2017) who studied the residence time distribution in single and two-phase

flows through screen mixers. Similarly, and in order to delineate the effect of screen geometry on k_{LA} , the results were plotted against various variants of Re, namely, the empty pipe Reynolds number, Re_{pipe} , the wire Reynolds number, Re_b , the mesh Reynolds number, Re_M , the individual-jet Reynolds number, Re_j , and the macroscopic jet Reynolds number, Re_{jet} . When plotted against the empty pipe Reynolds number (Figure 10a and Figure 11a) it can be seen that the results obtained for the four different screen geometries at the largest gas holdup, are relatively close to each other and it is very hard to distinguish the effect of the screen geometry. However, when using a different characteristic length for calculating Re, different trends can be discerned (Figure 10b-e and Figure 11b-e). For example, when using the wire diameter or the mesh size as the characteristic length, plotting k_{LA} values against Re_b or Re_M clearly shows that the smaller the wire or the mesh size is, the larger the value of k_{LA} will be. Similarly, when using the hydraulic diameter of the individual jet as the characteristic length to obtain Re_j a similar trend is observed, where higher k_{LA} values are observed for the finer screens. However, an opposite trend is observed when utilizing the macroscopic jet Reynolds number, Re_{jet} , which is equivalent to the empty pipe Re divided by the screen open area. It was found that the smaller the screen open area, the larger the value of Re_{jet} . The results for the remaining operating and design condition are presented in Appendix I (Figure 23, 24, 25 and 26).

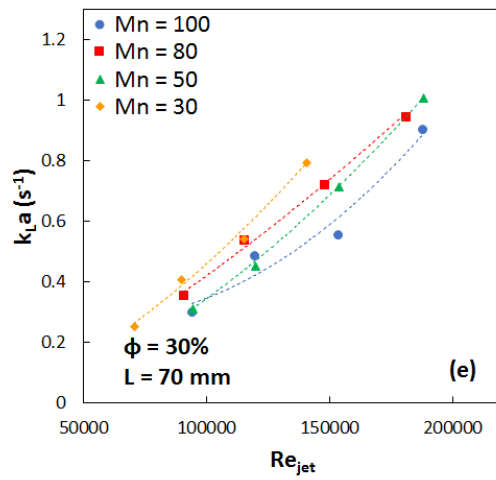
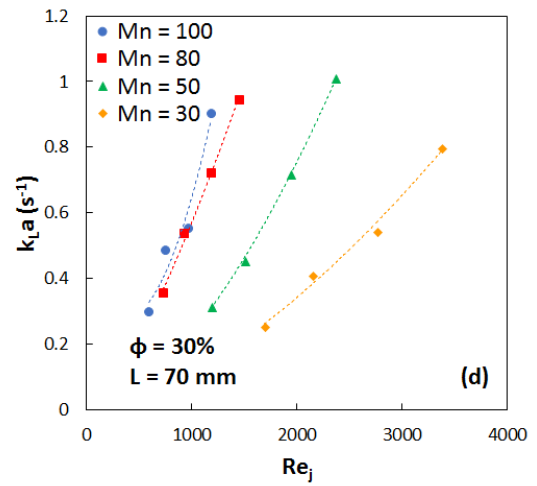
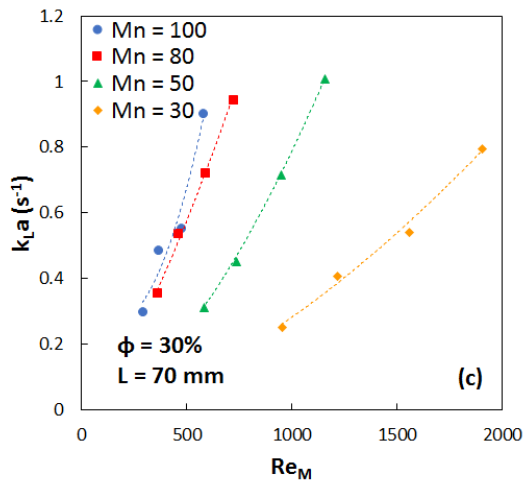
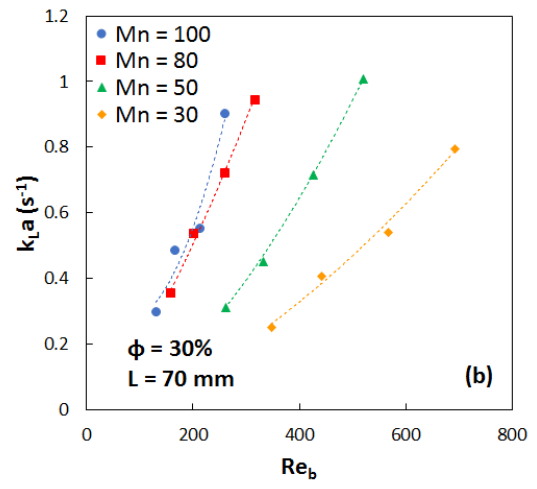
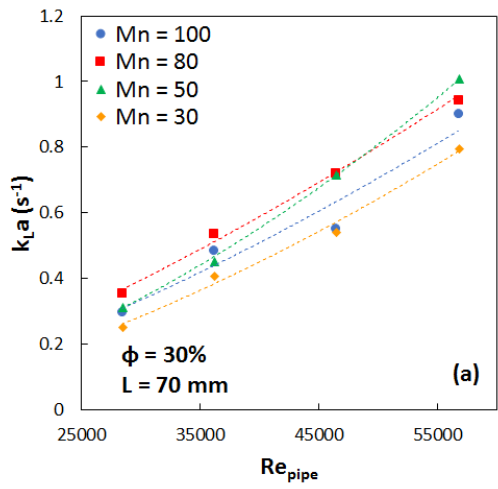


Figure 10: The variation of k_{La} with Reynolds number for all four screen geometries ($L = 70$ mm): (a) Re , (b) Re_b , (c) Re_M , (d) Re_j and (e) Re_{jet}

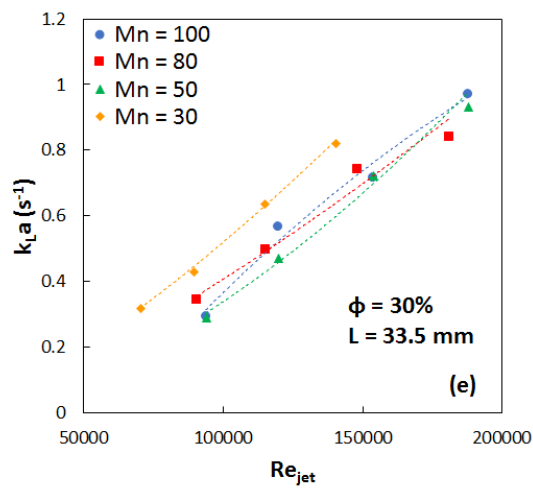
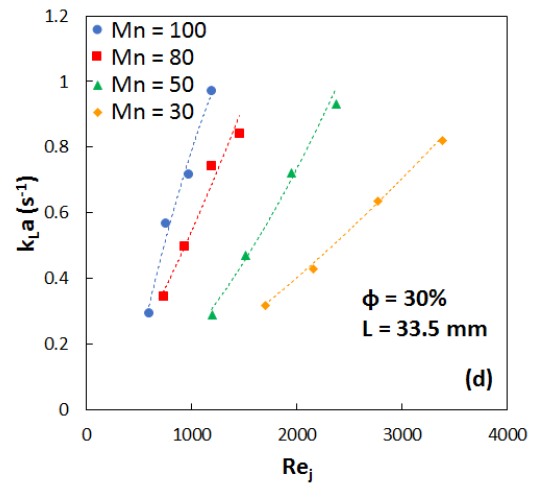
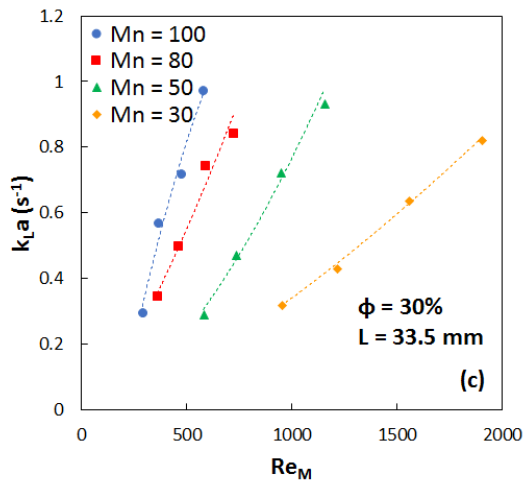
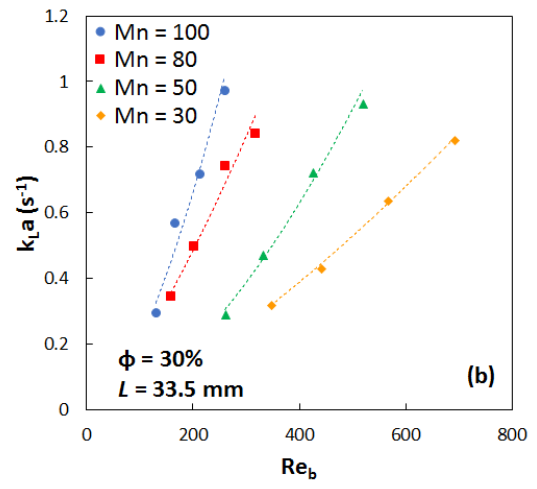
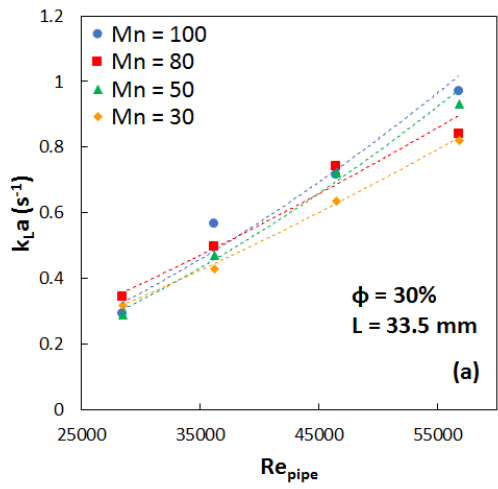


Figure 11: The variation of k_{LA} with Reynolds number for all four screen geometries ($L = 33.5$ mm): (a) Re , (b) Re_b , (c) Re_M , (d) Re_j and (e) Re_{jet}

4.5. Energy requirements

An indicator of the economic feasibility of a process is the energy required to operate it. A good indicator that addresses the concerns of mixing equipment users rather than designers is the energy needed to process a unit of the flow mixture, E_{spm} . This concept was first applied by Koglin et al. (1981) then applied by Al Taweel and Walker (1983), Al Taweel et al. (2005) and Azizi and Al Taweel (2015). The specific energy consumption per unit mass of liquid treated, E_{spm} , is highly dependent on the pressure drop and the gas and liquid flow rates. Because the total superficial velocity and gas holdup have a positive effect on k_{LA} , similar trends were obtained when plotting k_{LA} versus E_{spm} for the two reactor designs as depicted in Figure 12 and Figure 13.

Providing larger power inputs to the system enhanced the overall mass transfer for all investigated conditions. The highest E_{spm} values occurred at low gas holdup ($\phi = 10\%$) and high total superficial velocity ($U_T = 2$ m/s), which is in line with the findings of Azizi and Al Taweel (2015) who found a decrease in E_{spm} with an increase in the dispersed phase holdup. This behaviour was attributed to the reduction in the total pressure drop with increasing ϕ as well as the shorter residence times associated with larger total superficial velocities (Azizi and Al Taweel, 2015). Furthermore, the E_{spm} values at $L = 33.5$ mm (0.005 – 0.037 kWh/tonne) were found to be double those at the larger inter-screen spacing of $L = 70$ mm (0.002 – 0.019 kWh/tonne). This is due to the fact that a larger number of screen mixers is inserted to the reactor which consequently

leads to a larger pressure drop. Although the specific energy consumption was doubled, no significant increase in k_{LA} was observed between these two reactor designs.

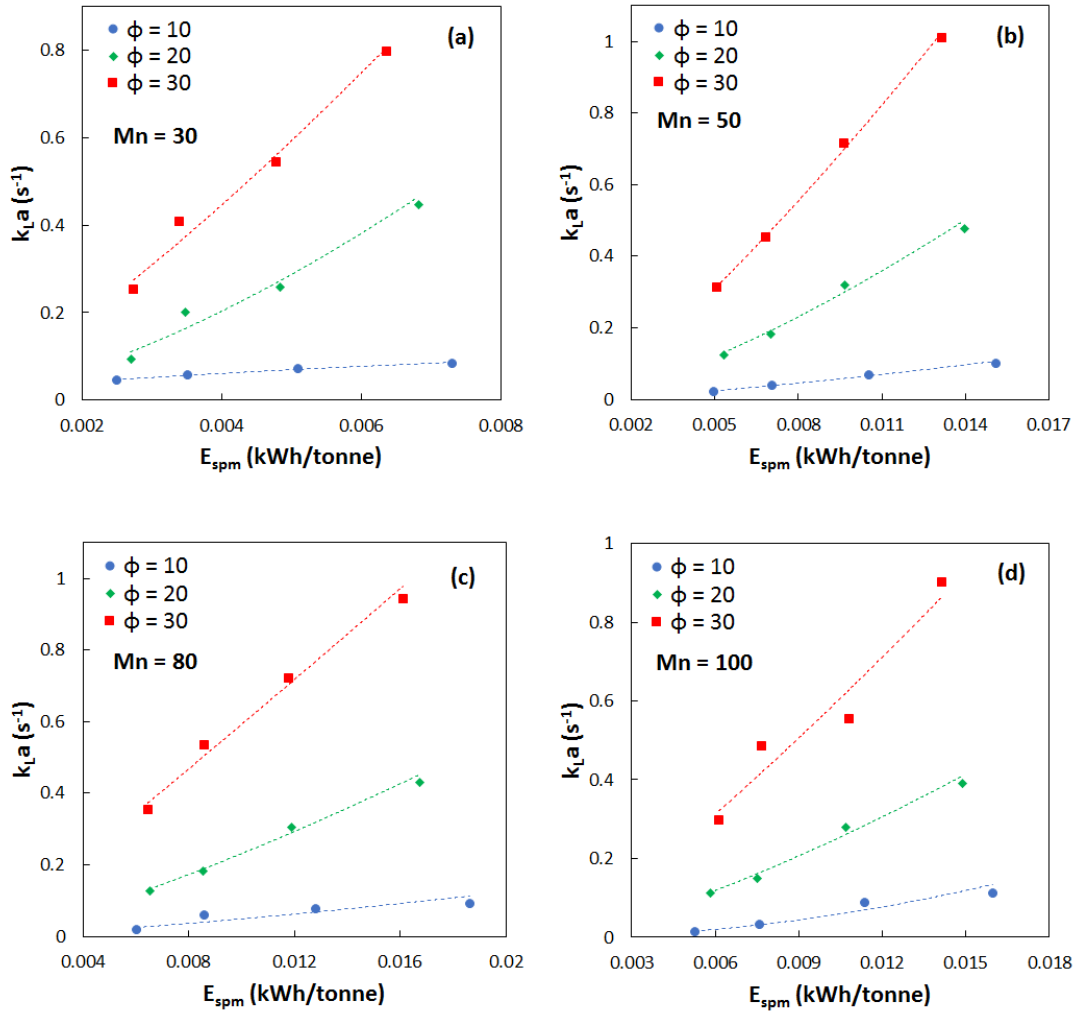


Figure 12: k_{LA} versus the energy needed to process a unit of the flowing mixture, E_{spm} , ($L = 70$ mm): (a) Mesh 30, (b) Mesh 50, (c) Mesh 80 and (d) Mesh 100

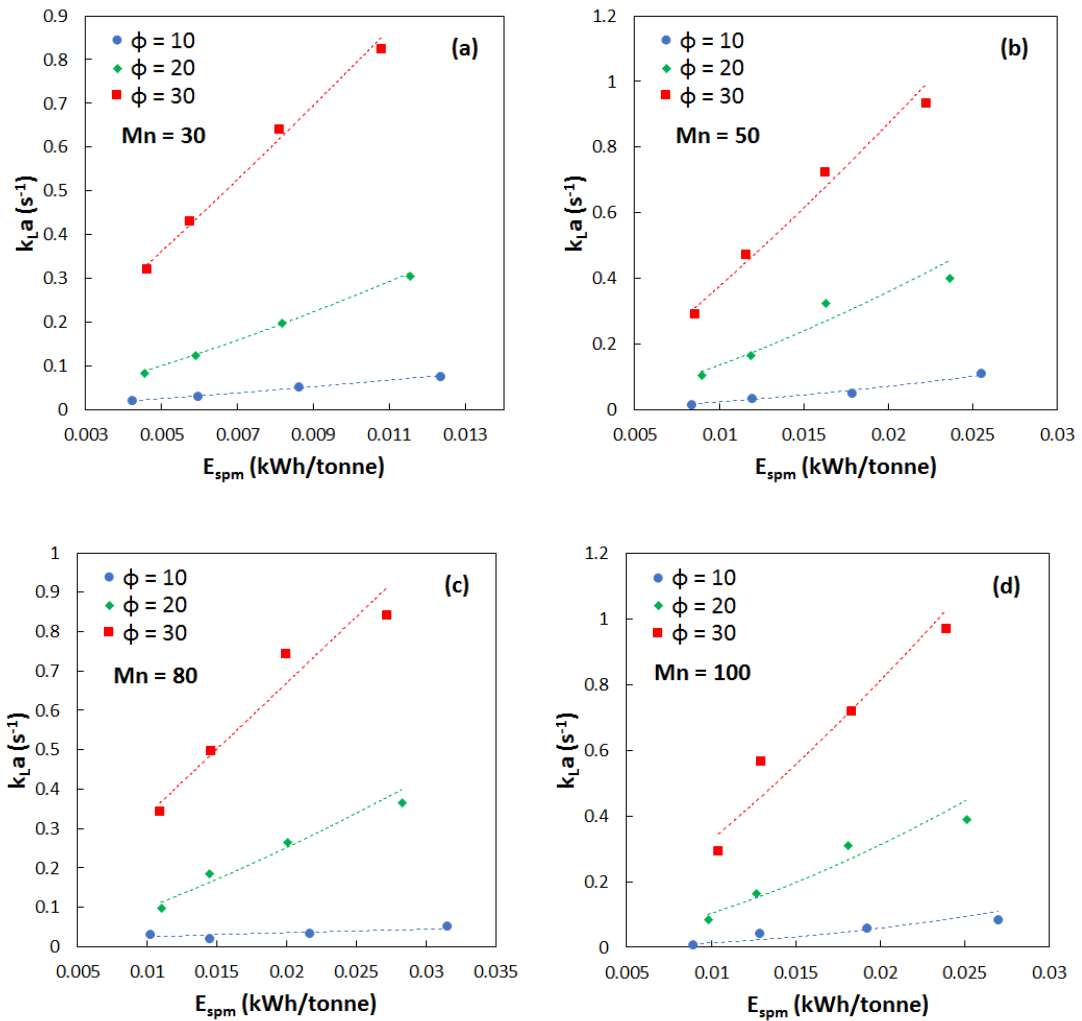


Figure 13: $k_{L,a}$ versus the energy needed to process a unit of the flowing mixture, E_{spm} , ($L = 33.5$ mm): (a) Mesh 30, (b) Mesh 50, (c) Mesh 80 and (d) Mesh 100

4.6. Effect of inter-screen spacing

In addition to investigating the effect of superficial velocity and gas holdup on the volumetric mass transfer coefficient, the effect of inter-screen spacing on the overall mass transfer performance of the reactor was also studied. It should be noted that decreasing the inter-screen spacing allowed an increase in the number of mixing

elements in the mixing section. However, k_{LA} values were found not to be affected by this change as it is evident from Figure 14. As can be clearly discerned, k_{LA} values for both reactor configurations fell within $\pm 20\%$ from each other. This indicates that the current system has become limited by the reaction kinetics as opposed to mass transfer limitations.

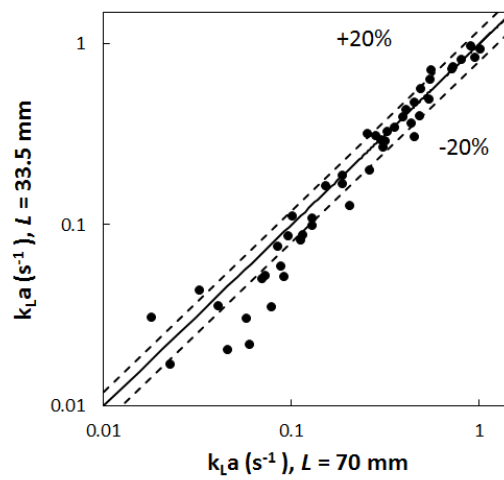


Figure 14: Parity plot of determined k_{LA} at $L = 33.5 \text{ mm}$ against k_{LA} at $L = 70 \text{ mm}$

CHAPTER 5

CONCLUSION

Intensifying CO₂ absorption in RO water was investigated using a tubular reactor equipped with screen-type static mixers. Four different screen geometries were investigated under two different reactor designs (i.e. inter-screen spacing, $L = 33.5$ mm and $L = 70$ mm). The efficiency of the reactor was evaluated from the calculated volumetric mass transfer coefficients that were determined from the dissolved concentrations of CO₂ in water. Two techniques were used to track the amount of dissolved CO₂ namely, pH measurements as well as direct CO₂ measurements using a CO₂ analyzer. These two measurement techniques differed by less than 10% when comparing pH measurements to pH values back-calculated from CO₂ measurements. For both reactor designs, it was found that k_{La} increased with an increase in the total superficial velocity as well as gas holdup and reached maximum values of 1.01 s^{-1} ($L = 70$ mm, $Mn = 50$) and 0.97 s^{-1} ($L = 33.5$ mm, $Mn = 100$). In addition, it was found that using the proper characteristic length when calculating the Reynolds number can help in better discerning the performance of these mixers. Higher k_{La} values were thus obtained using screens characterized by small open area, small wire diameter and mesh size. No significant enhancement in k_{La} values was recorded when changing the inter-screen spacing from 70 mm to 33.5 mm and doubling the number of elements in the reactor. This led to the conclusion that CO₂ absorption in RO water is kinetically limited and only longer residence times would be required to further enhance the absorption

process. Furthermore, the k_{La} values recorded in the present work were found to be one to two orders of magnitude higher than conventional gas-liquid contactors such as mechanically agitated tanks and bubble columns and were in same order of static mixers and advanced flow reactors.

APPENDIX I

FIGURES

A. Pressure Drop Measurements

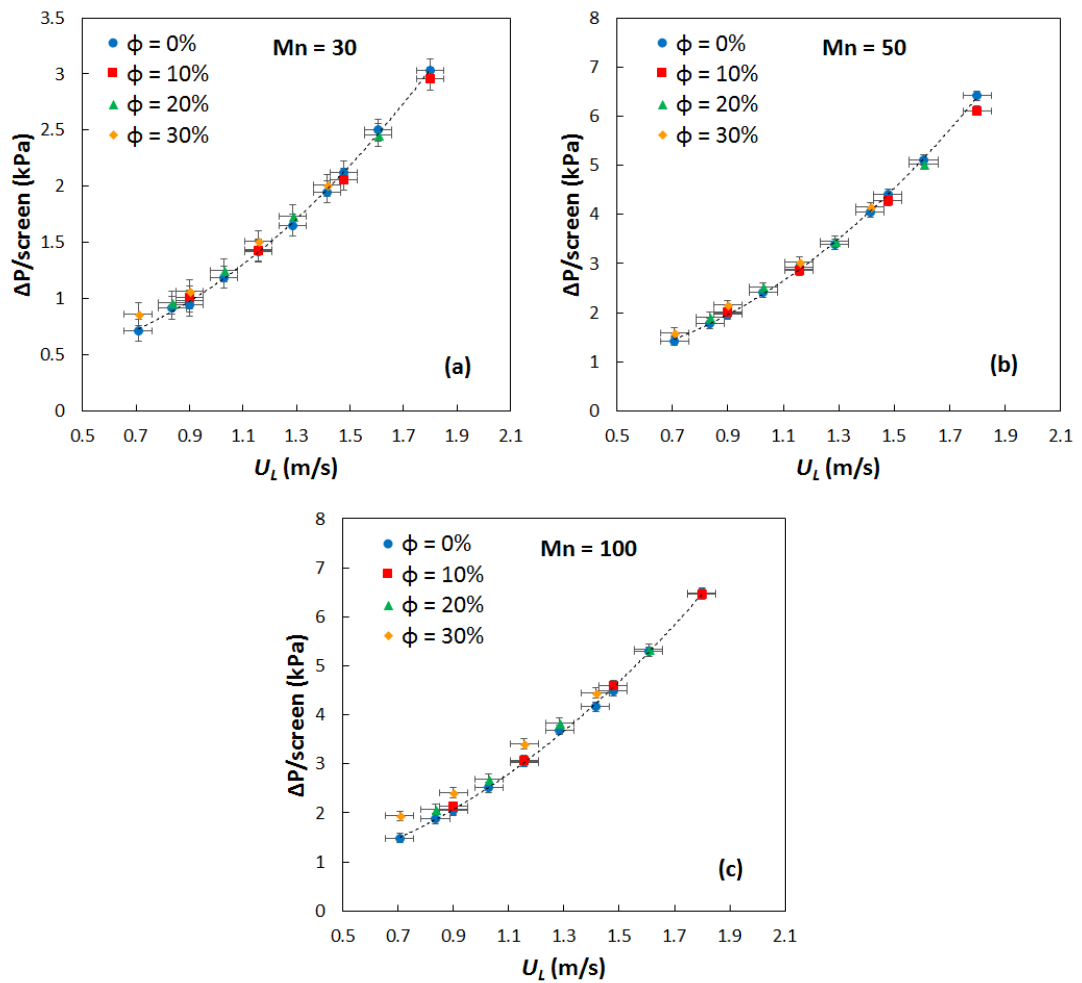


Figure 15: Effect of gas holdup and superficial liquid velocity on the pressure drop per screen: (a) Mesh 30, (b) Mesh 50 and (c) Mesh 100

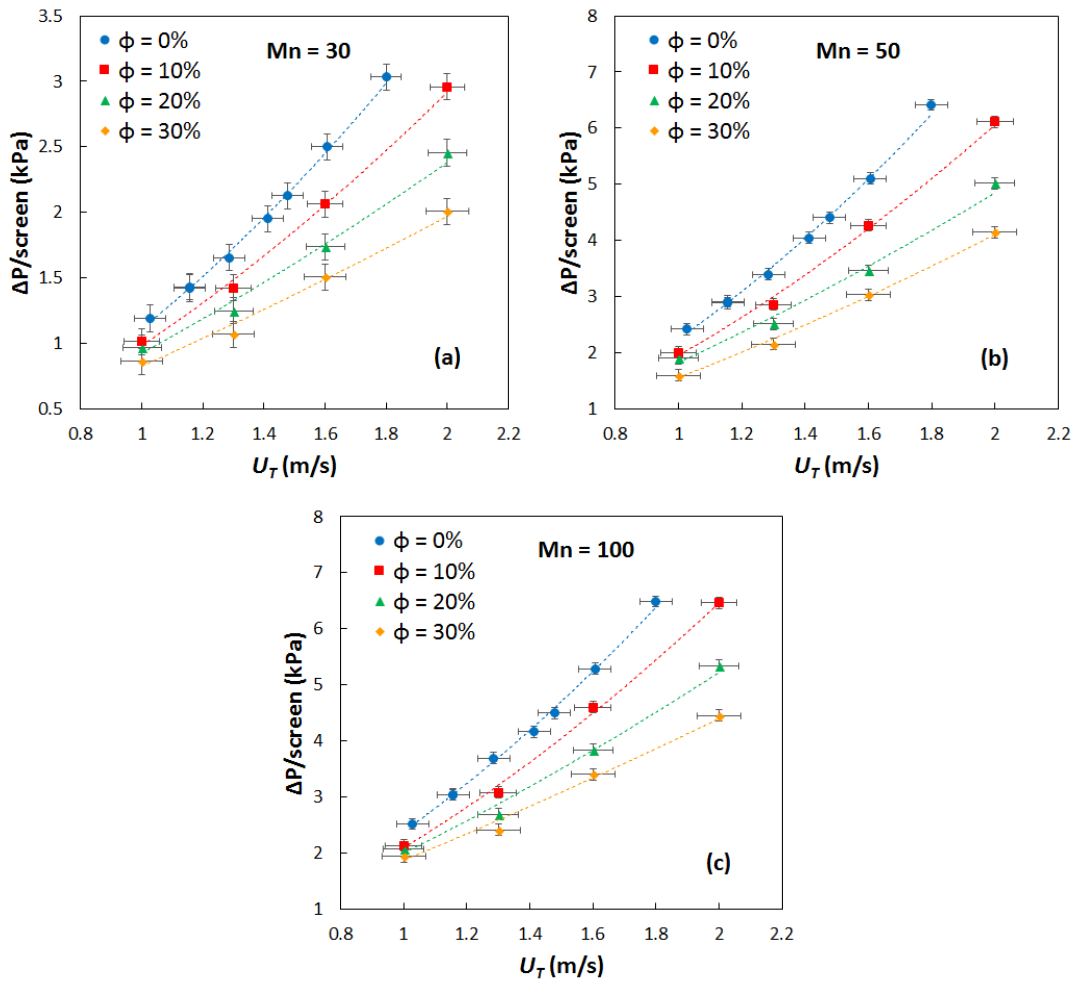


Figure 16: Effect of gas holdup and total superficial velocity on pressure drop per screen: (a) Mesh 30, (b) Mesh 50 and (c) Mesh 100

B. Volumetric Mass Transfer Coefficient

1. Part 1: $L = 70$ mm

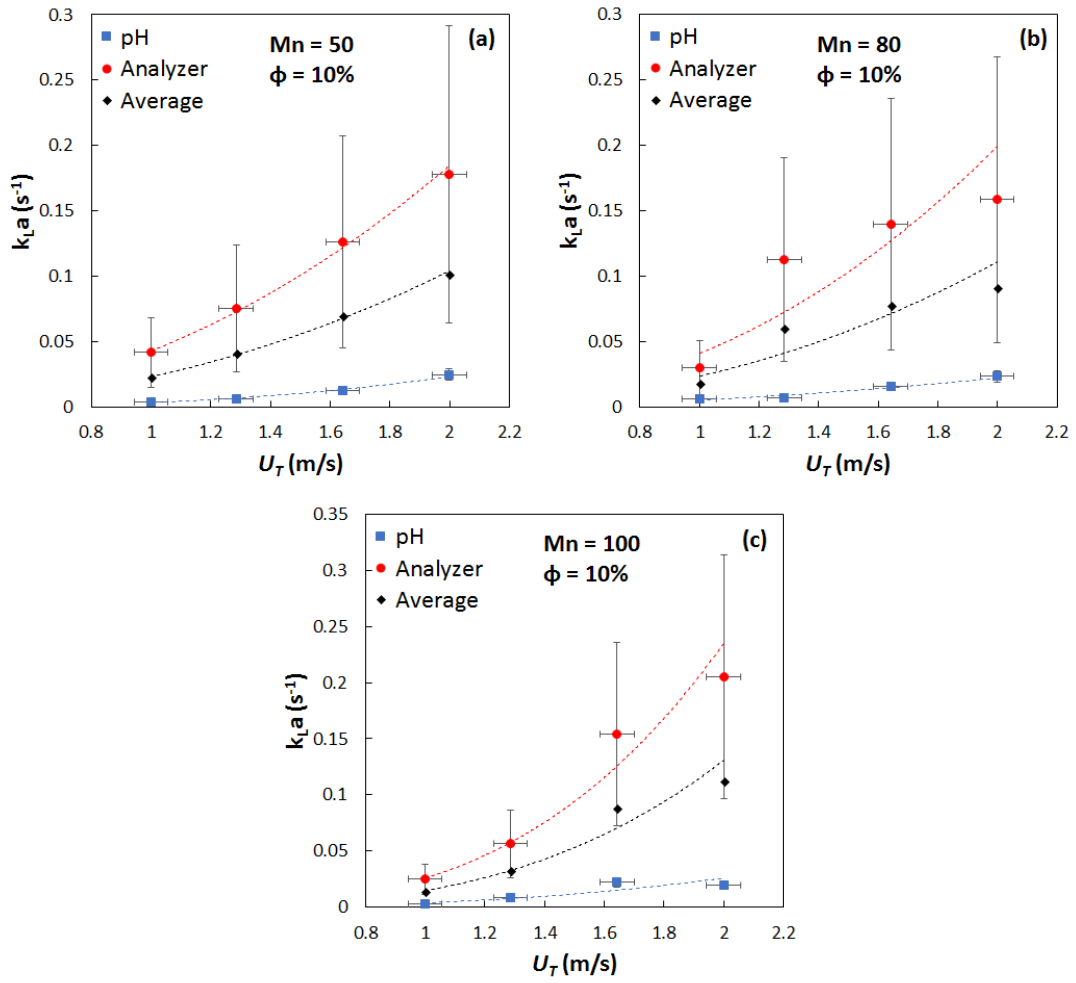


Figure 17: k_{La} from pH, CO₂ analyzer and average k_{La} versus U_T at $\phi = 10\%$ ($L = 70$ mm): (a) Mesh 50, (b) Mesh 80 and (c) Mesh 100

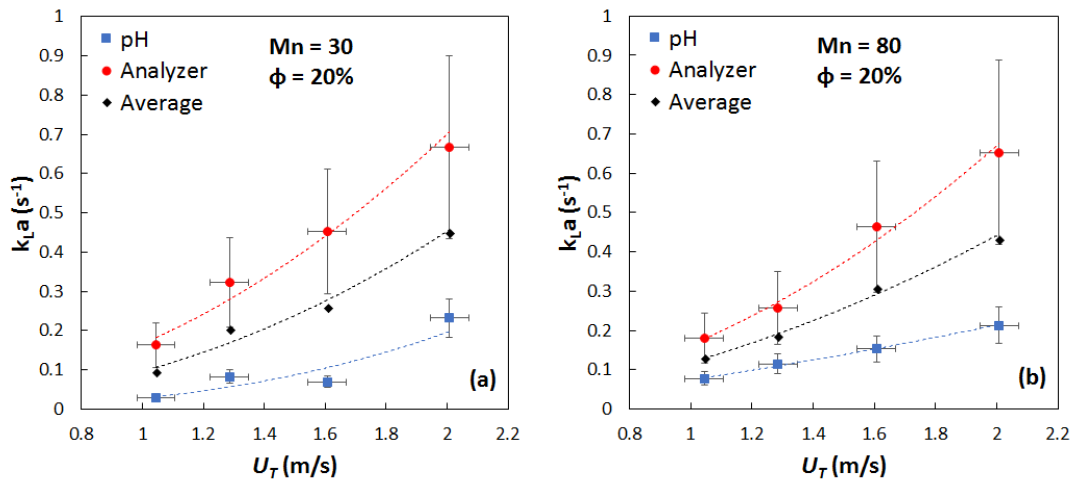


Figure 18: k_{LA} from pH, CO₂ analyzer and average k_{LA} versus U_T at $\phi = 20\%$ ($L = 70$ mm): (a) Mesh 30 and (b) Mesh 80

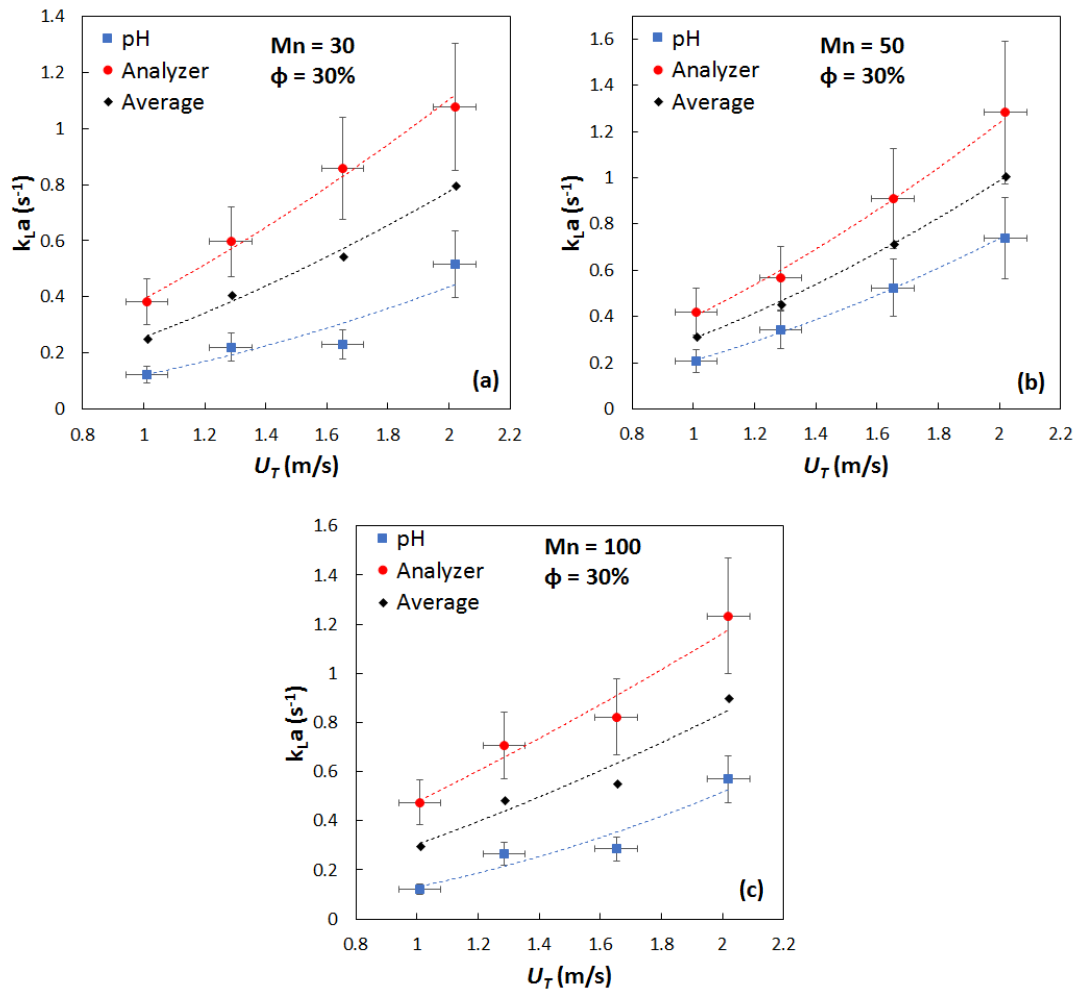


Figure 19: k_{La} from pH, CO₂ analyzer and average k_{La} versus U_T at $\phi = 30\%$ ($L = 70$ mm): (a) Mesh 30, (b) Mesh 50 and (c) Mesh 100

2. Part 2: $L = 33.5 \text{ mm}$

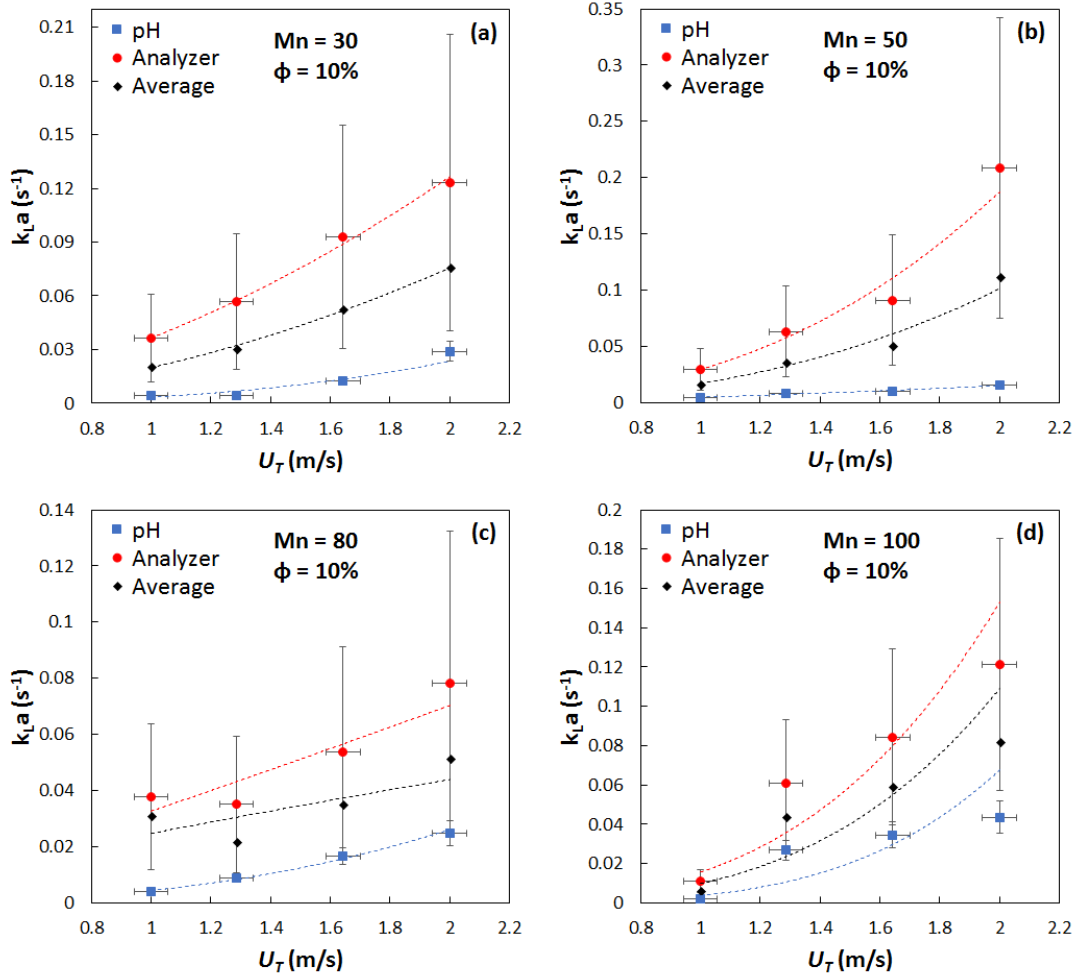


Figure 20: $k_{L,a}$ from pH, CO_2 analyzer and average $k_{L,a}$ versus U_T at $\phi = 10\%$ ($L = 33.5 \text{ mm}$): (a) Mesh 30, (b) Mesh 50, (c) Mesh 80 and (d) Mesh 100

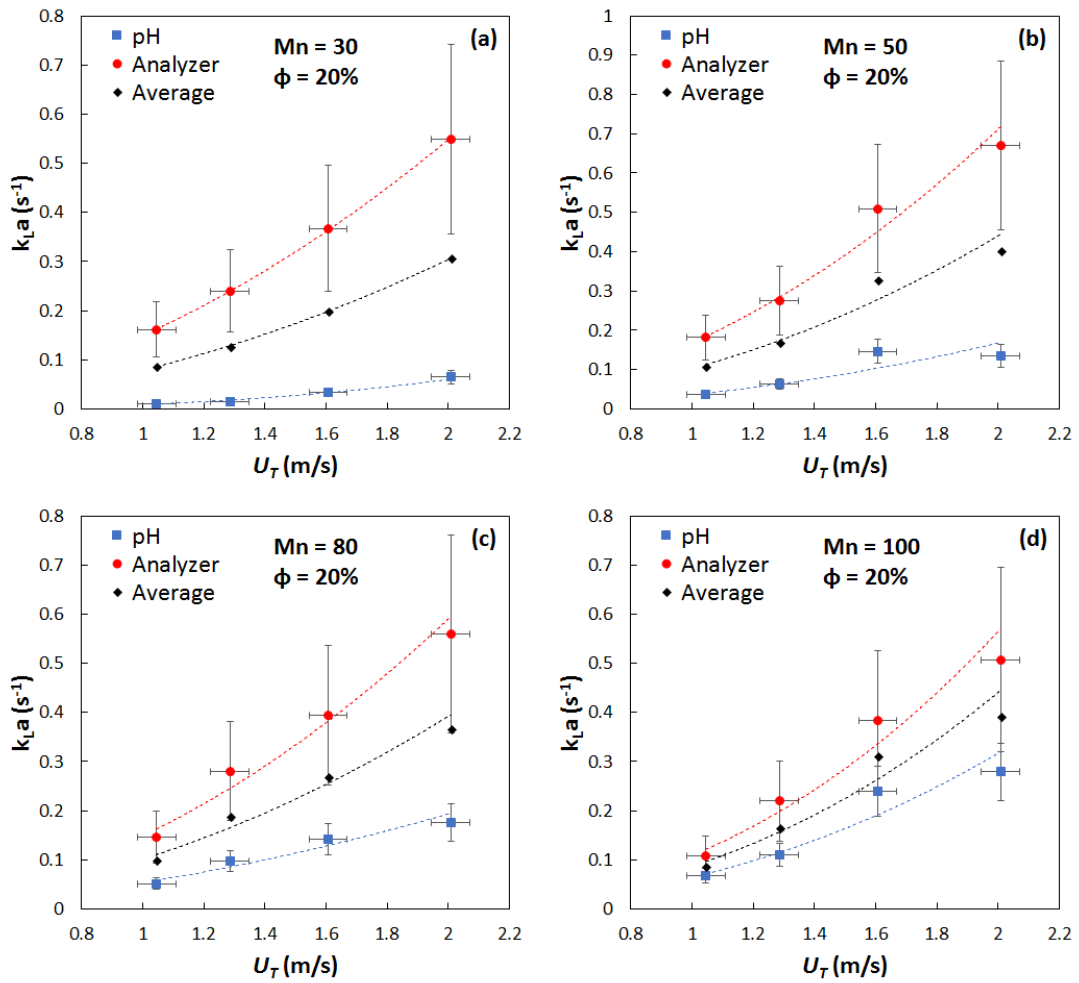


Figure 21: k_{La} from pH, CO₂ analyzer and average k_{La} versus U_T at $\phi = 20\%$ ($L = 33.5$ mm): (a) Mesh 30, (b) Mesh 50, (c) Mesh 80 and (d) Mesh 100

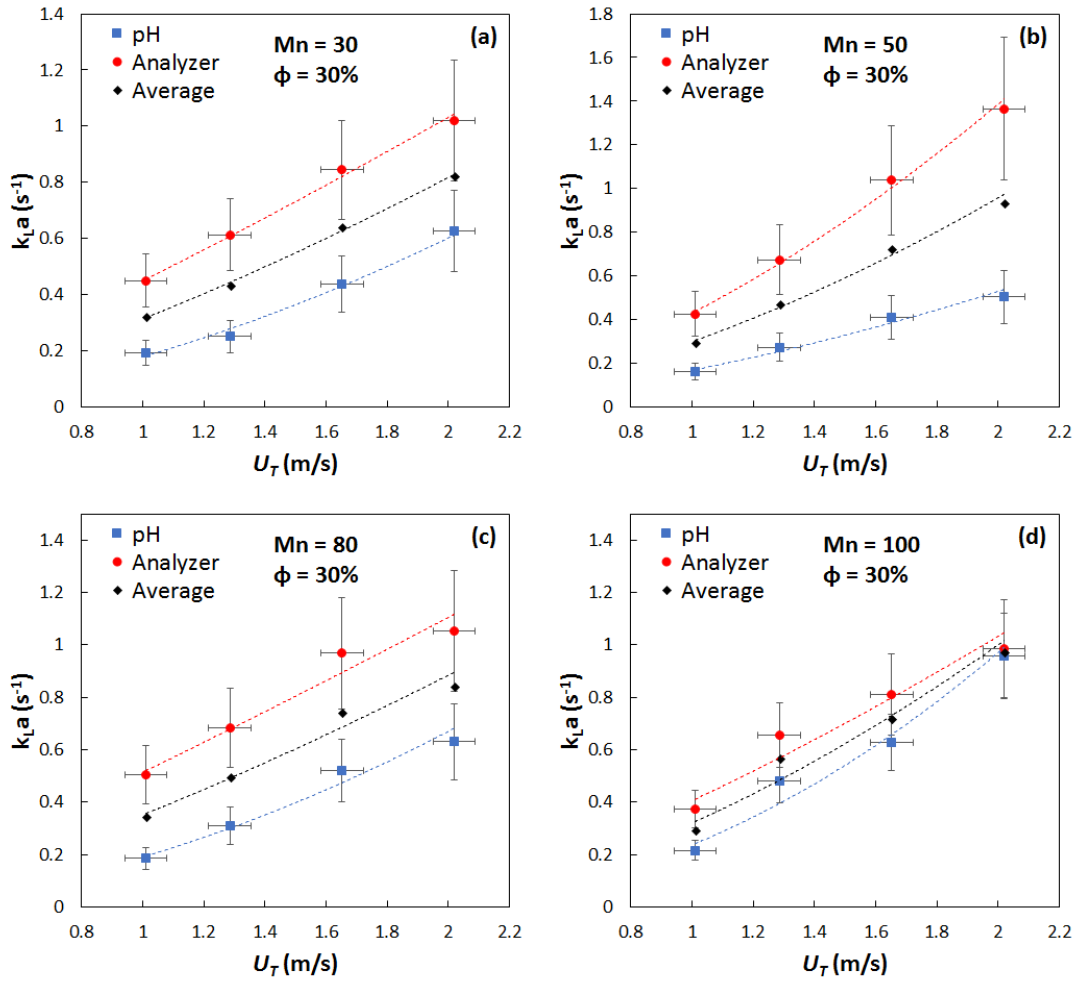


Figure 22: k_{La} from pH, CO_2 analyzer and average k_{La} versus U_T at $\phi = 30\%$ ($L = 33.5$ mm): (a) Mesh 30, (b) Mesh 50, (c) Mesh 80 and (d) Mesh 100

C. Effect of Reynolds number

1. Part 2: $L = 70$ mm

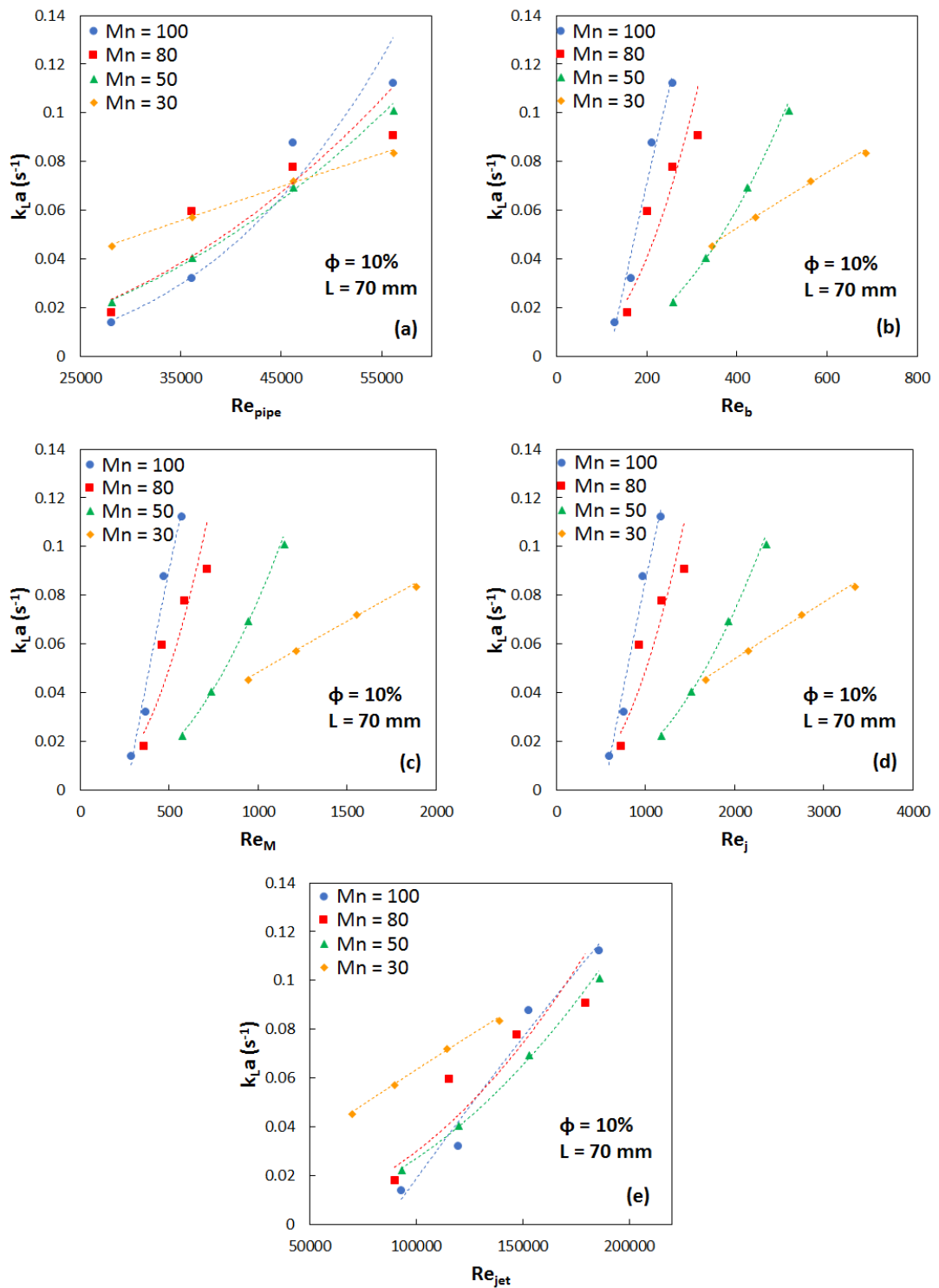


Figure 23: The variation of k_{La} with Reynolds number for all four screen geometries ($L = 70$ mm and $\phi = 10\%$): (a) Re_{pipe} , (b) Re_b , (c) Re_M , (d) Re_j and (e) Re_{jet}

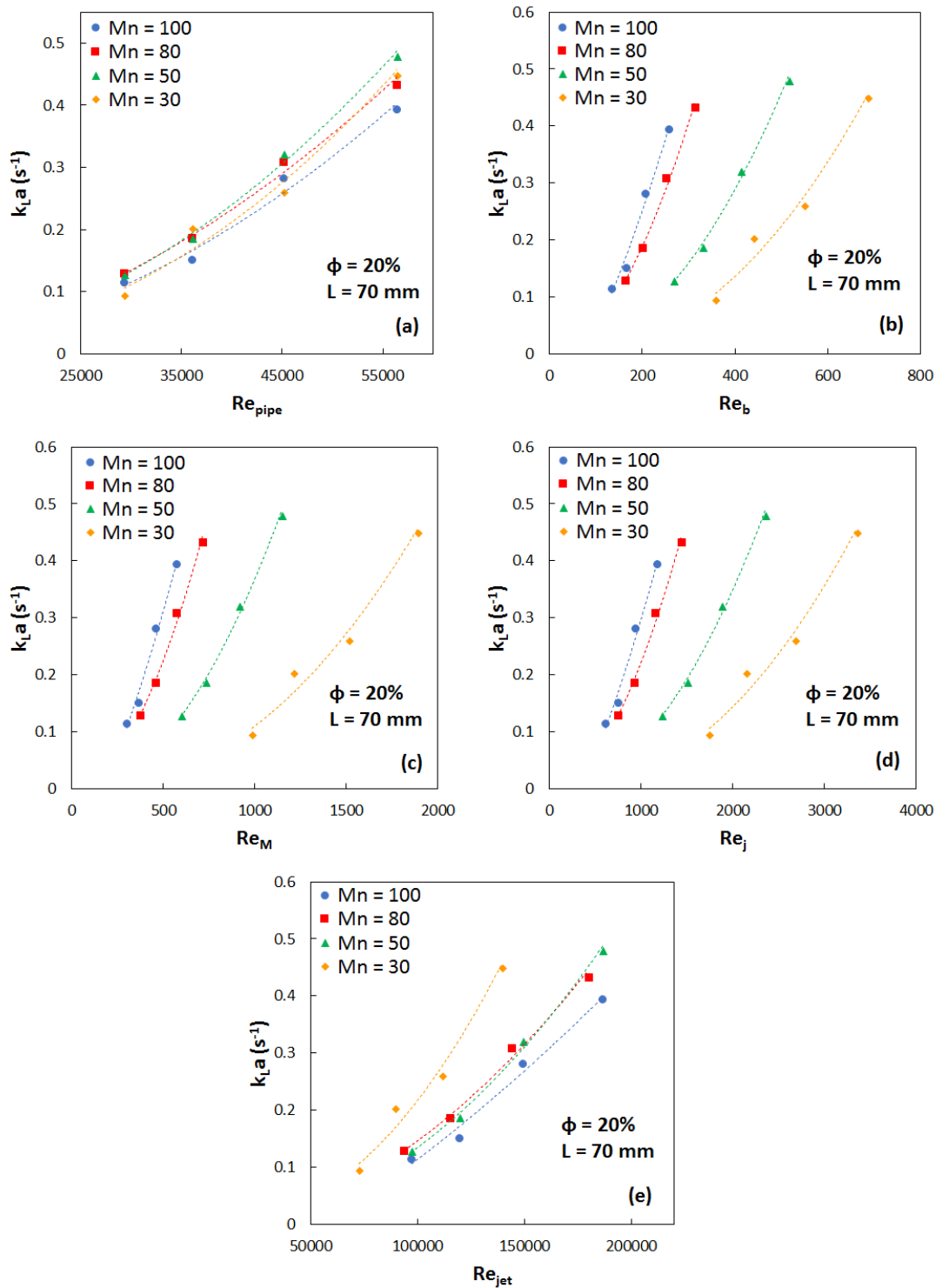


Figure 24: The variation of k_{La} with Reynolds number for all four screen geometries ($L = 70$ mm and $\phi = 20\%$): (a) Re_{pipe} , (b) Re_b , (c) Re_M , (d) Re_j and (e) Re_{jet}

2. Part 2: $L = 33.5 \text{ mm}$

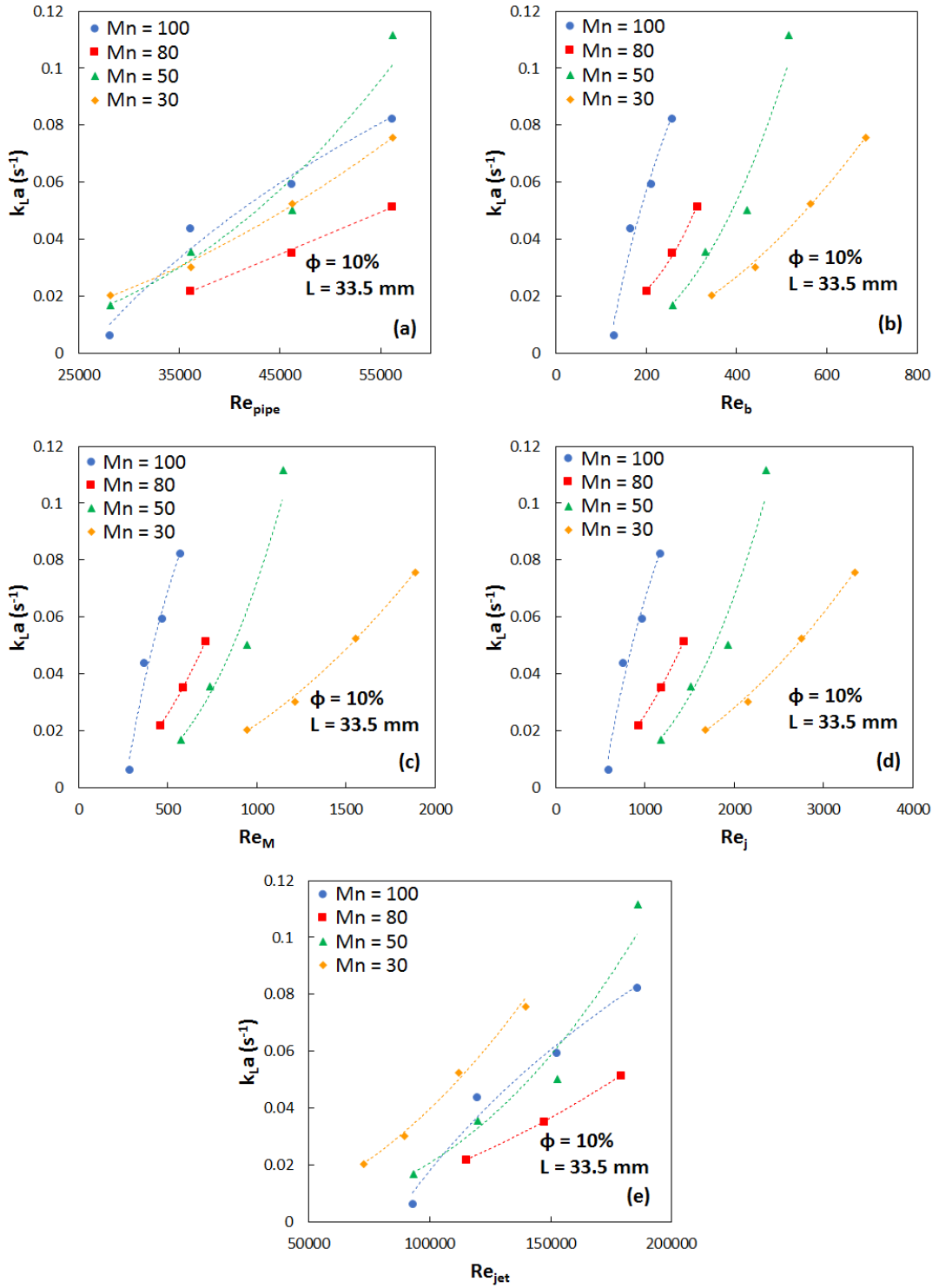


Figure 25: The variation of $k_L a$ with Reynolds number for all four screen geometries ($L = 33.5$ mm and $\phi = 10\%$): (a) Re_{pipe} , (b) Re_b , (c) Re_M , (d) Re_j and (e) Re_{jet}

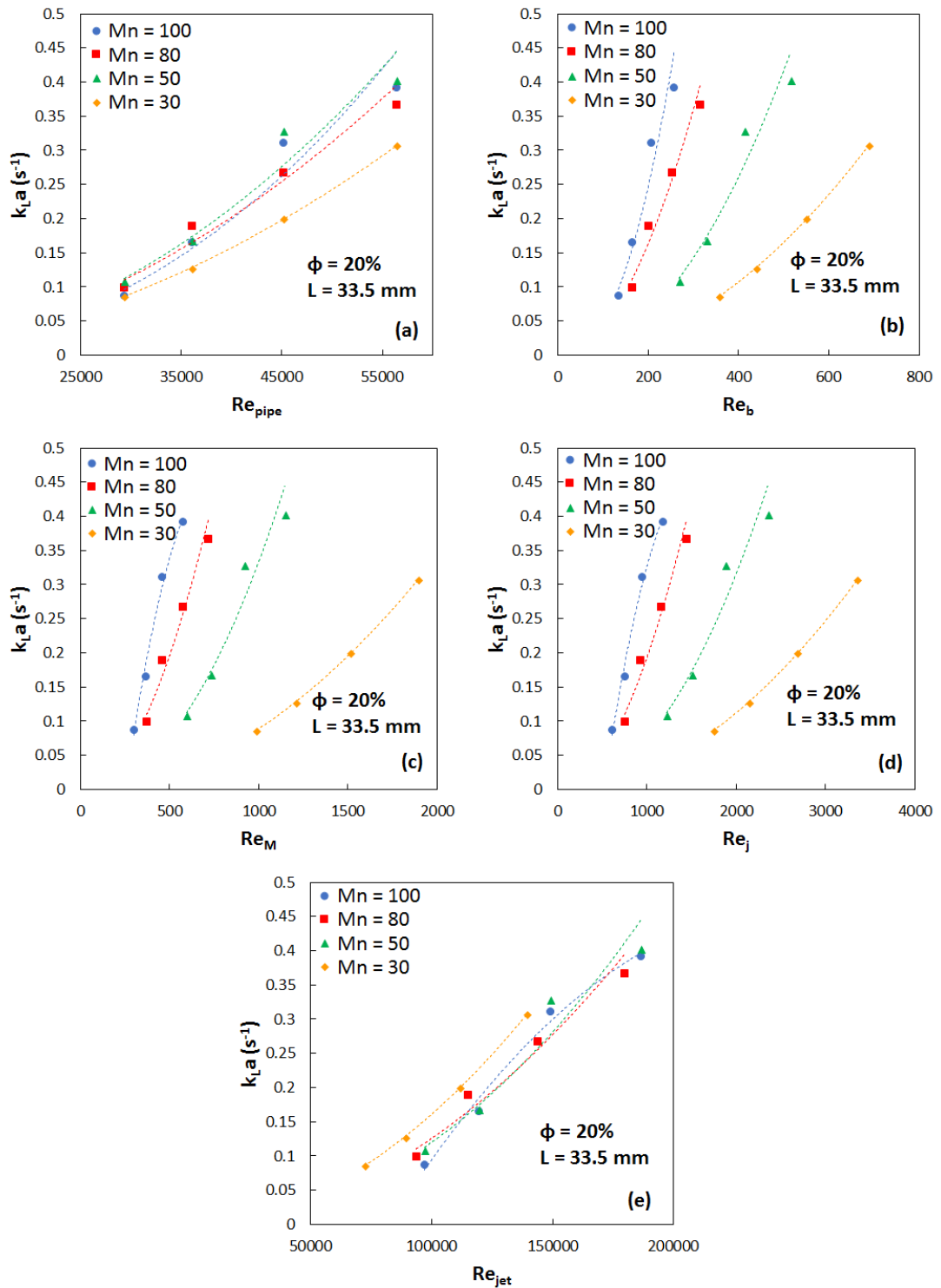


Figure 26: The variation of k_{La} with Reynolds number for all four screen geometries ($L = 33.5$ mm and $\phi = 20\%$): (a) Re_{pipe} , (b) Re_b , (c) Re_M , (d) Re_j and (e) Re_{jet}

APPENDIX II

RAW DATA FROM EXPERIMENTS

The units in the following tables are m/s for the velocity (U_T), bar for pressure, and mg/L for the CO₂ analyzer output or [CO₂]

Part 1: $L = 70$ mm

Table 3: Raw data for $Mn = 30$ at $L = 70$ mm and $\phi = 10\%$

U_T	1		1.3		1.6		2	
P_{in}	0.348		0.515		0.634		0.921	
P_{out}	0.186		0.319		0.384		0.593	
sample	pH	[CO ₂]	pH	[CO ₂]	pH	[CO ₂]	pH	[CO ₂]
0	6.2	0	6.94	0	6.65	0	6.32	0
1	5.78	0	5.82	0	5.77	0	5.74	0
2	5.32	7	5.33	15	5.31	14	5.2	32
3	5.05	73	5.05	74	5.03	69	4.95	85
4	4.98	89	4.95	93	4.93	107	4.9	111
5	4.96	94	4.96	97	4.94	100	4.91	100
6	4.94	113	4.93	110	4.92	115	4.88	116

Table 4: Raw data for $Mn = 30$ at $L = 70$ mm and $\phi = 20\%$

U_T	1		1.3		1.6		2	
P_{in}	0.332		0.467		0.534		0.742	
P_{out}	0.178		0.288		0.316		0.460	
sample	pH	[CO ₂]	pH	[CO ₂]	pH	[CO ₂]	pH	[CO ₂]
0	6.88	0	6.62	0	6.72	0	6.63	0
1	5.35	8	5.11	25	5.1	33	5.32	4
2	4.93	46	4.8	90	4.8	105	4.7	138
3	4.73	130	4.61	202	4.54	267	4.5	299
4	4.69	183	4.56	241	4.5	309	4.43	364
5	4.72	173	4.58	238	4.51	313	4.42	364
6	4.62	212	4.54	270	4.48	348	4.39	412

Table 5: Raw data for Mn = 30 at $L = 70$ mm and $\phi = 30\%$

UT	1		1.3		1.6		2	
P_{in}	0.331		0.437		0.572		0.639	
P_{out}	0.189		0.277		0.373		0.399	
sample	pH	[CO ₂]	pH	[CO ₂]	pH	[CO ₂]	pH	[CO ₂]
0	6.78	0	6.58	0	6.67	0	6.29	0
1	4.81	95	4.7	138	4.77	167	4.82	97
2	4.6	166	4.55	187	4.54	229	4.49	230
3	4.46	296	4.41	341	4.36	419	4.31	441
4	4.42	347	4.36	415	4.33	491	4.26	524
5	4.44	330	4.38	383	4.35	465	4.27	523
6	4.4	446	4.36	457	4.31	549	4.25	578

Table 6: Raw data Mn = 50 at $L = 70$ mm and $\phi = 10\%$

U _T	1		1.3		1.6		2	
P_{in}	0.409		0.669		0.827		0.959	
P_{out}	0.167		0.358		0.400		0.379	
sample	pH	[CO ₂]	pH	[CO ₂]	pH	[CO ₂]	pH	[CO ₂]
0	6.57	0	6.71	0	6.57	0	6.62	0
1	5.8	0	5.66	0	5.64	0	5.73	0
2	5.35	7	5.26	19	5.11	40	5.15	75
3	5.11	40	5	76	4.95	96	4.94	107
4	5.06	53	4.95	82	4.96	95	4.89	109
5	5.05	69	4.98	78	4.94	109	4.88	112
6	5.01	79	4.93	103	4.92	116	4.85	123

Table 7: Raw data Mn = 50 at $L = 70$ mm and $\phi = 20\%$

U _T	1		1.3		1.6		2	
P_{in}	0.467		0.578		0.738		0.933	
P_{out}	0.238		0.298		0.381		0.445	
sample	pH	[CO ₂]	pH	[CO ₂]	pH	[CO ₂]	pH	[CO ₂]
0	6.75	0	6.55	0	6.65	0	6.59	0
1	5.19	5	5.05	29	5.02	21	5.2	0
2	4.72	104	4.69	117	4.61	168	4.6	258
3	4.59	186	4.54	238	4.45	338	4.4	447
4	4.64	155	4.57	201	4.47	316	4.41	428
5	4.63	162	4.58	191	4.46	302	4.42	433
6	4.59	200	4.55	229	4.44	348	4.41	452

Table 8: Raw data Mn = 50 at $L = 70$ mm and $\phi = 30\%$

U_T	1		1.3		1.6		2	
P_{in}	0.353		0.500		0.677		0.801	
P_{out}	0.153		0.253		0.356		0.390	
sample	pH	[CO ₂]	pH	[CO ₂]	pH	[CO ₂]	pH	[CO ₂]
0	6.84	0	6.57	0	6.47	0	6.65	0
1	4.74	110	4.63	160	4.66	137	4.75	83
2	4.46	202	4.38	230	4.37	299	4.32	364
3	4.39	338	4.33	387	4.25	507	4.23	614
4	4.43	283	4.34	349	4.27	455	4.25	566
5	4.41	493	4.35	353	4.26	474	4.24	576
6	4.4	504	4.33	429	4.24	520	4.23	623

Table 9: Raw data Mn = 80 at $L = 70$ mm and $\phi = 10\%$

U_T	1		1.3		1.6		2	
P_{in}	0.467		0.639		0.885		1.038	
P_{out}	0.191		0.278		0.386		0.343	
sample	pH	[CO ₂]	pH	[CO ₂]	pH	[CO ₂]	pH	[CO ₂]
0	6.47	0	6.65	0	6.44	0	6.57	0
1	5.68	0	5.73	0	5.6	0	5.6	0
2	5.2	20	5.24	46	5.03	72	4.96	72
3	5.07	26	4.98	74	4.92	80	4.89	87
4	5.04	31	4.95	126	4.91	108	4.9	105
5	5.05	37	4.96	120	4.89	123	4.89	97
6	5.03	42	4.93	114	4.89	127	4.86	117

Table 10: Raw data Mn = 80 at $L = 70$ mm and $\phi = 20\%$

U_T	1		1.3		1.6		2	
P_{in}	0.446		0.624		0.734		1.019	
P_{out}	0.182		0.300		0.313		0.452	
sample	pH	[CO ₂]	pH	[CO ₂]	pH	[CO ₂]	pH	[CO ₂]
0	6.46	0	6.5	0	6.45	0	6.63	0
1	4.98	27	4.82	73	5.13	33	5.38	0
2	4.66	140	4.59	143	4.64	214	4.67	269
3	4.61	139	4.54	164	4.54	242	4.52	319
4	4.6	138	4.53	174	4.48	299	4.43	370

5	4.63	112	4.55	168	4.49	293	4.45	376
6	4.59	172	4.53	168	4.48	327	4.42	381

Table 11: Raw data Mn = 80 at $L = 70$ mm and $\phi = 30\%$

U_T	1		1.3		1.6		2	
P_{in}	0.435		0.583		0.679		0.886	
P_{out}	0.199		0.292		0.304		0.401	
sample	pH	[CO ₂]	pH	[CO ₂]	pH	[CO ₂]	pH	[CO ₂]
0	6.9	0	6.56	0	6.58	0	6.64	0
1	4.57	186	4.48	231	4.75	139	4.75	153
2	4.46	288	4.38	318	4.33	361	4.3	426
3	4.41	275	4.33	340	4.28	401	4.25	491
4	4.39	287	4.32	349	4.29	485	4.24	563
5	4.42	253	4.34	314	4.28	480	4.25	549
6	4.4	347	4.31	391	4.29	507	4.24	569

Table 12: Raw data Mn = 100 at $L = 70$ mm and $\phi = 10\%$

U_T	1		1.3		1.6		2	
P_{in}	0.409		0.533		0.804		0.994	
P_{out}	0.157		0.204		0.351		0.386	
sample	pH	[CO ₂]	pH	[CO ₂]	pH	[CO ₂]	pH	[CO ₂]
0	6.5	0	6.6	0	6.47	0	6.45	0
1	5.81	0	5.62	0	5.6	0	5.6	0
2	5.44	0	5.2	27	5.08	38	5.04	88
3	5.3	27	5.08	57	4.91	103	4.85	126
4	5.24	23	5.11	47	4.99	77	4.88	104
5	5.23	30	5	78	4.85	137	4.81	138
6	5.24	36	5.04	79	4.86	114	4.82	143

Table 13: Raw data Mn = 100 at $L = 70$ mm and $\phi = 20\%$

U_T	1		1.3		1.6		2	
P_{in}	0.390		0.481		0.669		0.968	
P_{out}	0.147		0.187		0.283		0.455	
sample	pH	[CO ₂]	pH	[CO ₂]	pH	[CO ₂]	pH	[CO ₂]
0	6.31	0	6.55	0	6.6	0	6.54	0
1	5.13	50	5	68	5	85	4.97	59

2	4.79	101	4.72	109	4.7	186	4.56	216
3	4.72	146	4.63	189	4.57	286	4.46	332
4	4.76	107	4.7	145	4.64	238	4.53	290
5	4.71	154	4.6	197	4.56	278	4.4	364
6	4.74	138	4.65	174	4.57	284	4.44	366

Table 14: Raw data Mn = 100 at $L = 70$ mm and $\phi = 30\%$

U_T	1		1.3		1.6		2	
P_{in}	0.384		0.514		0.654		0.817	
P_{out}	0.156		0.247		0.303		0.381	
sample	pH	[CO ₂]	pH	[CO ₂]	pH	[CO ₂]	pH	[CO ₂]
0	6.6	0	6.32	0	6.55	0	6.54	0
1	4.75	191	4.59	217	4.6	221	4.55	232
2	4.54	229	4.45	290	4.45	322	4.35	352
3	4.49	286	4.4	383	4.35	449	4.27	509
4	4.53	233	4.44	274	4.4	369	4.3	454
5	4.47	292	4.39	380	4.35	423	4.25	536
6	4.5	282	4.41	348	4.38	442	4.28	513

Part 2: $L = 33.5$ mm

Table 15: Raw data Mn = 30 at $L = 33.5$ mm and $\phi = 10\%$

U_T	1		1.3		1.6		2	
P_{in}	0.493		0.651		0.819		1.068	
P_{out}	0.263		0.355		0.415		0.488	
sample	pH	[CO ₂]	pH	[CO ₂]	pH	[CO ₂]	pH	[CO ₂]
0	6.52	0	6.59	0	6.56	0	5.95	0
1	5.88	0	5.64	0	5.71	0	5.4	0
2	5.4	2	5.35	13	5.27	14	5.02	58
3	5.22	23	5.11	39	5.04	64	4.9	71
4	5.14	50	5.07	60	4.98	73	4.83	80
5	5.09	56	5.01	70	4.95	84	4.87	82
6	5.03	76	4.98	86	4.91	102	4.82	100

Table 16: Raw data Mn = 30 at $L = 33.5$ mm and $\phi = 20\%$

U_T	1		1.3		1.6		2	
P_{in}	0.458		0.564		0.747		0.915	
P_{out}	0.240		0.296		0.407		0.453	
sample	pH	CO ₂	pH	CO ₂	pH	CO ₂	pH	CO ₂
0	6.84	0	6.84	0	6.68	0	6.6	0
1	5.45	12	5.33	18	5.2	27	5.35	5
2	5.1	96	5.08	101	4.95	119	4.8	181
3	4.95	138	4.88	184	4.73	258	4.59	283
4	4.93	167	4.86	209	4.71	280	4.56	342
5	4.88	202	4.83	232	4.67	311	4.51	372
6	4.84	253	4.79	288	4.64	385	4.48	410

Table 17: Raw data Mn = 30 at $L = 33.5$ mm and $\phi = 30\%$

U_T	1		1.3		1.6		2	
P_{in}	0.464		0.534		0.665		0.831	
P_{out}	0.266		0.295		0.355		0.437	
sample	pH	CO ₂	pH	CO ₂	pH	CO ₂	pH	CO ₂
0	6.59	0	6.54	0	6.62	0	6.62	0
1	4.64	129	4.6	140	4.67	154	4.7	133
2	4.47	275	4.48	290	4.4	302	4.35	328
3	4.4	330	4.36	376	4.3	432	4.25	481
4	4.39	345	4.37	379	4.32	467	4.27	517
5	4.37	403	4.34	450	4.31	542	4.25	634
6	4.35	527	4.31	573	4.29	635	4.23	698

Table 18: Raw data Mn = 50 at $L = 33.5$ mm and $\phi = 10\%$

U_T	1		1.3		1.6		2	
P_{in}	0.619		0.851		1.082		1.218	
P_{out}	0.219		0.315		0.354		0.562	
sample	pH	CO ₂	pH	CO ₂	pH	CO ₂	pH	CO ₂
0	6.67	0	6.7	0	6.56	0	6.62	0
1	5.88	0	5.54	0	5.68	0	5.5	0
2	5.38	0	5.18	34	5.25	37	5.1	77
3	5.24	25	5.09	44	5.1	68	4.94	96
4	5.18	26	5.03	68	4.99	76	4.89	100
5	5.09	48	4.98	72	5.02	84	4.88	104

6	5.06	55	4.96	86	4.98	93	4.85	118
---	------	----	------	----	------	----	------	-----

Table 19: Raw data Mn = 50 at $L = 33.5$ mm and $\phi = 20\%$

U_T	1		1.3		1.6		2	
P_{in}	0.674		0.754		0.911		1.266	
P_{out}	0.300		0.285		0.287		0.336	
sample	pH	CO ₂	pH	CO ₂	pH	CO ₂	pH	CO ₂
0	6.4	0	6.6	0	6.51	0	6.51	0
1	5.1	42	4.95	72	4.9	66	5.2	0
2	4.8	138	4.72	144	4.58	237	4.58	310
3	4.75	138	4.66	182	4.51	288	4.51	368
4	4.71	181	4.62	231	4.49	332	4.52	402
5	4.66	197	4.59	253	4.48	364	4.5	425
6	4.64	227	4.57	278	4.46	396	4.49	434

Table 20: Raw data Mn = 50 at $L = 33.5$ mm and $\phi = 30\%$

U_T	1		1.3		1.6		2	
P_{in}	0.589		0.693		0.935		1.094	
P_{out}	0.264		0.276		0.372		0.393	
sample	pH	CO ₂	pH	CO ₂	pH	CO ₂	pH	CO ₂
0	6.81	0	6.5	0	6.41	0	6.86	0
1	4.64	136	4.56	207	4.5	252	4.78	139
2	4.48	280	4.42	368	4.37	441	4.35	535
3	4.42	314	4.37	371	4.32	502	4.29	602
4	4.41	363	4.36	405	4.3	557	4.3	630
5	4.4	403	4.34	480	4.28	617	4.3	698
6	4.37	481	4.32	566	4.26	687	4.28	753

Table 21: Raw data Mn = 80 at $L = 33.5$ mm and $\phi = 10\%$

U_T	1		1.3		1.6		2	
P_{in}	0.687		0.945		1.260		1.191	
P_{out}	0.301		0.392		0.454		0.609	
sample	pH	CO ₂	pH	CO ₂	pH	CO ₂	pH	CO ₂
0	6.68	0	6.65	0	6.44	0	6.3	0
1	5.55	0	5.53	0	5.5	0	5.49	0
2	5.2	0	5.14	27	4.99	29	4.92	37
3	5.13	0	4.98	36	4.92	39	4.86	46

4	5.15	3	4.95	36	4.91	60	4.93	61
5	5.12	16	4.96	50	4.89	66	4.92	62
6	5.08	29	4.93	65	4.89	75	4.87	88

Table 22: Raw data Mn = 80 at $L = 33.5$ mm and $\phi = 20\%$

U_T	1		1.3		1.6		2	
P_{in}	0.661		0.829		1.143		1.217	
P_{out}	0.312		0.360		0.504		0.503	
sample	pH	CO ₂	pH	CO ₂	pH	CO ₂	pH	CO ₂
0	6.4	0	6.65	0	6.54	0	6.65	0
1	4.8	98	4.75	130	4.74	140	5.29	0
2	4.67	131	4.64	158	4.54	204	4.49	285
3	4.62	105	4.59	157	4.49	230	4.43	302
4	4.69	108	4.6	158	4.48	224	4.41	340
5	4.62	164	4.55	186	4.46	276	4.42	375
6	4.57	210	4.5	244	4.44	344	4.4	392

Table 23: Raw data Mn = 80 at $L = 33.5$ mm and $\phi = 30\%$

U_T	1		1.3		1.6		2	
P_{in}	0.676		0.824		1.003		1.325	
P_{out}	0.358		0.412		0.446		0.560	
sample	pH	CO ₂	pH	CO ₂	pH	CO ₂	pH	CO ₂
0	6.94	0	6.46	0	6.4	0	6.67	0
1	4.6	224	4.5	272	4.4	324	4.48	238
2	4.47	358	4.39	366	4.29	406	4.26	441
3	4.42	286	4.34	325	4.24	455	4.21	555
4	4.43	328	4.31	396	4.25	509	4.23	532
5	4.4	327	4.32	391	4.23	540	4.21	585
6	4.45	406	4.34	466	4.22	604	4.17	692

Table 24: Raw data Mn = 100 at $L = 33.5$ mm and $\phi = 10\%$

U_T	1		1.3		1.6		2	
P_{in}	0.679		0.854		1.254		1.045	
P_{out}	0.361		0.410		0.582		0.615	
sample	pH	CO ₂	pH	CO ₂	pH	CO ₂	pH	CO ₂
0	6.77	0	6.61	0	6.41	0	6.32	0
1	5.6	0	5.32	0	5.36	0	4.89	0

2	5.24	0	4.9	32	4.84	58	4.8	59
3	5.19	1	4.83	48	4.78	73	4.75	76
4	5.21	4	4.84	60	4.81	68	4.84	69
5	5.27	5	4.83	69	4.8	77	4.83	80
6	5.17	10	4.82	64	4.78	104	4.76	111

Table 25: Raw data Mn = 100 at $L = 33.5$ mm and $\phi = 20\%$

U_T	1		1.3		1.6		2	
P_{in}	0.663		0.827		1.030		1.114	
P_{out}	0.376		0.444		0.485		0.520	
sample	pH	CO ₂	pH	CO ₂	pH	CO ₂	pH	CO ₂
0	6.25	0	6.21	0	6.48	0	6.4	0
1	4.77	38	4.74	65	4.74	44	5.09	16
2	4.69	85	4.6	132	4.47	208	4.44	202
3	4.64	65	4.55	153	4.43	235	4.39	300
4	4.65	108	4.52	166	4.43	270	4.42	271
5	4.68	96	4.62	162	4.43	307	4.43	354
6	4.63	103	4.54	175	4.39	303	4.39	306

Table 26: Raw data Mn = 100 at $L = 33.5$ mm and $\phi = 30\%$

U_T	1		1.3		1.6		2	
P_{in}	0.663		0.766		0.993		1.173	
P_{out}	0.393		0.412		0.490		0.488	
sample	pH	CO ₂	pH	CO ₂	pH	CO ₂	pH	CO ₂
0	6.85	0	6.42	0	6.3	0	6.3	0
1	4.57	201	4.44	282	4.41	279	4.55	195
2	4.42	211	4.32	295	4.26	310	4.23	425
3	4.36	285	4.26	370	4.21	429	4.19	497
4	4.35	254	4.29	306	4.24	425	4.22	444
5	4.39	279	4.28	366	4.23	426	4.22	497
6	4.34	397	4.22	468	4.18	554	4.17	603

APPENDIX III

SAMPLE CALCULATION (k_{La})

The sample calculation presented is for one experimental run.

The operating and design conditions are summarized in the table below:

Table 27: Sample calculation operating and design conditions

Condition	Value
Mesh Number	50
Number of screen elements	8
Inter screen spacing (mm)	70
Screen open area (%)	30.25
Dispersed phase holdup (%)	30
Water flow rate, Q_L , (L/min)	41.6
Gas flow rate, Q_g , (L/min)	17.85
Temperature (k)	295
Water TDS (ppm)	45

There are several variables that need to be calculated prior to calculating k_{La} .

The residence time is calculated using the total superficial velocity, U_T ,

$$t = \frac{d}{U_T} \quad (1)$$

Where:

U_T is determined from the gas and liquid flow rates as shown below:

$$U_T \text{ (m/s)} = \frac{Q_L + Q_g}{1000 \times 60 \times A_c} = 2 \quad (2)$$

Where A_c is the cross-section area of the column and is equal to:

$$A_c = \frac{\pi D^2}{4} = \frac{\pi(0.025^2)}{4} = 4.91 \times 10^{-4} \text{ m}^2 \quad (3)$$

The local pressure, P_{local} is obtained using the average of the P_{bot} at the inlet of the reactor from table 2:

$$P_{local \text{ in}}(P_a) = P_{atm} + (P_{bot} \times 100000) \quad (4)$$

Where $P_{atm} = 101325 \text{ atm}$

Equilibrium concentration, C^* , is the concentration of physically dissolved CO_2 and H_2CO_3 in equilibrium with P_{CO_2} in the gas phase. It is obtained using Henry's law (equation (3) in the methodology section).

Henry's constant and k_1 were determined using the equations in the methodology section and presented in the table below:

Table 28: Calculated variables

Variable	value
H_{CO_2} (M/atm)	0.0365
K_1 (M)	4.9E-07
S (g/kg)	0.045

The salinity was calculated from water TDS as shown below:

$$S = \frac{TDS}{\rho_w} \quad (5)$$

$[\text{H}^+]$ is obtained from the pH values by:

$$[\text{H}^+] = 10^{-pH} \quad (6)$$

It should be noted that the pH measurements are fitted using curve fit in MATLAB using two exponentials. The fitted pH values are the ones used for determining the CO_2 concentrations.

The $[CO_2]$ which is either calculated from pH measurements or directly measured using the CO_2 analyzer (methodology section), and the transient term $d[CO_2]/dt$ is calculated using the following equation:

$$\frac{d[CO_2]}{dt} = \frac{[CO_2]_2 - [CO_2]_1}{t_2 - t_1} \quad (7)$$

Where the subscripts (1 and 2) denotes the sample position.

The volume of the liquid processes in the reactor, V_L , is obtained using the following equation:

$$V_L(L) = \frac{Q_L}{60} \times t \quad (8)$$

Now all the variables are calculated, the k_{LA} can be obtained by re-arranging equation (9) in methodology section as shown below:

$$k_{La} = \frac{\frac{dc_{H_2CO_3}}{dt} \times \frac{Q_g H_{CO_2}}{V_L RT}}{\frac{Q_g H_{CO_2}}{V_L RT} \times ((c_{H_2CO_3})_1^* - c_{H_2CO_3}) \times \left[\frac{2}{2 + (K_1/c_{H_2CO_3})^{0.5}} \right] - \frac{dc_{H_2CO_3}}{dt}} \quad (9)$$

$$= \frac{N \text{ (Numerator)}}{D \text{ (Denominator)}}$$

“Diff” term was defined as shown below for each sample position and an average value was then calculated.

$$Diff = k_{La} \times D - N \quad (10)$$

From this average value, excel solver was used to solve for k_{La} such that Diff term is zero, therefore the k_{La} of the system is obtained.

Using pH:

The table below summarizes the set of raw data and variables calculated to determine k_{LA} .

Table 29: Data Used to Calculate k_{LA}

Sample	d (cm)	time (s)	P_{local} (atm)	pH	pH_fit	C*	[H ⁺]
0	0	0.000	1.79	6.65	6.29	6.5E-02	5.1E-07
1	15	0.074	1.78	4.75	4.83	6.5E-02	1.5E-05
2	29	0.144	1.68	4.32	4.45	6.1E-02	3.5E-05
3	43	0.213	1.59	4.23	4.32	5.8E-02	4.8E-05
4	50	0.248	1.54	4.25	4.29	5.6E-02	5.1E-05
5	57	0.282	1.49	4.24	4.27	5.5E-02	5.4E-05
6	71	0.352	1.40	4.23	4.24	5.1E-02	5.8E-05

Table 30: Calculated variables for determining k_{LA} using pH

[CO ₂]	C*- [CO ₂]	d[CO ₂]/dt	V _L	A
5.39E-07	6.54E-02	-	0	-
4.38E-04	6.45E-02	5.89E-03	0.052	18.7
2.57E-03	5.89E-02	3.08E-02	0.100	9.68
4.62E-03	5.34E-02	2.95E-02	0.148	6.53
5.33E-03	5.09E-02	2.07E-02	0.172	5.61
5.91E-03	4.86E-02	1.68E-02	0.196	4.93
6.88E-03	4.42E-02	1.39E-02	0.244	3.95

“A” is calculated as using equation (9) (methodology section). It should be noted that

“A” is a function of the k_{LA} value that needs to be calculated. So, an initial guess for k_{LA} (usually $k_{LA} = 1$) is used before solving for k_{LA} .

The k_{LA} obtained using pH method was found to be 0.74 s^{-1} .

Using CO₂ analyzer:

Table 31: Calculated variables for determining k_{La} using CO₂ analyzer

[CO ₂] (mg/L)	[CO ₂] fit (mg/L)	[CO ₂] (M)	C*-[CO ₂]	d[CO ₂]/dt	V _L	A
0	0	0	-	-	0	-
83	94	0.0021	6.28E-02	0.0289	0.052	6.20
364	341	0.0078	5.37E-02	0.0810	0.100	3.21
514	510	0.0116	4.64E-02	0.0553	0.148	2.16
566	565	0.0128	4.34E-02	0.0359	0.172	1.86
576	600	0.0136	4.09E-02	0.0231	0.196	1.63
623	611	0.0139	3.72E-02	0.0037	0.244	1.31

The k_{La} obtained using CO₂ analyzer was found to be 1.28 s⁻¹.

The average k_{La} which was used in this study is:

$$k_{La} (s^{-1}) = \frac{0.74 + 1.28}{2} = 1.01 \quad (11)$$

It should be noted that these calculation methods can also be performed on MATLAB by solving the differential equation and all the set of variables. The values for k_{La} shown are obtained from the specially developed MATLAB code that perform similar to the solution presented above using excel data sheet.

APPENDIX IV

ERROR ANALYSIS

Physical quantities measured are subject to errors and they are classified as precision errors and bias errors.

Table 32 summarizes the measurement tool with its associated errors.

Table 32: Errors associated with measured physical quantities

Physical quantity measured	Error
Q _L	1.5 (L/min)
Q _g	4%
pH	0.03
[CO ₂] - CO ₂ analyzer	40 mg/L
Pressure transducer	0.4 kPa

In order to determine the error propagation on calculated terms, the following equation was applied.

$$\Delta y_i = y(x_1, x_2, \dots, x_i + \Delta x_i, \dots, x_n) - y(x_1, x_2, \dots, x_n) \quad (12)$$

So, if x_i has a precision error of Δx_i then the resulting error on y (Δy_i) can be calculated.

From the errors associated to the pressure transducer, the error on ΔP /screen was calculated as shown below:

$$Error\ on\ \frac{\Delta P}{screen}\ (kPa) = \frac{\Delta P_{bottom} - \Delta P_{top}}{8} = \frac{0.4 + 0.4}{8} = 0.1 \quad (13)$$

From ΔQ_L and ΔQ_g , the errors on U_L and U_g can be calculated as shown below:

$$\Delta U_L (m/s) = \frac{\Delta Q_L}{1000 \times 60 \times A_c} = 0.05 \quad (14)$$

$$\Delta U_g (m/s) = \frac{\Delta Q_g}{1000 \times 60 \times A_c} \quad (15)$$

Where A_c is the cross-section area of the reactor and is equal to:

$$A_c = \frac{\pi D^2}{4} = \frac{\pi(0.025^2)}{4} = 4.91 \times 10^{-4} m^2 \quad (16)$$

From ΔQ_L and ΔQ_g , the errors on ϕ and U_T are calculated as shown below:

$$\Delta\phi (\%) = \frac{Q_g + \Delta Q_g}{Q_L + \Delta Q_L + Q_g + \Delta Q_g} \times 100 \quad (17)$$

$$\Delta U_T (m/s) = \Delta U_L + \Delta U_g \quad (18)$$

the errors associated to U_g , U_T and ϕ are summarized in Table 33:

Table 33: Error analysis for superficial velocity of gas and liquid mixture

Q_g (L/min)	Q_L (L/min)	ΔQ_g (L/min)	$\Delta\phi$ (%)	ΔU_g (m/s)	ΔU_T (m/s)
2.94	26.5	0.118	1.43	0.004	0.055
3.79	34.07	0.151	0.36	0.0051	0.057
4.84	43.53	0.193	0.47	0.0066	0.058
5.89	53	0.236	1.02	0.008	0.059
6.15	24.61	0.246	1.61	0.0084	0.06
7.57	30.28	0.303	0.73	0.0103	0.062
9.46	37.85	0.379	0.03	0.0129	0.064
11.83	47.32	0.473	0.64	0.0161	0.067
8.92	20.82	0.357	2.16	0.0121	0.064
11.36	26.5	0.454	1.12	0.0154	0.067
14.6	34.07	0.584	0.27	0.0198	0.071
17.85	41.64	0.714	0.27	0.0242	0.076

From ΔU_T the error on residence time (Δt) can be calculated as shown below:

$$\Delta t (s) = t - \frac{d}{U_T + \Delta U_T} \quad (19)$$

The percent error on residence time is calculated as shown in the following equation:

$$\% \text{ error } (\Delta t) = \frac{\Delta t}{t} \times 100 \quad (20)$$

The values are summarized in Table 34:

Table 34: Error on residence time

U_T (m/s)	ΔU_T (m/s)	t (s)	Δt	% error (t)
1.01	0.055	0.71	0.043	6.1
1.29	0.057	0.55	0.023	4.2
1.65	0.058	0.43	0.017	4.0
2.02	0.059	0.36	0.014	3.8
1.04	0.06	0.68	0.037	5.4
1.29	0.062	0.55	0.025	4.6
1.61	0.064	0.44	0.017	3.8
2.01	0.067	0.35	0.011	3.2
1.00	0.064	0.70	0.036	5.1
1.29	0.067	0.55	0.027	5.0
1.64	0.071	0.43	0.015	3.5
2.00	0.076	0.35	0.009	2.7

In what follows, a sample calculation for the error propagation on pH, CO₂ concentrations, E_{spm} , k_{LA} and Reynolds number is demonstrated.

Experimental run: Mn = 80, $U_T = 1.6$ m/s, $\phi = 30\%$ and L = 70 mm

In order to determine the error propagation on k_{LA} , a sample calculation for one experimental was demonstrated. The errors associated to the measurement methods were first analyzed.

- Error on calculated CO₂ concentrations

The error on pH measurements propagates to the calculated CO₂ concentrations. To quantify this error, the CO₂ concentration was calculated with ΔpH as shown below:

$$[CO_2]_{(e)} = \frac{10^{-2(pH - \Delta pH)}}{K_1} \quad (21)$$

The percent error was calculated as shown below:

$$\% \text{ error } ([CO_2]) = \frac{[CO_2]_{(e)} - [CO_2]}{[CO_2]} \times 100 \quad (22)$$

Table 35 summarizes the values calculated for the experimental run

Table 35: Error propagation on the calculated CO₂ from pH

pH	[CO ₂] - pH	[CO ₂] _(e)	Δ[CO ₂]	% error ([CO ₂])
6.41	0	0	0	15
4.5	90	103	13	15
4.37	163	188	24	15
4.32	206	236	30	15
4.3	226	259	33	15
4.28	247	284	37	15
4.26	271	311	40	15

- Error on back calculated pH

On the other hand, the error on the CO₂ analyzer also resulted in an error on the back calculated pH. pH_(e) was calculated with Δ[CO₂] as shown below to determine the percentage error.

$$pH_{(e)} = -\frac{1}{2} \log(K_1 \times ([CO_2] + \Delta[CO_2])) \quad (23)$$

The percent error was calculated as shown below:

$$\% \text{ error } (pH) = \frac{pH_{(e)} - pH}{pH} \times 100 \quad (24)$$

Table 36 summarizes the values of a sample calculation for the experimental run

Table 36: Error propagation on back calculated pH from CO₂ analyzer

[CO ₂]	calculated pH	pH _(e)	ΔpH	% error (pH)
0	6.47	6.47	0.000	0.0
252	4.28	4.24	0.032	0.7
441	4.15	4.14	0.019	0.5
502	4.13	4.11	0.017	0.4
557	4.10	4.09	0.015	0.4
617	4.08	4.07	0.014	0.3
687	4.06	4.05	0.012	0.3

- Error on k_{La}

To determine the error propagation on k_{La} , $k_{La(e)}$ was calculated with the errors demonstrated previously. The percentage error was determined using the following equation:

$$\% \text{ error } (k_{La}) = \frac{k_{La(e)} - k_{La}}{k_{La}} \times 100 \quad (25)$$

Table 37 summarizes the values for the errors on k_{La} .

Table 37: Error propagation on k_{La}

	k_{La}	k_{La_e}	% error (k_{La})
pH	0.74	0.90	22
CO ₂ analyzer	1.28	1.47	15
average	1.01	1.19	18

- Error on E_{spm}

The E_{spm} for the specified experimental run is 0.013152 kWh/tonne.

The error on E_{spm} was calculated by determining ΔE_{spm} as shown below:

$$\begin{aligned}
\Delta E_{spm}(\text{kWh/tonne}) & \quad (26) \\
& = E_{spm} \\
& \quad - \frac{(\Delta P + 0.1) \cdot (Q_L + \Delta Q_L + Q_G + \Delta Q_G)}{\rho_{mix}} \times (t + \Delta t) \\
& = 0.00046
\end{aligned}$$

The percentage error on E_{spm} is calculated as follows:

$$\% \text{ error } (E_{spm}) = \frac{\Delta E_{spm}}{E_{spm}} \times 100 = 3.5 \% \quad (27)$$

- Error on Reynolds number

The error propagation on Reynolds number was also calculated for the specified experimental run. All Reynolds numbers, Re , Re_b , Re_M , Re_j and Re_{jet} , are dependent on U_T . So, they are affected by ΔU_T . Table 38 summarizes the variation of Reynolds number affected by ΔU_T and the percentage error.

Table 38: Error on Reynolds number

	Value	Δ (change)	% error
Re	56734	1947	3.4
Re _b	519	18	3.4
Re _M	1153	40	3.4
Re _j	2365	81	3.4
Re _{jet}	187549	6436	3.4

BIBLIOGRAPHY

- Abou Hweij, K., Azizi, F., 2015. Hydrodynamics and residence time distribution of liquid flow in tubular reactors equipped with screen-type static mixers. *Chem. Eng. J.* 279, 948–963. <https://doi.org/10.1016/j.cej.2015.05.100>
- Afkhamipour, M., Mofarahi, M., 2017. Review on the mass transfer performance of CO₂ absorption by amine-based solvents in low- and high-pressure absorption packed columns. *RSC Adv.* 7, 17857–17872. <https://doi.org/10.1039/C7RA01352C>
- Al-Anezi, K., Hilal, N., 2006. Effect of carbon dioxide in seawater on desalination: A comprehensive review. *Sep. Purif. Rev.* 35, 223–247. <https://doi.org/10.1080/15422110600867365>
- Al-Deffeeri, N.S., 2008. The release of CO₂ in MSF distillers and its use for the recarbonation plant: a case study. *Desalination* 222, 579–591. <https://doi.org/10.1016/j.desal.2007.01.124>
- Al-Hindi, M., Azizi, F., 2017. Absorption and desorption of carbon dioxide in several water types. *Can. J. Chem. Eng.* 96, 274–284. <https://doi.org/10.1002/cjce.22901>
- Al Taweel, A.M., Azizi, F., Siriijeerachai, G., 2013. Static mixers: Effective means for intensifying mass transfer limited reactions. *Chem. Eng. Process. Process Intensif.* 72, 51–62. <https://doi.org/10.1016/j.cep.2013.08.009>
- Al Taweel, A.M., Chen, C., 1996. A novel static mixer for the effective dispersion of immiscible liquids. *Chem. Eng. Res. Des.* 74, 2018.
- Al Taweel, A.M., Yan, J., Azizi, F., Odedra, D., Gomaa, H.G., 2005. Using in-line static mixers to intensify gas-liquid mass transfer processes. *Chem. Eng. Sci.* 60, 6378–6390. <https://doi.org/10.1016/j.ces.2005.03.011>
- Ali, a T.B., Alali, M., Alzaid, M., Bunch, M., Menacherry, S., 2011. Numerical simulation model of geological storage of carbon dioxide in onshore Gippsland Basin, Victoria. *Soc. Pet. Eng. - 9th Eur. Form. Damage Conf.* 2011 2, 796–812.
- Álvarez, E., Gómez-Díaz, D., Navaza, J.M., Sanjurjo, B., 2008. Continuous removal of carbon dioxide by absorption employing a bubble column. *Chem. Eng. J.* 137, 251–256. <https://doi.org/10.1016/j.cej.2007.04.027>
- Alves, S.S., Maia, C.I., Vasconcelos, J.M.T., 2004. Gas-liquid mass transfer coefficient in stirred tanks interpreted through bubble contamination kinetics. *Chem. Eng. Process. Process Intensif.* 43, 823–830. <https://doi.org/10.1016/S0255->

2701(03)00100-4

- Aroonwilas, A., Veawab, A., Tontiwachwuthikul, P., 1999. Behavior of the Mass-Transfer Coefficient of Structured Packings in CO₂ Absorbers with Chemical Reactions. *Ind. Eng. Chem. Res.* 38, 2044–2050. <https://doi.org/10.1021/ie980728c>
- Azizi, F., Abou Hweij, K., 2017. Liquid-Phase Axial Dispersion of Turbulent Gas-Liquid Co-Current Flow Through Screen-Type Static Mixers. *AIChE J.* 63, 1390–1403. <https://doi.org/10.1002/aic>
- Azizi, F., Al Taweel, A.M., 2015. Mass Transfer in an Energy-Efficient High-Intensity Gas-Liquid Contactor. *Ind. Eng. Chem. Res.* 54, 11635–11652. <https://doi.org/10.1021/acs.iecr.5b01078>
- Azizi, F., Al Taweel, A.M., 2012. Inter-phase mass transfer in turbulent liquid-liquid dispersions: A comparative analysis of models. *Chem. Eng. J.* 179, 231–241. <https://doi.org/10.1016/j.cej.2011.10.063>
- Azizi, F., Al Taweel, A.M., 2011. Hydrodynamics of liquid flow through screens and screen-type static mixers. *Chem. Eng. Commun.* 198, 726–742. <https://doi.org/10.1080/00986445.2011.532748>
- Azizi, F., Al Taweel, A.M., 2007. Population balance simulation of gas-liquid contacting. *Chem. Eng. Sci.* 62, 7436–7445. <https://doi.org/10.1016/j.ces.2007.08.083>
- Bauer, F., Hulteberg, C., Persson, T., Tamm, D., 2013. Biogas upgrading – Review of commercial technologies. Swedish Gas Technol. Centre, SGC 82. [https://doi.org/SGC Rapport 2013:270](https://doi.org/SGC%20Rapport%202013%3A270)
- Belaissaoui, B., Favre, E., 2018. Novel dense skin hollow fiber membrane contactor based process for CO₂ removal from raw biogas using water as absorbent. *Sep. Purif. Technol.* 193, 112–126. <https://doi.org/10.1016/j.seppur.2017.10.060>
- Berglund, M., Börjesson, P., 2006. Assessment of energy performance in the life-cycle of biogas production. *Biomass and Bioenergy* 30, 254–266. <https://doi.org/10.1016/j.biombioe.2005.11.011>
- Bishnoi, S., Rochelle, G.T., 2000. Absorption of carbon dioxide into aqueous piperazine: Reaction kinetics, mass transfer and solubility. *Chem. Eng. Sci.* 55, 5531–5543. [https://doi.org/10.1016/S0009-2509\(00\)00182-2](https://doi.org/10.1016/S0009-2509(00)00182-2)
- Bloder, J., Gautsch, J., Germann, K., Murer, G., 2005. U.S. Patent No. 6,874,351. Washington, DC: Patent and Trademark Office. <https://doi.org/10.1145/634067.634234>.

- Boodhoo, K., Harvey, A., 2013a. Process Intensification: An Overview of Principles and Practice. *Process Intensif. Green Chem. Eng. Solut. Sustain. Chem. Process.* 1–31. <https://doi.org/10.1002/9781118498521.ch1>
- Boodhoo, K., Harvey, A., 2013b. Process Intensification for Green Chemistry: Engineering Solutions for Sustainable Chemical Processing. *Process Intensif. Green Chem. Eng. Solut. Sustain. Chem. Process.* 2018. <https://doi.org/10.1002/9781118498521>
- Boributh, S., Assabumrungrat, S., Laosiripojana, N., Jiraratananon, R., 2011. A modeling study on the effects of membrane characteristics and operating parameters on physical absorption of CO₂ by hollow fiber membrane contactor. *J. Memb. Sci.* 380, 21–33. <https://doi.org/10.1016/j.memsci.2011.06.029>
- Chavez, R.-H., Guadarrama, J.J. De, 2010. Comparison of structured packings in CO₂ absorber with chemical reactions. *Chem. Eng. Trans.* 21, 577–582. <https://doi.org/10.3303/CET1021097>
- Chen, B.H., Vallabh, R., 1970. Holdup and Mass transfer in Bubble Columns Containing Screen Cylinders. *Ind. Eng. Chem. Process Des. Dev.* 9, 121–126. <https://doi.org/10.1021/i260057a005>
- Dawoud, B., Amer, E., Gross, D., 2007. Experimental investigation of an adsorptive thermal energy storage. *Int. J. energy Res.* 31, 135–147. <https://doi.org/10.1002/er>
- Elhajj, J., Al-Hindi, M., Azizi, F., 2014. A Review of the Absorption and Desorption Processes of Carbon Dioxide in Water Systems. *Ind. Eng. Chem. Res.* 53, 2–22. <https://doi.org/10.1021/ie403245p>
- Evren, V., Çağatay, T., Özdural, A.R., 1999. Carbon dioxide-air mixtures: Mass transfer in recycling packed-bed absorption columns operating under high liquid flow rates. *Sep. Purif. Technol.* 17, 89–96. [https://doi.org/10.1016/S1383-5866\(99\)00014-3](https://doi.org/10.1016/S1383-5866(99)00014-3)
- Ganapathy, H., Steinmayer, S., Shooshtari, A., Dessiatoun, S., Ohadi, M.M., 2016. Process intensification characteristics of a microreactor absorber for enhanced CO₂ capture. *Appl. Energy* 162, 416–427. <https://doi.org/10.1016/j.apenergy.2015.10.010>
- Ghanem, A., Lemenand, T., Della Valle, D., Peerhossaini, H., 2014. Static mixers: Mechanisms, applications, and characterization methods - A review. *Chem. Eng. Res. Des.* 92, 205–228. <https://doi.org/10.1016/j.cherd.2013.07.013>
- Glade, H., Meyer, J.H., Will, S., 2005. The release of CO₂ in MSF and ME distillers and its use for the recarbonation of the distillate: A comparison. *Desalination* 182, 99–110. <https://doi.org/10.1016/j.desal.2005.04.012>

- Golkhar, A., Keshavarz, P., Mowla, D., 2013. Investigation of CO₂ removal by silica and CNT nanofluids in microporous hollow fiber membrane contactors. *J. Memb. Sci.* 433, 17–24. <https://doi.org/10.1016/j.memsci.2013.01.022>
- Gómez-Díaz, D., Navaza, J.M., 2005. Gas/liquid mass transfer processes in a carbon dioxide/alkane system. *J. Chem. Technol. Biotechnol.* 80, 812–818. <https://doi.org/10.1002/jctb.1251>
- Hasib-ur-Rahman, M., Siaj, M., Larachi, F., 2010. Ionic liquids for CO₂ capture- Development and progress. *Chem. Eng. Process. Process Intensif.* 49, 313–322. <https://doi.org/10.1016/j.cep.2010.03.008>
- Hasson, D., Bendrihem, O., 2006. Modeling remineralization of desalinated water by limestone dissolution. *Desalination* 190, 189–200. <https://doi.org/10.1016/j.desal.2005.09.003>
- Heyouni, A., Roustan, M., Do-Quang, Z., 2002. Hydrodynamics and mass transfer in gas-liquid flow through static mixers. *Chem. Eng. Sci.* 57, 3325–3333. [https://doi.org/10.1016/S0009-2509\(02\)00202-6](https://doi.org/10.1016/S0009-2509(02)00202-6)
- Hill, G.A., 2006. Measurement of overall volumetric mass transfer coefficients for carbon dioxide in a well-mixed reactor using a pH probe. *Ind. Eng. Chem. Res.* 45, 5796–5800. <https://doi.org/10.1021/ie060242t>
- Jackson, R.B., Le Quéré, C., Andrew, R.M., Canadell, J.G., Peters, G.P., Roy, J., Wu, L., 2017. Warning signs for stabilizing global CO₂ emissions. *Environ. Res. Lett.* 12, 110202. <https://doi.org/10.1088/1748-9326/aa9662>
- Koglin, B., Pawlowski, J., Schnoring, H., 1981. Kontinuierliches Emulgieren mit Rotor/StatorMaschinen. *Chemie Ing. Tech.* 53, 641–647. <https://doi.org/10.1002/cite.330530813>
- Kordac, M., Linek, V., 2008. Dynamic Measurement of Carbon Dioxide Volumetric Mass Transfer Coefficient in a Well-Mixed Reactor Using a pH probe: Analysis of the Salt and Saturation Effects. *Ind. Eng. Chem. Res.* 47, 1310–1317.
- Laakkonen, M., Alopaeus, V., Aittamaa, J., 2006. Validation of bubble breakage, coalescence and mass transfer models for gas-liquid dispersion in agitated vessel. *Chem. Eng. Sci.* 61, 218–228. <https://doi.org/10.1016/j.ces.2004.11.066>
- Lee, J.S., Lee, J.W., Kang, Y.T., 2015. CO₂ absorption/regeneration enhancement in DI water with suspended nanoparticles for energy conversion application. *Appl. Energy* 143, 119–129. <https://doi.org/10.1016/j.apenergy.2015.01.020>
- Lee, J.W., Jung, J.Y., Lee, S.G., Kang, Y.T., 2011. CO₂ bubble absorption

- enhancement in methanol-based nanofluids. *Int. J. Refrig.* 34, 1727–1733.
<https://doi.org/10.1016/j.ijrefrig.2011.08.002>
- Lee, J.W., Kang, Y.T., 2013. CO₂ absorption enhancement by Al₂O₃ nanoparticles in NaCl aqueous solution. *Energy* 53, 206–211.
<https://doi.org/10.1016/j.energy.2013.02.047>
- Lee, J.W., Torres Pineda, I., Lee, J.H., Kang, Y.T., 2016. Combined CO₂ absorption/regeneration performance enhancement by using nanoabsorbents. *Appl. Energy* 178, 164–176. <https://doi.org/10.1016/j.apenergy.2016.06.048>
- Lezhnin, S., Eskin, D., Leonenko, Y., Vinogradov, O., 2003. Dissolution of air bubbles in a turbulent water pipeline flow. *Heat Mass Transf. und Stoffuebertragung* 39, 483–487. <https://doi.org/10.1007/s00231-002-0313-z>
- Lin, C.C., Chu, C.R., 2015. Mass transfer performance of rotating packed beds with blade packings in carbon dioxide absorption into sodium hydroxide solution. *Sep. Purif. Technol.* 150, 196–203. <https://doi.org/10.1016/j.seppur.2015.06.025>
- Lin, C.C., Kuo, Y.W., 2016. Mass transfer performance of rotating packed beds with blade packings in absorption of CO₂ into MEA solution. *Int. J. Heat Mass Transf.* 97, 712–718. <https://doi.org/10.1016/j.ijheatmasstransfer.2016.02.033>
- Lisitsin, D., Hasson, D., Semiat, R., 2008. The potential of CO₂ stripping for pretreating brackish and wastewater desalination feeds. *Desalination* 222, 50–58.
<https://doi.org/10.1016/j.desal.2007.02.063>
- Luo, Y., Luo, J.Z., Chu, G.W., Zhao, Z.Q., Arowo, M., Chen, J.F., 2017. Investigation of effective interfacial area in a rotating packed bed with structured stainless steel wire mesh packing. *Chem. Eng. Sci.* 170, 347–354.
<https://doi.org/10.1016/j.ces.2016.10.023>
- MacDowell, N., Florin, N., Buchard, A., Hallett, J., Galindo, A., Jackson, G., Adjiman, C.S., Williams, C.K., Shah, N., Fennell, P., 2010. An overview of CO₂ capture technologies. *Energy Environ. Sci.* 3, 1645. <https://doi.org/10.1039/c004106h>
- Maceiras, R., Nóvoa, X.R., Álvarez, E., Cancela, M.A., 2007. Local mass transfer measurements in a bubble column using an electrochemical technique. *Chem. Eng. Process. Process Intensif.* 46, 1006–1011.
<https://doi.org/10.1016/j.cep.2007.05.010>
- Mansourizadeh, A., 2012. Experimental study of CO₂ absorption/stripping via PVDF hollow fiber membrane contactor. *Chem. Eng. Res. Des.* 90, 555–562.
<https://doi.org/10.1016/j.cherd.2011.08.017>

- Millero, F.J., 1995. Thermodynamics of the carbon dioxide system in the ocean. *Geochim. Cosmochim. Acta* 59, 661–677.
- Momeni, A., Aghajani, M., Zargar, G., 2012. A simulation study of carbon dioxide sequestration in a depleted oil reservoir. *Pet. Sci. Technol.* 30, 751–765. <https://doi.org/10.1080/10916466.2010.490809>
- Moucha, T., Rejl, F.J., Kordač, M., Labík, L., 2012. Mass transfer characteristics of multiple-impeller fermenters for their design and scale-up. *Biochem. Eng. J.* 69, 17–27. <https://doi.org/10.1016/j.bej.2012.08.007>
- Munter, R., 2010. Comparison of Mass Transfer Efficiency and Energy Consumption in Static Mixers. *Ozone Sci. Eng.* 32, 399–407. <https://doi.org/10.1080/01919512.2010.517492>
- Nieves-Remacha, M.J., Kulkarni, A.A., Jensen, K.F., 2013. Gas–Liquid Flow and Mass Transfer in an Advanced-Flow Reactor. *Ind. Eng. Chem. Res.* 52, 8996–9010. <https://doi.org/10.1021/ie4011707>
- Nock, W.J., Walker, M., Kapoor, R., Heaven, S., 2014. Modeling the water scrubbing process and energy requirements for CO₂ capture to upgrade biogas to biomethane. *Ind. Eng. Chem. Res.* 53, 12783–12792. <https://doi.org/10.1021/ie501280p>
- Olivier, J.G.J., Schure, K.M., Peters, J.A.H.W., 2017. TRENDS IN GLOBAL CO₂ AND TOTAL GREENHOUSE GAS EMISSIONS 2017 Report Trends in global CO₂ and total greenhouse gas emissions: 2017 Report.
- Panja, N.C., Rao, D.P., 1993. Measurement of gas-liquid parameters in a mechanically agitated contactor. *Chem. Eng. J.* 52, 121–129. [https://doi.org/10.1016/0300-9467\(93\)80061-R](https://doi.org/10.1016/0300-9467(93)80061-R)
- Persson, M., 2003. Evaluation of Upgrading Techniques for Biogas. *Environ. Eng.* <https://doi.org/SGC142>
- Peschel, A., Hentschel, B., Freund, H., Sundmacher, K., 2012. Design of optimal multiphase reactors exemplified on the hydroformylation of long chain alkenes. *Chem. Eng. J.* 188, 126–141. <https://doi.org/10.1016/j.cej.2012.01.123>
- Pineda, I.T., Choi, C.K., Kang, Y.T., 2014. CO₂ gas absorption by CH₃OH based nanofluids in an annular contactor at low rotational speeds. *Int. J. Greenh. Gas Control* 23, 105–112. <https://doi.org/10.1016/j.ijggc.2014.02.008>
- Roes, A.W.M., Zeeman, A.J., Bukkems, F.H., 1984. HIGH INTENSITY GAS / LIQUID MASS TRANSFER IN THE BUBBLY FLOW REGION DURING CO-

CURRENT UPFLOW THROUGH STATIC MIXERS . 87, 231–238.

- Rubia, M.D. La, García-Abuín, A., Gómez-Díaz, D., Navaza, J.M., 2010. Interfacial area and mass transfer in carbon dioxide absorption in TEA aqueous solutions in a bubble column reactor. *Chem. Eng. Process. Process Intensif.* 49, 852–858. <https://doi.org/10.1016/j.cep.2010.06.003>
- Smyth, B.M., Murphy, J.D., O'Brien, C.M., 2009. What is the energy balance of grass biomethane in Ireland and other temperate northern European climates? *Renew. Sustain. Energy Rev.* 13, 2349–2360. <https://doi.org/10.1016/j.rser.2009.04.003>
- Tamir, A., Herskowitz, D., Herskowitz, V., 1990. Jet Absorbers. *Chem. Eng. Commun.* 28, 165.
- Taweel, A.M., AL, Walker, L.D., 1983. Liquid Dispersion in Static In-Line Mixers. *Eng. Chem.* 61, 527.
- Thaker, K., Rao, D.P., 2007. Effects of gas redispersion and liquid height on gas-liquid hydrodynamics in a multistage bubble column. *Chem. Eng. Res. Des.* 85, 1362–1374. [https://doi.org/10.1016/S0263-8762\(07\)73176-3](https://doi.org/10.1016/S0263-8762(07)73176-3)
- Tokumura, M., Baba, M., Kawase, Y., 2007. Dynamic modeling and simulation of absorption of carbon dioxide into seawater 62, 7305–7311. <https://doi.org/10.1016/j.ces.2007.08.074>
- Torres Pineda, I., Kang, Y.T., 2016. CO₂ absorption enhancement by nanoabsorbents in Taylor-Couette absorber. *Int. J. Heat Mass Transf.* 100, 39–47. <https://doi.org/10.1016/j.ijheatmasstransfer.2016.04.086>
- Torres Pineda, I., Lee, J.W., Jung, I., Kang, Y.T., 2012. CO₂ absorption enhancement by methanol-based Al₂O₃ and SiO₂ nanofluids in a tray column absorber. *Int. J. Refrig.* 35, 1402–1409. <https://doi.org/10.1016/j.ijrefrig.2012.03.017>
- Turunen, I., Haario, H., 1994. Mass Transfer in Tubular Static Reactors Mixers Equipped With 49, 5257–5269.
- Vázquez, G., Cancela, M.A., Varela, R., Alvarez, E., Navaza, J.M., 1997. Influence of surfactants on absorption of CO₂ in a stirred tank with and without bubbling. *Chem. Eng. J.* 67, 131–137. [https://doi.org/10.1016/S1385-8947\(97\)00047-8](https://doi.org/10.1016/S1385-8947(97)00047-8)
- Wang, Y., Zhao, L., Otto, A., Robinius, M., Stolten, D., 2017. A Review of Post-combustion CO₂ Capture Technologies from Coal-fired Power Plants. *Energy Procedia* 114, 650–665. <https://doi.org/10.1016/j.egypro.2017.03.1209>
- Wappel, D., Gronald, G., Kalb, R., Draxler, J., 2010. Ionic liquids for post-combustion

- CO₂ absorption. *Int. J. Greenh. Gas Control* 4, 486–494.
<https://doi.org/10.1016/j.ijggc.2009.11.012>
- Weiss, R.F., 1974. Carbon dioxide in water and seawater: the solubility of a non-ideal gas. *Mar. Chem.* 2, 203–215. [https://doi.org/10.1016/0304-4203\(74\)90015-2](https://doi.org/10.1016/0304-4203(74)90015-2)
- Withers, A., 2005. Options for recarbonation, remineralisation and disinfection for desalination plants. *Desalination* 179, 11–24.
<https://doi.org/10.1016/j.desal.2004.11.051>
- Xu, B., Gao, H., Luo, X., Liao, H., Liang, Z., 2016. Mass transfer performance of CO₂ absorption into aqueous DEEA in packed columns. *Int. J. Greenh. Gas Control* 51, 11–17. <https://doi.org/10.1016/j.ijggc.2016.05.004>
- Yue, J., Chen, G., Yuan, Q., Luo, L., Gonthier, Y., 2007. Hydrodynamics and mass transfer characteristics in gas-liquid flow through a rectangular microchannel. *Chem. Eng. Sci.* 62, 2096–2108. <https://doi.org/10.1016/j.ces.2006.12.057>
- Zhang, J., Xu, S., Li, W., 2012. High shear mixers: A review of typical applications and studies on power draw, flow pattern, energy dissipation and transfer properties. *Chem. Eng. Process. Process Intensif.* 57–58, 25–41.
<https://doi.org/10.1016/j.cep.2012.04.004>
- ZHANG, P., SHI, Y., WEI, J., 2007. Kinetics region and model for mass transfer in carbon dioxide absorption into aqueous solution of 2-amino-2-methyl-1-propanol. *Sep. Purif. Technol.* 56, 340–347. <https://doi.org/10.1016/j.seppur.2007.02.010>